

NOAA Technical Memorandum ERL NSSL-72

UPDRAFT PROPERTIES

DEDUCED FROM RAWINSOUNDINGS

Robert P. Davies-Jones  
James H. Henderson

Property of  
NWC Library  
*University of Oklahoma*

National Severe Storms Laboratory  
Norman, Oklahoma  
November 1974

UNITED STATES  
DEPARTMENT OF COMMERCE  
Frederick B. Dent, Secretary

NATIONAL OCEANIC AND  
ATMOSPHERIC ADMINISTRATION  
Robert M. White, Administrator

Environmental Research  
Laboratories  
Wilmot N. Hess, Director



## CONTENTS

	Page
LIST OF FIGURES	v
LIST OF TABLES	vi
ABSTRACT	ix
1. INTRODUCTION	1
1.1 Literature Review of Updraft Measurements	1
1.1.1 Vertical Velocity and Temperature Measurements	1
1.1.2 Pressure Measurements	3
1.1.3 Liquid Water Contents	3
1.1.4 Horizontal Wind Measurements	3
1.1.5 Summary	4
1.2 History of Updraft Soundings	4
1.3 Instrument Limitations	5
2. CHARACTERISTICS OF INDIVIDUAL UPDRAFTS	6
2.1 The NSSL Upper Air Networks	6
2.2 Selection of Updraft and Environment Soundings	8
2.3 Synoptic Locations of Storms	10
2.4 Description of Soundings	10
2.4.1 Environment Soundings	10
2.4.2 Updraft Soundings	12
2.5 Radar Echo Descriptions	13
2.6 Summary	15
3. STATISTICS OF UPDRAFT SOUNDINGS	15
3.1 Release Times and Points of Environment Soundings	15
3.2 Statistics of Eight 1.2 km Thick Layers	15
3.3 Mean Updraft and Environment Soundings	18
3.4 Mean Vertical Velocity Profiles	27
3.5 Dynamical Interpretations	27
3.6 Summary	28
4. DISCUSSION OF MEASUREMENTS INSIDE HIGH SPEED THUNDERSTORM UPDRAFTS	28
4.1 Introduction	28
4.2 Data Analysis	29
4.3 The Diagnostic Model	32

	Page
4.4 Results	34
4.4.1 Dibble Updraft	34
4.4.2 Other Updrafts	38
4.5 Conclusions	38
5. CONCLUSIONS	38
6. ACKNOWLEDGMENTS	44
7. REFERENCES	45
APPENDIX A: DATA BASE	51
APPENDIX B: THERMODYNAMIC ENERGY EQUATION	117

## LIST OF FIGURES

<u>Figure</u>		<u>Page</u>
1	Updraft sounding taken at Columbia, Mo, at 0237 CST, 14 October 1954.	4
2	Map showing positions relative to NSSL radar (NRO) of upper air stations mentioned in this report.	8
3	Position of environment stations relative to updraft stations.	16
4	Relative release time versus relative distance for each pair of updraft and environment soundings.	16
5	Scatter diagram of $\bar{w}$ versus $\overline{\Delta T_v}$ for eight 1.2 km thick layers.	20
6	Scatter diagrams of $\bar{w}$ versus $\overline{\theta_w}$ (for lower two layers) and $\overline{\theta_s}$ (for upper six layers).	22
7	Mean updraft versus mean environment profiles for all 34 storms.	25
8	Mean updraft versus mean environment profiles for seven fastest updrafts.	27
9	Watonga updraft data: (left) Stuve diagram of updraft and environment soundings; (center) vertical profiles of $\theta_w$ and $\theta_s$ for updraft and environment; (right) updraft vertical velocity and excess virtual temperature profiles.	30
10	Fort Sill updraft data.	30
11	Dibble updraft data.	31
12	Edmond updraft data.	31
13	Observed $\theta$ profile <sub>1</sub> and model profiles for various values of $b_1$ and $w_1 = 2.5 \text{ m sec}^{-1}$ for Dibble updraft.	35
14	Observed vertical velocity profile and model profiles with different virtual mass coefficients for Dibble updraft.	36
15	Observed vertical velocity profile versus model profiles with different values of K for Dibble updraft.	37
16	Updraft radius, normalized by cloud radius, as function of height in non-entraining case for $w_1 = 2.5$ and $5 \text{ m sec}^{-1}$ .	39
17	Dibble updraft: model profiles of (a) virtual temperature excess, (b) liquid water and precipitation mixing ratios, (c) radar reflectivity, in non-entraining case.	40

<u>Figure</u>		<u>Page</u>
18	Edmond updraft: (a) observed and model $\theta$ profiles, (b) model virtual temperature excess and liquid water mixing ratio profiles, and (c) observed and model vertical velocity profiles.	41
19	Same as figure 18 but for Watonga updraft.	42
20	Same as figure 18 but for Fort Sill updraft.	43
A1-A34	Updraft and environment soundings, updraft vertical velocity profiles, radar photographs, synoptic weather summaries, weather and cloud observations for individual cases.	52-115

LIST OF TABLES

<u>Table</u>		<u>Page</u>
1	Summary of rawinsonde networks and operations, 1966-1973.	7
2	List of updraft and environment soundings, and ascent rates of updraft balloons with respect to still air.	9
3	Stability indices for environmental soundings.	11
4	Statistics of starting times and locations of environment soundings relative to corresponding updraft soundings.	17
5	Values of $\bar{w}$ , $\overline{\Delta T}_v$ , $\bar{\theta}_s$ , $\bar{\theta}_w$ , $\delta\bar{\theta}_s$ for each layer.	19
6	Correlation coefficients between $\bar{w}$ and $\overline{\Delta T}_v$ , $\bar{\theta}_s$ , $\bar{\theta}_w$ for each of eight 1.2 km-thick layers.	24

## ABSTRACT

Between 1966 and 1973, National Severe Storms Laboratory mesonet network soundings were taken near thunderstorms and squall lines. Thirty-four of these soundings sampled updrafts at various levels. Because of instrumental noise and atmospheric fine structure, many of the individual soundings were hard to interpret. However, significant results were obtained from the data as a whole and from the four fastest updraft cases.

Typically, the updrafts were associated with moderate thunderstorms that formed in baroclinic regions with maritime tropical air near the surface overlaid by dryer air aloft. The immediate environments were potentially, conditionally, and latently unstable but were stable with respect to parcel displacement from the lifted condensation level. The updrafts were generally located in regions of strong radar reflectivity gradient at 0° antenna tilt. The updraft soundings often showed pseudo-adiabatic lapse rates immediately above the updraft condensation level. With the aid of a Squires-Turner one-dimensional cloud model, it is shown that the four fastest updrafts had cores that extended at least to mid-levels and were virtually undiluted by environmental air. This finding casts doubt on the applicability of models that assume instantaneous mixing across the updraft to cumulonimbi.

Statistical analysis of the data confirms that updrafts are warm core at mid- and upper levels and that they are relatively cool at low levels (below 700 mb). Important effects of perturbation pressure gradient forces are emphasized. We also find that local updraft speed is positively correlated at the 95% confidence level with local potential wet-bulb temperature between 0.9 and 9.3 km MSL. The average vertical velocity is a maximum at a relatively low height (4.8 km MSL); this agrees with other experiments that involve tracking objects released below cloud base. However, flight train icing and other extraneous factors may be influencing this result. The average horizontal winds in the updraft and environment agree with recent conceptual Great Plains thunderstorm models.

# UPDRAFT PROPERTIES DEDUCED FROM RAWINSOUNDINGS

Robert P. Davies-Jones and James H. Henderson\*

## 1. INTRODUCTION

### 1.1 Literature Review of Updraft Measurements<sup>1</sup>

Several methods of measuring wind, vertical currents, and thermodynamic variables in thunderstorm updrafts are described. The results of the current study (on updraft rawinsoundings) are not included in this review, although parts of it have already been published (Davies-Jones and Henderson, 1973; Davies-Jones, 1974). It will become apparent that even today updraft structure is poorly understood.

#### 1.1.1 Vertical Velocity and Temperature Measurements

The first aircraft measurements of updrafts were taken in non-severe thunderstorms during the Thunderstorm Project (Byers and Braham, 1949). No penetrations were made above 7.6 km. Typical updraft diameters were 1.5 km. Average vertical currents across the updraft were estimated from altitude changes of the aircraft. Vertical velocity increased with elevation up to the 7.6 km ceiling, and the maximum recorded speed was  $25 \text{ m sec}^{-1}$ . Temperature excesses up to 5C were also measured during the penetrations. The rate at which the radar echo tops ascended indicated that the maximum updraft speeds occurred in the layer from 10.7 to 13.7 km.

Steiner and Rhyne (1962) reported a vertical gust of  $63 \text{ m sec}^{-1}$  recorded during an aircraft penetration at 12.2 km of a 15.2 km high storm. Associated strong turbulence was encountered.

Sinclair (1973) penetrated a northeastern Colorado severe thunderstorm at 9.1 km MSL in a F101B aircraft and recorded a peak mean vertical velocity of  $26 \text{ m sec}^{-1}$  and a maximum temperature excess of 13C. He concluded that in some cases the updraft core ascended practically undiluted to 9.1 km. Undiluted updraft cores have been hypothesized by Ludlam (1966), Newton (1966), and Roach (1967) to explain storm tops reaching levels predicted by parcel theory, and have been detected from aircraft penetrations of the lower regions of convective clouds near Flagstaff, Arizona, by MacCready and Takeuchi (1968).

Saunders (1962) made optical measurements of the penetration of cumulonimbi into the stratosphere and of the ascent rates of cloud turrets. Note that the vertical speed in a cloud is about twice that of the cap, since

---

\*Present affiliation National Weather Service Forecast Office, Birmingham, Alabama

<sup>1</sup>Excluding turbulence characteristics and microphysics.

cloud tops resemble convective bubbles or thermals (Turner, 1962). Saunders determined that the speeds at which the tops of cloud towers approached the tropopause were proportional to the depths of stratospheric penetrations in the ratio  $10 \text{ m sec}^{-1}$  per km. The maximum penetration and ascent rate were 2.5 km and  $25 \text{ m sec}^{-1}$ , respectively. In this case, the thermal probably contained air rising at  $50 \text{ m sec}^{-1}$ . Roach (1967) also observed towers with growth rates of  $25 \text{ m sec}^{-1}$  and stratospheric penetrations up to 7 km. Vonnegut and Moore (1958) showed that according to simple parcel theory an updraft speed at the tropopause of  $20 \text{ m sec}^{-1}$  is implied by each km of penetration. Thus Saunder's results are compatible with parcel theory. Ludlum (1959) performed similar work using radar rather than visual observations. He measured a stratospheric penetration of 2.4 km and a radar turret ascent rate of  $27 \text{ m sec}^{-1}$ .

Battan and Theiss (1966) and Donaldson (1967), using vertically pointing Doppler radars, found peak updraft speeds of 15 to  $20 \text{ m sec}^{-1}$  near a thunderstorm top ( $\sim 10 \text{ km}$ ). Vertical time sections of updraft velocity indicate aggregates of rising bubbles rather than a rising jet. However, the updrafts were probably non-steady and three dimensional, and thus not totally contained in the time sections.

Bushnell (1973) measured a  $25 \text{ m sec}^{-1}$  updraft speed 4 km above cloud base with a dropsonde. Wichmann (1951) described observations in cumulonimbi over Germany by sailplane pilots. Updraft speeds varied from 2 to  $6 \text{ m sec}^{-1}$  at cloud base, and reached 20 to  $30 \text{ m sec}^{-1}$  at midlevels ( $< 8 \text{ km}$ ). The updrafts were smooth and concentrated in narrow chimneys.

Sulakvelidze et al. (1967) used radar tracking of no-lift pilot balloons with corner reflectors to determine in-cloud vertical velocities. They found maximum vertical velocities of  $22 \text{ m sec}^{-1}$  or less occurring at a (surprisingly) low height of 1 to 4 km above cloud base. They claimed that icing of the balloons in supercooled clouds had an insignificant effect on their results. Marwitz (1972, 1973) and Grandia (1973) experimented with aircraft-dispersed chaff released below cloud base and obtained similar profiles in some cases. In other cases, their data show vertical velocity profiles with nearly zero slope near the top of the radar weak echo region. Since no decrease was indicated before the chaff was lost in high reflectivity above the weak echo region<sup>2</sup>, their conclusion that the maximum was attained in all cases is contestable. Calculations based on an assumed liquid water concentration of  $2 \text{ gm m}^{-3}$  show that ice accumulating on the chaff should not affect the results significantly during the first 5 min of ascent above the freezing level. Marwitz's data also show the vertical velocity in an updraft steadily decreasing with time, with the maximum reduced from  $27 \text{ m sec}^{-1}$  to  $19 \text{ m sec}^{-1}$  in 30 min.

---

<sup>2</sup>Radar weak echo regions mark strong updrafts at low and midlevels (Browning, 1964).

Hart and Cooper (1968) used radar-tracked superpressure balloons with a 1.2 km float altitude and a bursting altitude of 3.7 km to study thunderstorm inflow. One balloon package was carried up to 10.4<sub>1</sub> km in a storm. Allowing an instrument package fall velocity of 10 m sec<sup>-1</sup> after the balloon burst, they calculated a maximum updraft speed of 26 m sec<sup>-1</sup> at 7 km above ground. Vertical velocities below cloud base of 2.5 to 4 m sec<sup>-1</sup> (but occasionally as high as 10 m sec<sup>-1</sup>) were measured by the delivery aircraft. Auer and Sand (1966) found similar subcloud vertical velocities (4 to 6 m sec<sup>-1</sup>) and also noted that the updrafts were "smooth" at these levels.

Marwitz (1973) and Grandia (1973) determined from aircraft measurements that updraft air at cloud base often has a virtual temperature deficit of 2C and must be rising under the influence of perturbation pressure gradient forces (since the buoyancy force is downward). The updraft air originated from near the surface. Marwitz et al. (1970) had previously found that subcloud air is not well mixed.

#### 1.1.2 Pressure Measurements

The pressure field in and around a thunderstorm is impossible to measure (except at the surface) with present technology. The hydrostatic assumption is invalid so that pressure and height have to be measured independently. The uncertainties in height measurements are large enough to mask up to 5 mb horizontal pressure differences between updraft and environment.

#### 1.1.3 Liquid Water Contents

Measured liquid water contents as high as 40 g m<sup>-3</sup> in the upper parts of thunderstorms have been reported by Kyle and Sand (1973) and Roys and Kessler (1966). Such large liquid water concentrations must be suspended in updrafts.

#### 1.1.4 Horizontal Wind Measurements

In an environment with vertical wind shear, rising air should tend to partially conserve its horizontal momentum (so that the updraft should have lower horizontal wind shear than the environment), but it is also subject to forces of interaction with the environment such as form drag (Bates, 1961; Newton, 1966) and Magnus force (Fujita and Grandoso, 1968). In addition, the winds in the updraft are affected by entrainment (Warner, 1972) and may acquire significant rotational components through local stretching of vortex tubes. In Fankhauser's (1971) model<sup>3</sup> of a Great Plains cumulonimbus, the inflow is on the right-forward flank<sup>3</sup> of the storm, and a rotating updraft rises with an upshear slope. The vertical slope of echo-weak vaults (Browning, 1964) and the locations of the highest tops are evidence for this configuration.

Superpressure balloon trajectories (Hart and Cooper, 1968) showed that updrafts have nearly horizontal low-level inflows and nearly vertical slopes

<sup>3</sup>However, some storms have updrafts on the right-rear flank.

at midlevels. Marwitz (1973) observed from chaff trajectories that the velocity vector within the weak echo region of some (but not all) storms is constant with height and time. Marwitz also computed updraft slopes but apparently failed to correct for storm motion.

### 1.1.5 Summary

Updrafts may be warmer than their environments by 10C or more at upper levels and may contain large quantities of suspended liquid water (30 to 40 g m<sup>-3</sup>). We know that strong updrafts have peak vertical velocities of 25 m sec<sup>-1</sup> or more, although disagreement on the location of the maximum has not been resolved. Perhaps the maximum is high in the cloud during vigorous new convective growth and descends as (and if) an updraft becomes progressively more water-loaded. We need to know more about the shape, size, tilt, evolution, propagation, and rotation of updrafts and about how these factors vary in different environments. More detailed measurements are required before satisfactory parameterizations of the turbulence and microphysics can be devised for numerical cloud models.

## 1.2 History of Updraft Soundings

Inevitably, a few rawinsoundings sample thunderstorm updrafts. McComb and Beebe (1956) described one such updraft sounding (fig. 1) where the balloon ascended at 14.1 m sec<sup>-1</sup> between 604 and 436 mb. The first part of this rapid ascent was pseudo-adiabatic; then a sharp increase in temperature occurred just above the freezing level. The lapse rate was markedly superadiabatic as the balloon exited this updraft. McComb and Beebe made a plea that all updraft soundings be brought to the attention of the Severe Local Storms Forecast Center, and that the ascent rates in particular be saved. However, this work was not pursued.

Mesonetwork rawinsonde soundings taken by the National Severe Storms Laboratory (NSSL) in southwestern Oklahoma since 1966 have been processed and recorded on magnetic tape (Barnes et al., 1971). In 1970 and 1971 special effort was made to obtain in-storm soundings. A search through this archived data (over four thousand soundings) revealed 34 soundings in which the balloons

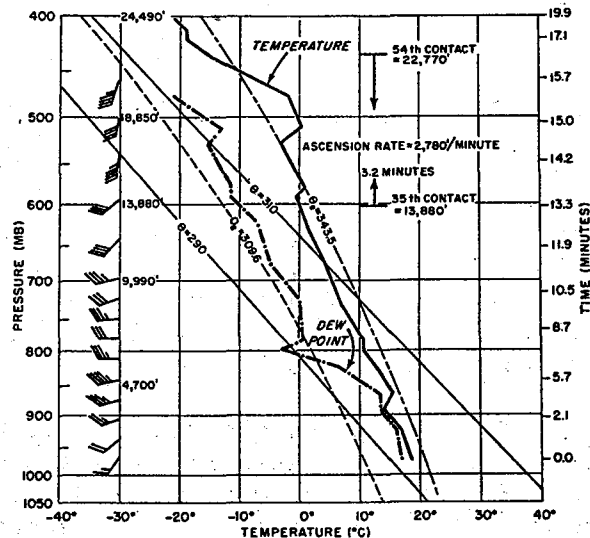


Figure 1. Updraft sounding taken at Columbia, Mo., at 0237 CST, October 14, 1954. Wind speeds to the nearest 5 knots (half barbs) and directions to the nearest 10° for the standard levels are shown on the left. Time after release is shown on the right (from McComb and Beebe, 1956).

rose  $5 \text{ m sec}^{-1}$  faster than the ascent rate in "still" air over vertical distances greater than 1 km. One of these soundings (Dibble, 24 May 1968, 1700 CST) has already been discussed by Barnes (1970, Davies-Jones and Ward (1971), and Barnes (1971). Henderson (1971, 1972) used two updraft soundings in his analysis of a thunderstorm that moved through the network on 29 April 1970.

This present work is an in-depth report on the properties of NSSL updraft soundings.

### 1.3 Instrument Limitations

Since standard rawinsondes are not designed for release into severe thunderstorms, possible instrument errors must be identified. Washout of the humidity element undoubtedly occurred on some of the runs. Flow through the humidity duct may also have been restricted. Inaccuracies in the temperature data are likely because the element is unshielded and subject to wetting and icing (Byers and Braham, 1949, p. 28). When the element is completely wet, it records the wet-bulb temperature or the water temperature. Note that the temperature of large water drops may be significantly different from the local air temperature (Caplan, 1966). Above the melting level, undercooled water freezes on contact with the element, giving spurious indications not easily identified (Barnes, 1970). The temperature of undercooled water must rise to  $0^{\circ}\text{C}$  before freezing, since a water-ice mixed phase can exist only at this temperature (Byers, 1965, p. 27). Element icing could account for the sharp temperature increases in figure 1. Ice accumulation probably increases the element's thermal lag greatly above the freezing level. Under non-icing conditions, lag errors are believed small even at these unusually fast ascent rates since the elements and circuitry are essentially the same as tested for dropsondes with fall speeds of  $25 \text{ m sec}^{-1}$  (Severin, 1971). Temperature errors can also be caused by moisture shunting some vulnerable component in the temperature circuit (Hodge and Harmantas, 1965). Other relevant sources of error are poor recorder sensitivity, baselining inaccuracies and calibration errors. Errors in horizontal wind velocities should be negligible owing to the high elevation angles of rapidly ascending balloons.

To compute updraft velocities, we must first assume that heights can be calculated hydrostatically from the data. Tests show that updraft profiles and buoyancy forces were changed insignificantly by applying the "dynamic" corrections described by Davies-Jones and Ward (1971). Also, to compute true hydrostatic heights, we need to know the surface pressure and the profile of virtual temperature over the station at a single instant of time. Since balloons have a finite ascent rate and travel horizontally as well as vertically, the computed hydrostatic heights are a function of balloon trajectory in cases where large horizontal gradients of virtual temperature exist. Thus, errors in updraft soundings may arise from updraft tilt, from entrainment of the balloon into the updraft above its base, or from the presence of a steep pseudo-cold front with a deep layer of cold air outflow behind. These are not serious sources of error in the updraft profile but

suggest (when combined with the "dynamic" corrections) that measured hydrostatic pressure differences of 5 mb or less between updraft and environment do not necessarily imply actual pressure differences (Davies-Jones and Ward, 1971; Barnes, 1970, 1971).

Second, we must assume that the balloons ascend at a constant rate,  $w_B$ , with respect to the air. Since balloons rise at nearly constant rates below 10 km under stable conditions, the assumption is reasonable provided that the balloons do not accumulate large masses of water or ice, are not beaten down by falling precipitation, and do not change shape appreciably. Since the balloons were over-inflated and their lift was not measured<sup>4</sup>,  $w_B$  was assumed to be the average velocity between the surface ( $\sim 350$  m MSL) and 900 m MSL. In some cases balloons burst prematurely. Tracking falling balloon packages indicated terminal velocities of 15 to 20 m sec<sup>-1</sup>. Strong updrafts could carry packages higher after a balloon burst, but since no sudden decreases of 15 to 20 m sec<sup>-1</sup> in vertical velocity (without corresponding changes in temperature) occurred, we assumed that the balloons burst at their apogees.

We conclude that although the data may be questionable in heavy precipitation regions, they warrant investigation because better quality data are unavailable.

## 2. CHARACTERISTICS OF INDIVIDUAL UPDRAFTS

In this section an objective definition of updraft sounding is made. We then discuss the optimum choice of a sounding representative of the storms' environment. Examination of radar data and weather charts reveals the types of storms and synoptic scale environments under investigation. The positions of updrafts relative to radar echoes are described, and some general observations on the soundings are made. Individual sounding data, updraft vertical velocity profiles, radar, cloud and weather observations, and synoptic situations are contained in appendix A.

### 2.1 The NSSL Upper Air Networks

The 1966 to 1973 NSSL upper air networks and operations are summarized in table 1. In 1966 and 1967 the average station spacing was 85 km and several soundings were taken at fixed observation times (every 90 min) on days favorable for severe weather. In 1968 the station spacing was reduced by over 50% to obtain soundings closer to storms, and the time differential between ascents was reduced to 60 min. The 1969 and 1970 networks with further reduction in spacing and flexible release schedules were designed to provide even more in- and near-storm data. Operations in 1971 through 1973 were greatly curtailed with only three stations taking observations. In 1970 and 1971 updraft soundings were obtained by design by releasing the

<sup>4</sup>Balloons were filled to a volume necessary to produce a 4 to 7 m sec<sup>-1</sup> ascent.

Table 1. Summary of Rawinsonde Networks and Operations 1966 - 1973

YEAR	PERIOD OF OPERATION	AREA BOUNDED BY NETWORK (km <sup>2</sup> )	NUMBER OF STATIONS	AVERAGE STATION SPACING (km)	TIME BETWEEN SERIAL SOUNDINGS (min)	NORMAL TERMINATION PRESSURE (mb)	NUMBER OF SOUNDINGS
1966	Apr 1 - Jun 15	31000	11	85	90	100	1274
1967	Apr 15 - Jun 15	26000	10	85	90	100	965
1968	Apr 22 - May 31	5300	10*	39	60	400	688
1969	Apr 21 - May 29	2700	8	30	irregular	400	482
1970	Apr 5 - May 31	2900	9	30	irregular	400	489
1971	Apr 19 - Jun 12	1200	3	54	irregular	400 or 250	156
1972	Apr 11 - Jun 27	1200	3	54	irregular	400 or 100	45
1973	Apr 21 - Jun 4	1200	3	54	irregular	100 or 400	81

\*Two stations had dual instrumentation

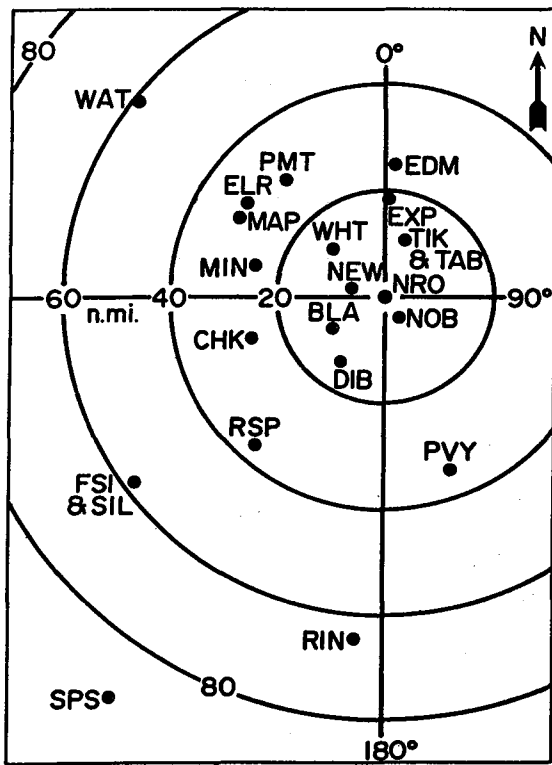


Figure 2. Map showing positions relative to the NSSL radar (NRO) of upper air stations mentioned in this report. Range marks are at 20 n mi (37 km) intervals.

balloon immediately after passage of the wind-shift line (this is generally before the onset of rain). This maneuver was aided by direct radio communication between the radar site and the raob station. Annual network maps are given by Barnes et al. (1971) and Nelson (1973). Figure 2 is a composite map showing the position relative to the NSSL radar (which is at Norman, Oklahoma) of those stations mentioned in this report.

## 2.2 Selection of Updraft and Environment Soundings

In a prior study, Davies-Jones and Henderson (1973) studied the properties of 33 updraft soundings. A more objective search in the same data archive resulted in five original updraft soundings being discarded and six being added. (Some environment soundings were also changed.)

Updraft soundings were located objectively as follows. In each sounding the vertical velocity ( $m \text{ sec}^{-1}$ ) of the air,  $w(z)$ , at height  $z$  (m MSL) is computed from the interpolated data (tabulated every 150 m) by the formula

$$w(z) = \frac{(z+150) - (z-150)}{t(z+150) - t(z-150)} - w_B$$

where  $t(z)$  is elapsed time (sec) and  $w_B$  is the balloon ascent rate ( $m \text{ sec}^{-1}$ ) with respect to still air (computed as described in sec. 1.3). Several balloons started rising faster above 10.5 km MSL, far from any radar echoes. We assume that these accelerations were caused by changes in the balloons' aerodynamic characteristics rather than actual updrafts. Attention was therefore restricted to levels below 10.5 km where we can assume approximately constant ascent rates relative to still air. Eighty-four soundings were located in which  $w$  exceeded  $5 m \text{ sec}^{-1}$  at one level or more. Since we are interested in "sustained" updrafts, we define an updraft sounding as one in which  $w > 5 m \text{ sec}^{-1}$  for eight or more levels (not necessarily consecutive). There are 34 such soundings (see table 2 for listing and computed balloon ascent rates with respect to still air) taken on 18 different days. Eight of these soundings were obtained in a single squall-line that passed through the network on 14 May 1970. There were no updraft soundings in 1972 and 1973.

Table 2. List of Updraft and Environment Soundings, and Ascent Rate of Updraft Balloons with Respect to Still Air

CASE NO.	DATE	UPDRAFT		ENVIRONMENT		UPDRAFT $w_B$ (m sec <sup>-1</sup> )
		Station	CST	Station	CST	
1	6-05-66	WAT	1822	CHK	1830	3.6
2	6-15-66	FSI	2250	TIK	2315	7.3
3	5-05-67	TIK	1115	PVY	1057	4.5
4	5-30-67	SPS	1051	RIN	1050	7.2
5	5-30-67	RIN	1222	PVY	1230	4.5
6	5-30-67	PVY	1656	RIN	1703	4.1
7	5-30-67	RIN	1826	SPS	1832	4.1
8	5-24-68	DIB	1602	RSP	1602	3.8
9	5-24-68	DIB	1700	RSP	1602	8.2
10	5-31-68	NEW	1706	DIB	1600	4.5
11	5-31-68	SIL	1744	FSI	1700	1.4
14	4-26-69	EXP	1651	NRO	1613	6.3
13	5-06-69	NRO	1512	BLA	1510	5.4
14	5-07-69	ELR	2135	MIN	2107	5.6
15	4-16-70	ELR	1026	MIN	1002	5.4
16	4-23-70	NOB	1502	BLA	1503	5.2
17	4-29-70	CHK	2134	BLA	2101	5.0
18	4-29-70	WHT	2233	NOB	2247	5.5
19	4-29-70	TAB	2242	NOB	2247	6.7
20	4-29-70	TAB	2341	NOB	2338	6.9
21	5-14-70	PMT	1810	WHT	1756	5.5
22	5-14-70	ELR	1846	CHK	1831	3.2
23	5-14-70	WHT	1916	BLA	1913	6.9
24	5-14-70	CHK	1945	NOB	1920	5.8
25	5-14-70	TAB	2009	NOB	1958	5.6
26	5-14-70	CHK	2010	NOB	1958	6.3
27	5-14-70	BLA	2011	NOB	1958	7.1
28	5-14-70	WHT	2024	NOB	1958	3.3
29	5-29-70	TAB	1441	CHK	1445	7.2
30	6-02-71	EDM	2118	NRO	2119	7.0
31	6-07-71	MAP	1945	NRO	1932	4.0
32	6-10-71	EDM	2211	EDM	2100	5.7
33	6-10-71	NRO	2225	NRO	2115	5.6
34	6-12-71	MAP	1358	EDM	1348	5.2

Soundings representative of the storms' environments, listed in table 2, were chosen, after careful examination of surface charts and radar film, to meet the following criteria whenever possible. They should be close in time and space to the updraft soundings. They should be released on the low-level inflow side of the storm into the unstable air masses in which the storms are embedded. The environment soundings should also be outside convective regions. Obviously, not all these requirements could be met in every case. For instance, in case 2 (see appendix A) the only available environment sounding was 90 km behind the squall line. Also, on days of widespread convection it was not always possible to pick an environment sounding outside regions of convection. In two cases (Nos. 7, 12) rain was falling and in two others (5, 10) thunder was heard at release time.

### 2.3 Synoptic Locations of Storms

The synoptic locations of each storm are given in appendix A. Thirty of the 34 storms were embedded in mT air masses at the surface. The other four storms formed in mP air; two of these cases were overrunning situations. Several different types of thunderstorms were present. However, the majority (23) were either cold-frontal (15) or in the class which forms in deepening low pressure areas without obvious fronts present (8). Others were pre-frontal (2, one with an associated bubble high), stationary frontal (3), overrunning (2), and air mass (2). The remaining two were difficult to classify; one was northwest of a stationary front, the other in a weak surface low.

### 2.4 Description of Soundings

For each updraft-environment pair, appendix A contains Stüve diagrams, potential wet-bulb temperature ( $\theta_w$ ), saturated potential wet-bulb temperature ( $\theta_w^s$ , defined as  $\theta_w$  with assumed relative humidity of 100%), updraft vertical velocity, and excess virtual temperature profiles. Some updraft balloons floated or burst. Descending portions of soundings were discarded. In cases where balloons descended briefly and then re-ascended (e.g., Nos. 19 and 31) the data were accepted again when the balloon passed its previous high point. This procedure was adopted so that each variable is a single valued function of height. In this section we make some general observations of the sounding set; statistical results are discussed later.

#### 2.4.1 Environment Soundings

A number of stability indices were computed from the 850 and 500 mb data<sup>5</sup> to show that the environments are almost without exception potentially, conditionally, and latently unstable and capable of sustaining thunderstorms. Two unusual indices were defined, the potential wet-bulb index,  $\theta_w^s(500) - \theta_w(850)$ , and the saturated potential wet-bulb index,  $\theta_w^s(500) - \theta_w^s(850)$ . Negative values indicate that the 850-500 mb layer is potentially ( $\partial\theta_w^s/\partial z < 0$ ) and conditionally ( $\partial\theta_w/\partial z < 0$ ) unstable. Table 3 shows that all the soundings are conditionally unstable, and all but one are potentially unstable. The

<sup>5</sup>The Lifted Index actually uses mean values in the lowest 0.9 km rather than 850 mb values. No correction for surface heating (as applied by SELS to the 12Z soundings) was made.

Table 3. Stability Index Values for Environmental Soundings. The Units of All These Indices Apart from the SWEAT Index Are Degrees Centigrade.

CASE(S)	DATE	STATION	CST	$\theta_w(500)$ $-\theta_w(850)$	$\theta_s(500)$ $-\theta_s(850)$	SHOWALTER INDEX	LIFTED INDEX	CROSS TOTALS	VERTICAL TOTALS	TOTAL TOTALS	SWEAT INDEX
1	6-05-66	CHK	1830	-5.7	-7.9	-3.5	-3.6	22	31	53	412
2	6-15-66	TIK	2315	-4.8	-9.4	-7.2	-7.7	26	34	61	236
3	5-05-67	PVY	1057	+0.4	-2.5	+4.6	-0.8	16	26	43	271
4	5-30-67	RIN	1050	-3.5	-5.4	-3.1	-5.4	24	30	54	270
5	5-30-67	PVY	1230	-4.2	-4.1	-5.9	-5.9	28	28	56	313
6	5-30-67	RIN	1703	-1.6	-4.7	+0.3	-3.4	20	29	49	344
7	5-30-67	SPS	1832	-1.6	-1.5	-0.3	-0.4	23	24	47	247
8-9	5-24-68	RSP	1602	-7.5	-5.3	-5.6	-6.4	26	29	55	379
10	5-31-68	DIB	1600	-1.7	-6.5	-0.9	-4.0	20	31	51	297
11	5-31-68	FSI	1700	-3.0	-2.7	-2.7	-3.0	25	25	50	370
12	4-26-69	NRO	1613	-3.2	-3.0	-4.3	-4.5	27	28	55	413
13	5-06-69	BLA	1510	-0.2	-2.6	-0.4	-0.9	23	25	48	204
14	5-07-69	MIN	2107	X	X	X	X	X	X	X	X
15	4-16-70	MIN	1002	-1.9	-2.6	-2.0	-3.4	26	28	54	338
16	4-23-70	BLA	1503	-4.6	-3.8	-3.6	-3.7	25	28	53	282
17	4-29-70	BLA	2101	-0.3	-6.6	-4.8	-6.4	26	31	56	279
18-19	4-29-70	NOB	2247	-4.6	-3.5	-3.9	-5.3	25	26	51	520
20	4-29-70	NOB	2338	-5.7	-3.8	-5.6	-5.9	27	27	54	577
21	5-14-70	WHT	1756	-3.9	-4.6	-1.5	-3.4	23	28	51	308
22	5-14-70	CHK	1831	-4.8	-5.1	-3.3	-4.6	24	29	54	381
23	5-14-70	BLA	1913	-2.6	-4.0	-1.9	-3.1	23	28	51	254
24	5-14-70	NOB	1920	-4.8	-4.7	-3.7	-4.6	25	29	54	328
25-28	5-14-70	NOB	1958	-4.4	-3.0	-2.3	-2.9	24	26	50	231
29	5-29-70	CHK	1445	-2.4	-5.1	+1.0	-0.9	19	28	47	X
30	6-02-71	NRO	2119	-6.3	-7.1	-7.6	-8.9	28	31	59	635
31	6-07-71	NRO	1932	-4.8	-9.4	-5.5	-8.6	24	34	58	517
32	6-10-71	EDM	2100	-4.0	-5.9	-3.3	-4.4	24	29	53	339
33	6-10-71	NRO	2115	-4.2	-6.0	-3.8	-5.3	24	29	53	350
34	6-12-71	EDM	1348	-4.9	-5.0	-1.9	-4.7	22	28	50	292

Threshold Values For

light to moderate thunderstorms	<0	<0	>18	>26	>44	
severe thunderstorms	<-3	<-3	>24	>26	>50	>300
tornadoes	<-6	<-6	>26	>26	>52	>400

X Missing Data

values of more familiar stability indices, also given in table 3, indicate environments favorable for thunderstorms and, in many cases, for severe thunderstorms. Many soundings have a pronounced dry over moist stratum as in the type I sounding (Fawbush and Miller, 1954); however, since they are so close to the storms, low-level inversions are either weak (cases 1, 3-4, 15-16, 18-19, 30, 32-33) or nonexistent. In many cases, a one-dimensional cloud model would not predict thunderstorms from the environment soundings because the level of free convection (LFC) is a considerable distance above cloud base. Presumably, perturbation pressure gradient forces, neglected by one-dimensional models, play a critical role in atmospheric convection.

#### 2.4.2 Updraft Soundings

Updraft soundings generally have a complicated structure, probably due to strong horizontal gradients and turbulence in the storms and to instrumental errors caused by harsh measuring conditions (precipitation, turbulence, unusually fast ascent rates, icing). Unfortunately, it is often impossible to separate atmospheric fine structure from the instrumental noise.

A common feature of soundings in saturated updrafts is a sudden warming from around  $-3^{\circ}\text{C}$  to near  $0^{\circ}\text{C}$  (e.g., cases 4, 5, 7, 10 to 11, 15 to 24, 26, 30, 34). As explained in section 1.3, this is evidence that supercooled water is freezing on the thermistor. In other cases (e.g., 1, 3, 9, 25, 27-29, 31-33), a similar feature is present, but either the temperature does not recover fully to  $0^{\circ}\text{C}$  or the whole effect occurs at a few degrees above freezing. Either the baseline calibration was inaccurate in these cases or some other effect occurred. Just above the level where all the undercooled water on the element has frozen, the recorded temperature drops sharply and often the apparent lapse rate is markedly superadiabatic. Superadiabatic lapse rates are also indicated where the balloons pass out of updraft cores through regions of strong horizontal gradients (e.g., cases 5-7, 10, 18, 23, 25-26, 34) or, due partly to the wet-bulb effect (Hodge, 1958), where the radiosondes exit clouds (e.g., cases 3, 8, 21, 32).

Pseudo-adiabatic lapse rates are observed immediately above updraft condensation levels in several cases (e.g., 1-6, 8-9, 11-12, 16-18, 21, 27-28, 31-32). Above the pseudo-adiabatic layer, the updraft temperature profile frequently becomes very jagged; this perhaps is caused by instrumental effects, passage of the balloon package out of the updraft core into the surrounding turbulent sheath, or turbulent breakdown of the updraft.

In all cases, the maximum vertical velocity peaks below 7 km MSL. However, this result may be strongly affected by ice formation on the flight train and by the buoyant balloon's tendency to rise out of tilted updrafts. The height of maximum vertical velocity no doubt depends on the storm's maturity and updraft tilt. Henderson (1972) showed, using radar data, that the low height (3 km MSL) of the peak vertical velocity in case 18 is due to heavy water loading of an almost vertical updraft. His conclusion is substantiated by high surface rainfall rates.

A rising parcel's vertical velocity depends on the net vertical impulse produced by the buoyancy, liquid water loading, drag, and perturbation

pressure gradient forces acting throughout its ascent. Hence, even if balloons describe parcel trajectories, simple correlations between vertical velocity and excess virtual temperature should not be expected. However, in several soundings, balloons do accelerate as the relative warmth of the local air increases. Other soundings are difficult to interpret; in fact, some exhibit buoyancy incapable of sustaining the observed updrafts. This could be due to the environment sounding poorly representing the close environment. Many updrafts are colder than their environment at low levels, and warmer at mid- and upper levels. In two cases (3, 30), there are significant rising motions in the cold air outflow of intense squall lines.

Above cloud base, the measured relative humidities in updrafts are generally very close to 100%, indicating that the updrafts are saturated. In a few cases (e.g., 22), the dewpoint and temperature curves are so strikingly similar that one suspects that the recorded dewpoint depression is not real but is due to bad baselining or washout of the carbon element. The dryness of the updrafts in cases 12 and 20 are highly questionable on physical grounds because the associated lapse rates are subadiabatic.

In general, the updraft winds have lower vector wind shears than the environment and are more southerly because of the tendency for low-level momentum to be conserved in rising air. In six cases (4, 18, 25, 27, 28, 30) the updraft winds have an easterly component through considerable depths (300 mb or more). Since all 34 storms had an eastward component of motion, we conclude that in at least these six cases the updraft tilted westward with height.<sup>6</sup> Note that conceptual thunderstorm models (e.g., Fankhauser, 1971) have updrafts that tilt in the upwind direction from low levels and then recurve downwind aloft.

We examine the soundings from a statistical viewpoint in section 3, and analyze the four fastest updrafts in section 4.

## 2.5 Radar Echo Descriptions

Appendix A contains NSSL WSR-57 whole-scope photographs of the radar echoes very close to the time that the updraft soundings were released. The contoured display (Wilk and Gray, 1970) reveals gray shades corresponding to different reflectivity thresholds. For each of the years 1966-71, the calibration levels and techniques were different. The radar data were best in 1970 and 1971.

The radar reports (RAREPS) from OKC (Oklahoma City, Oklahoma WSR-57) are listed in appendix A with a computer correction to position them with respect to Norman rather than OKC. These reports are used because the radar data gathered at NSSL are not amenable to analyses that reveal tops of echoes, and the intensity trend and echo configuration descriptions are not routinely reported. These RAREPS may differ in time by as much as 30 min from the NSSL

---

<sup>6</sup>No attempt was made to determine accurate storm vectors and compute winds relative to the storms.

whole scope photographs. Observing and reporting procedures are described in the Weather Radar Manual (1967).

The majority of the activity was interpreted by the OKC radar operators as TRW or TRW+. In only two instances were updraft echoes reported as TRW-, and these were new cells that eventually became more intense.

General cell movement was from the west or southwest with speeds between 5 and 20 m sec<sup>-1</sup>. No cell had an easterly component of motion. The mean speed was 13 m sec<sup>-1</sup>. Echo height ranged between 9 and 18 km with a 14 km mean. Due to the length of the data set, no effort was made to correlate tops with tropopause height, or cell motion with mean environmental winds.

Problems caused by having the radar in the observing network are illustrated by the five updrafts that were inside the radar ground pattern at observation time. Launching of radiosondes in precipitation should be avoided because the moisture causes errors like those in section 1.3. In 1970 and 1971, when a concerted effort was made to put balloons into updrafts, launches were attempted behind the gust front but ahead of the precipitation. As a result, only about one-third of the updraft balloons for these 2 years were launched in precipitation.

In most cases a visual observation at the time of launch was made. Visual observations and radar indications agrees in most cases. A photograph of the whole sky at the time of launch would have been helpful to post-analysis.

Three launches were made under severe weather conditions (U.S. Environmental Data Service, 1966, 1971). In case 1 a tornado was observed 11 km northwest of the site approximately 8 min before launch and was associated with the thunderstorm that the balloon eventually entered. In case 3 the balloon was launched into the leading edge of a line of severe thunderstorms. Approximately 5 min after launch, hail, heavy rain, and gusts to 35 m sec<sup>-1</sup> struck the launch site. Gusts of 55 m sec<sup>-1</sup> were reported in the vicinity. The instrument was destroyed by hail or lightning while it was still accelerating upward at 500 mb. Strong winds (30 m sec<sup>-1</sup>) were also associated with case 30.

The majority of the echoes in the vicinity of the observed updrafts had tight reflectivity gradients. Marwitz et al. (1972) also associated strong gradients with updraft areas. About half the echoes did not have hooks or indentations. Generally, the balloons entered on the right flank (with respect to movement) and rose through the outflow into the moist updraft. In four cases (3, 7, 8, 19) balloons were overrun aloft by the storm and entrained into an updraft. This aspect reveals complex interactions between the internal structure of the storms and the environments aloft. Two updrafts (cases 16 and 28) were at the left rear of the echo. Since the radar indicated strong updraft on the right, these cells must have had updrafts on both sides.

In four cases (21, 23, 31, 32) the balloons entered updrafts that had no associated radar echoes. We believe that these updrafts were associated with cumulus clouds that formed along the gust front of neighboring thunderstorms, and whose radar reflectivity was below the minimum detectable signal of the WSR-57. This belief might have been substantiated by sky photography.

## 2.6 Summary

Typically, the observed updrafts were associated with moderate thunderstorms that formed in baroclinic regions with mT air near the surface overlaid by dryer air aloft. Close proximity environment soundings were potentially, conditionally, and latently unstable, but generally the LFC was considerably higher than the lifted condensation level (LCL) so that the soundings were stable with respect to parcel displacement from the LCL. This casts doubt on the applicability of one-dimensional steady-state cumulus cloud models to non-airmass thunderstorm forecasting (a doubt also cast by Garrett, 1972).

The updraft soundings were complicated by atmospheric fine structure and instrumental noise. In many cases a sudden warming in recorded temperature from around  $-3\text{C}$  to  $0\text{C}$  signified onset of the freezing of undercooled water on the temperature element. Often, pseudo-adiabatic lapse rates were observed immediately above updraft condensation levels and up to the freezing level in a few cases. In at least six cases (and perhaps many more), the updraft tilted upwind with height. The updrafts were generally located in areas of tight radar reflectivity gradients at  $0^\circ$  elevation but were often not identifiable by indentations and hooks. A few updrafts were considerably ahead of radar echoes and must have been associated with cumulus convection along the leading edge of the gust front. In two cases significant rising motions were observed in the cold air outflow of intense squall lines.

## 3. STATISTICS OF UPDRAFT SOUNDINGS

### 3.1 Release Time and Points of Environment Soundings

In many cases, several soundings could have been used to represent the "environment." Whenever possible environmental soundings were picked on the low-level inflow side of the storm.

Figure 3 shows the position of the environment stations relative to the updraft stations. The mean vector position is 19 km at  $151^\circ$ . Relative release time versus distance is plotted in figure 4. The mean range of the environmental station is 43 km, and the average environmental balloon is launched 15 min before the updraft balloon. Other statistics presented in table 4 verify the close time and space proximity of the environment soundings. The above graphs and table represent surface values only. Relative times and positions change with altitude, since generally the environment balloon ascends slower than the updraft balloon and drifts further from its release site.

### 3.2 Statistics of Eight 1.2 km-Thick Layers

As discussed in section 1.3, the ascent rate of the balloon with respect to "still air" is assumed to be the average vertical velocity between the surface ( $\sim 350$  m MSL) and 900 m MSL, calculated independently for each balloon. The mean ascent rates for the updraft and environment balloons are both  $5.4 \text{ m sec}^{-1}$ ; the corresponding standard deviations are 1.5 and 0.9  $\text{m sec}^{-1}$ , respectively.

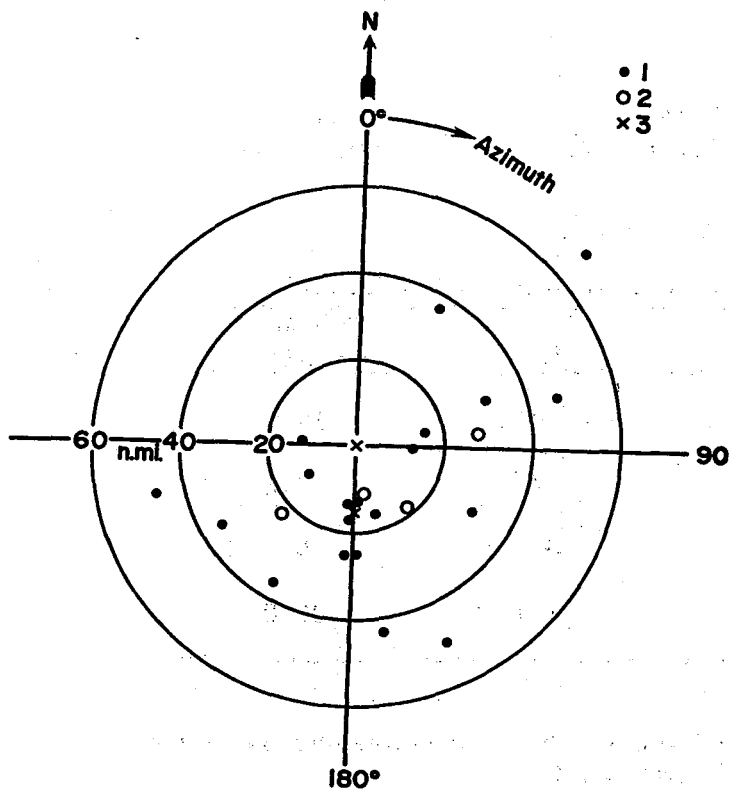


Figure 3. Position of environment stations relative to updraft stations. Single, double (2 points coincident) and triple points are denoted by  $\cdot$ ,  $\circ$ ,  $\times$ , respectively. Range marks are at 20 n mi (37 km) intervals.

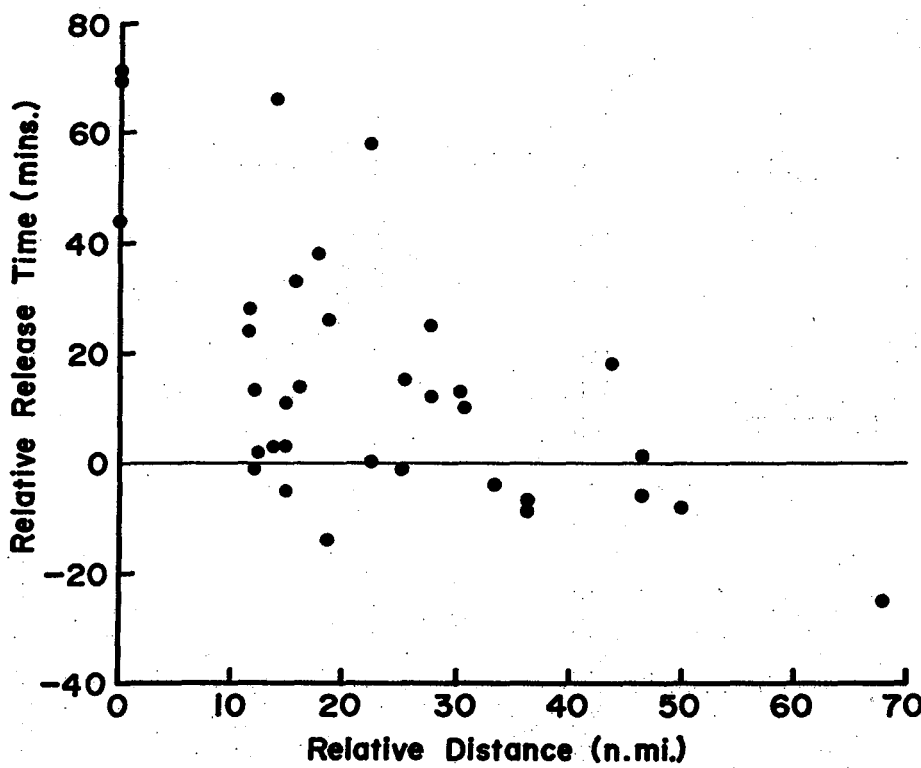


Figure 4. Relative release time versus relative distance for each pair of updraft and environment soundings. Relative release time is positive if environment sounding is taken prior to updraft sounding. To convert n mi to km multiply by 1.85.

Table 4. Statistics of Starting Times and Locations of Environmental Soundings Relative to Corresponding Updraft Soundings.

VARIABLE	MEAN	STANDARD DEVIATION	MEDIAN
Relative release time (min)	+15.3	23.9	+11.5
Relative range (km)	43.2	28.2	34.5
East distance (km)	+ 8.9	35.6	+ 0.9
North distance (km)	-16.3	32.8	-25.8

Note: Relative Release Times are Positive When Environment Balloons Are Launched Before Updraft Balloons.

We now present statistics pertaining to layer mean values in eight 1.2 km-thick layers from 0.9 km to 10.5 km. First, to illustrate notation, consider  $\theta(z)$ , the updraft saturated wet-bulb potential temperature.  $\theta(z)$  is tabulated at every interpolated level (multiples of 150 m) in each sounding. We denote by  $\bar{\theta}_s$  and  $\delta\theta_s$  the mean value and standard deviation of the interpolated data in a given 1.2 km layer of a sounding. For each such layer, the average and standard deviation of  $\bar{\theta}_s$  for all updraft soundings are called  $\bar{\theta}_w$  and  $\sigma(\bar{\theta}_w)$  and are listed in table 5, along with corresponding values for updraft vertical velocity ( $w$ ), virtual temperature excess ( $\Delta T_v$ ), wet-bulb potential temperature ( $\theta_w$ ). Also included is  $\bar{\delta\theta}_s$ , the average of  $\delta\theta$  over all the soundings. The sample size decreases with layer height because soundings terminated at different levels. Evaluation of  $\Delta T_v$  requires an environment sounding (in addition to the updraft sounding). Thus  $\Delta T_v$  can have a smaller sample size than the other variables because some environment soundings terminated in lower layers than their associated updraft soundings.

Even though no attempt was made to delete portions of soundings where the balloon was not in an updraft,  $w(z)$  and  $\Delta T_v(z)$  still have substantial maxima (8.3 m sec<sup>-1</sup> and 4.3C) at midlevels. Table 5 also shows that  $\bar{\theta}_w$  is constant within one degree over the eight layers. The increase in  $\bar{\delta\theta}_s$  from the third to the fourth level may be due to instrumental noise caused by ice forming on the temperature element (the mean freezing level in the updrafts is 4.5 km).

Scatter diagrams of  $\bar{w}$  versus  $\Delta T_v$  (for all eight layers),  $\bar{\theta}_w$  (for lowest two layers) and  $\bar{\theta}_s$  (for highest six layers), are presented in figures 5 and 6. (The reason for the switch from  $\bar{\theta}_w$  to  $\bar{\theta}_s$  is that, although  $\bar{\theta}_w$  has the advantage of being conservative for unsaturated as well as saturated adiabatic processes,  $\bar{\theta}_s$  is preferable above cloud base where it is more realistic to assume 100% relative humidity than to adopt the measured values.) The solid lines are regression lines of  $\bar{w}$  on the abscissa. The dashed envelopes describe the root-mean-squares of the  $w$  deviations about the regression lines. The correlation coefficients with 95% confidence limits are given in table 6. All the correlation coefficients are positive. However, not all correlations are statistically significant at the 5% level, namely those at upper levels where sample sizes are small and the weak correlations near the surface.

These statistics verify elementary concepts of convection in a conditionally and potentially unstable atmosphere; they confirm that for each layer, updraft speed is positively correlated with the relative warmth of the core and with  $\bar{\theta}_w$ , which is a measure of the static energy content of the air.

### 3.3 Mean Updraft and Environment Soundings

Figure 7 shows the average updraft sounding versus the average environmental sounding for all 34 storms. Mean quantities are presented only up to

<sup>7</sup> Saturated wet-bulb potential temperature is independent of mixing ratio since it is computed with an assumed relative humidity of 100%.

Table 5. Values of  $\bar{w}$ ,  $\frac{\bar{w}}{\Delta T_V}$ ,  $\bar{\theta}_s$ ,  $\bar{\theta}_w$ ,  $\frac{\delta\theta_s}{\Delta T_V}$  for each layer. Second column gives sample size for computing  $\frac{\bar{w}}{\Delta T_V}$ . This differs from the third column (sample size for other mean quantities) because in some cases the environment sounding terminated at a lower height than the updraft sounding. Values following  $\pm$  sign are standard deviations.

Layer (km)	No. of cases		$\bar{w}$ (m sec <sup>-1</sup> )	$\frac{\bar{w}}{\Delta T_V}$ (°C)	$\bar{\theta}_s$ (°C)	$\bar{\theta}_w$ (°C)	$\frac{\delta\theta_s}{\Delta T_V}$ (°C)
	$\frac{\bar{w}}{\Delta T_V}$	other means					
0.9 - 2.1	34	34	1.3±2.0	-1.1±1.9	21.8±2.2	20.3±1.8	0.7
2.1 - 3.3	34	34	3.6±3.8	0.0±1.6	20.7±1.7	19.9±1.9	0.5
3.3 - 4.5	33	33	6.6±4.2	1.4±1.6	20.2±2.0	19.4±2.2	0.4
4.5 - 5.7	32	33	8.3±5.7	4.0±2.8	20.3±2.0	19.7±2.2	0.8
5.7 - 6.9	28	29	5.1±6.3	4.3±3.7	20.3±2.3	19.7±2.5	0.7
6.9 - 8.1	7	16	3.8±5.2	1.4±2.4	20.0±2.1	19.4±2.2	0.5
8.1 - 9.3	6	9	3.0±3.8	1.9±4.3	20.4±1.8	19.9±1.9	0.3
9.3 - 10.5	6	6	0.4±1.3	0.7±1.8	19.6±0.7	19.3±0.8	0.3

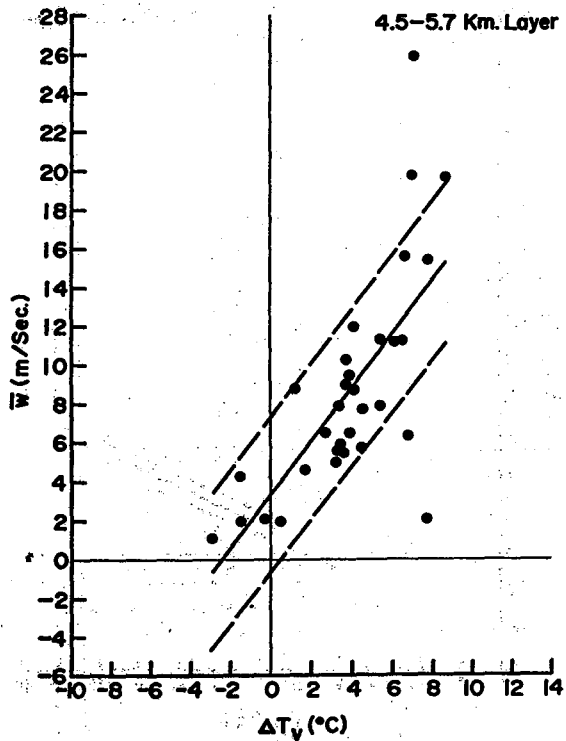
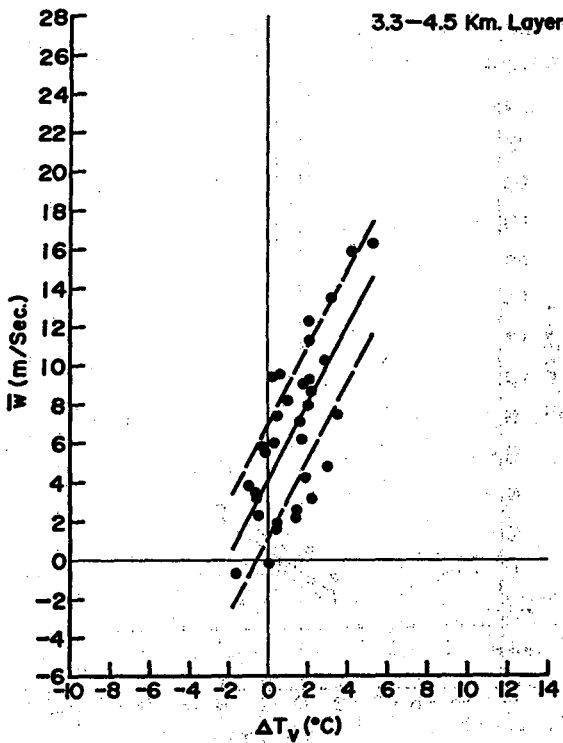
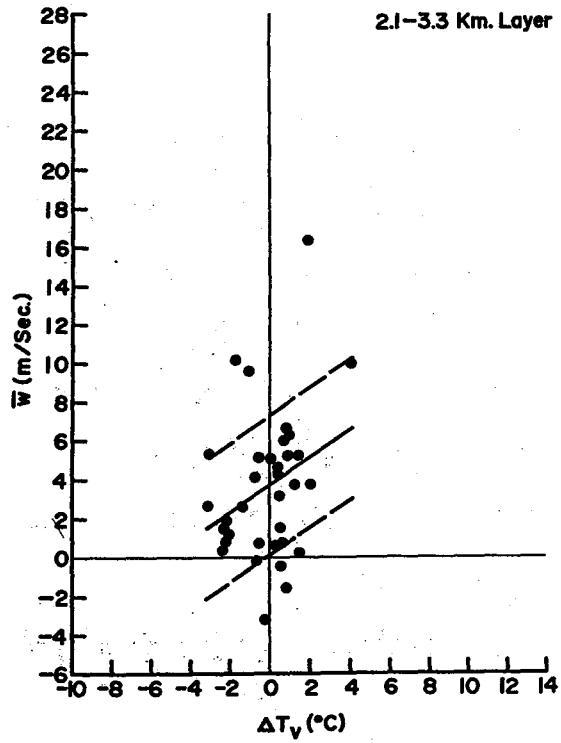
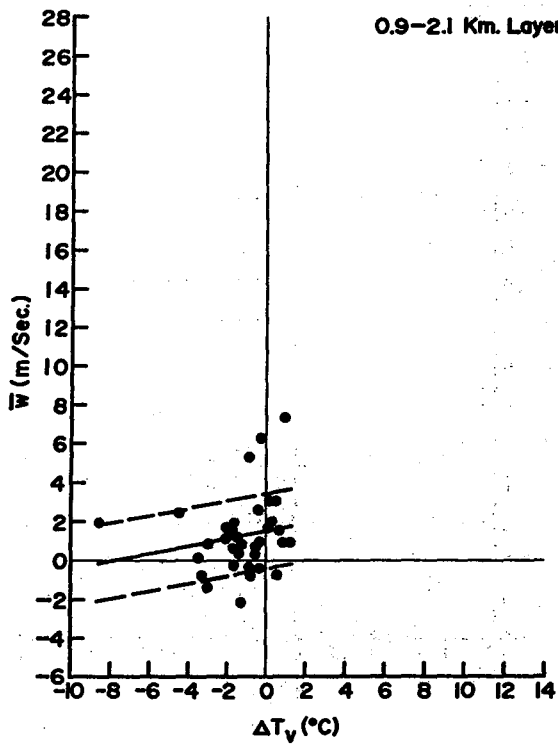


Figure 5. Scatter diagram of  $\bar{w}$  versus  $\Delta T_v$  for eight 1.2 km thick layers. The solid lines are regression lines of  $\bar{w}$  on the abscissa. The dashed envelopes describe the root-mean-squares of the  $\bar{w}$  deviations about the regression lines.

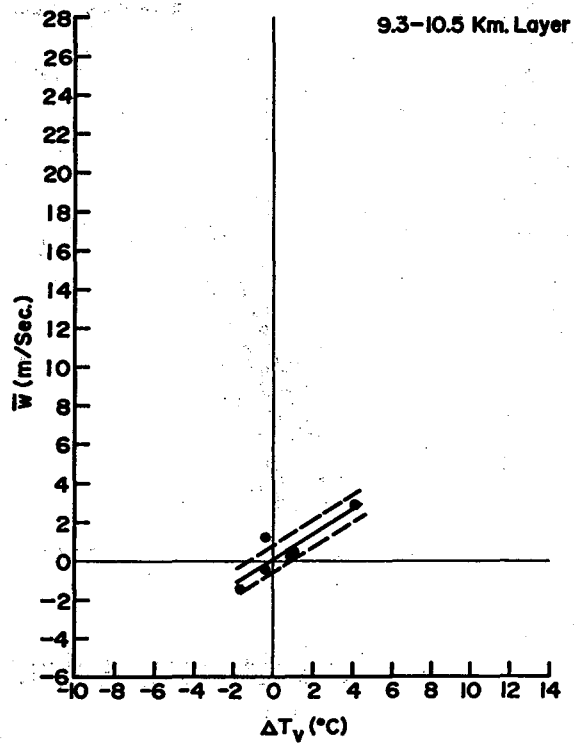
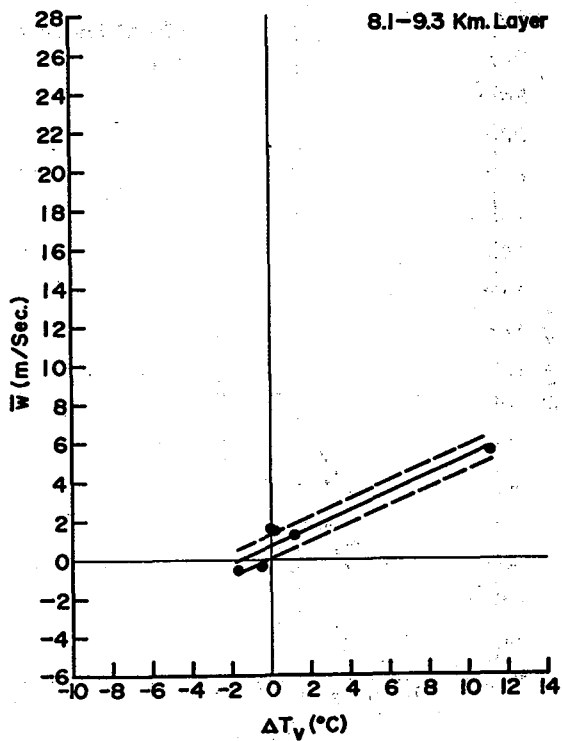
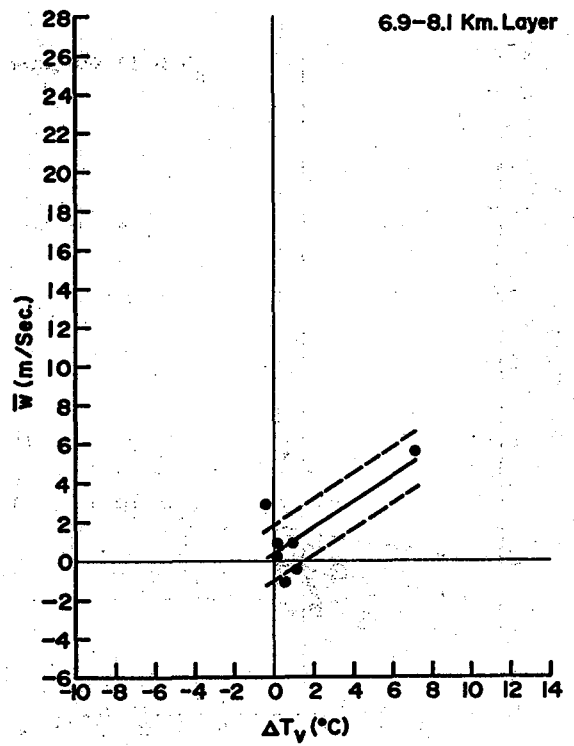
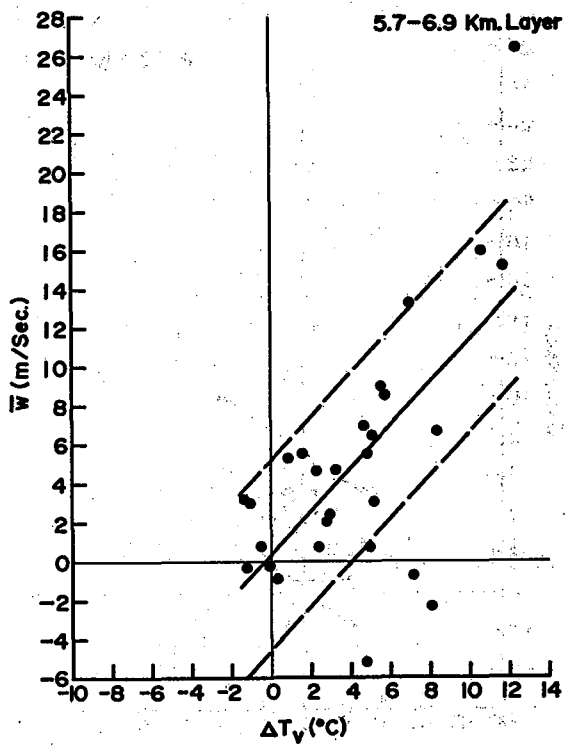


Figure 5. Continued. (continued from Figure 4) The vertical velocity  $\bar{w}$  is plotted against the vertical temperature gradient  $\Delta T_v$  for the four layers shown in Figure 4. The dashed lines represent the best fit to the data points.

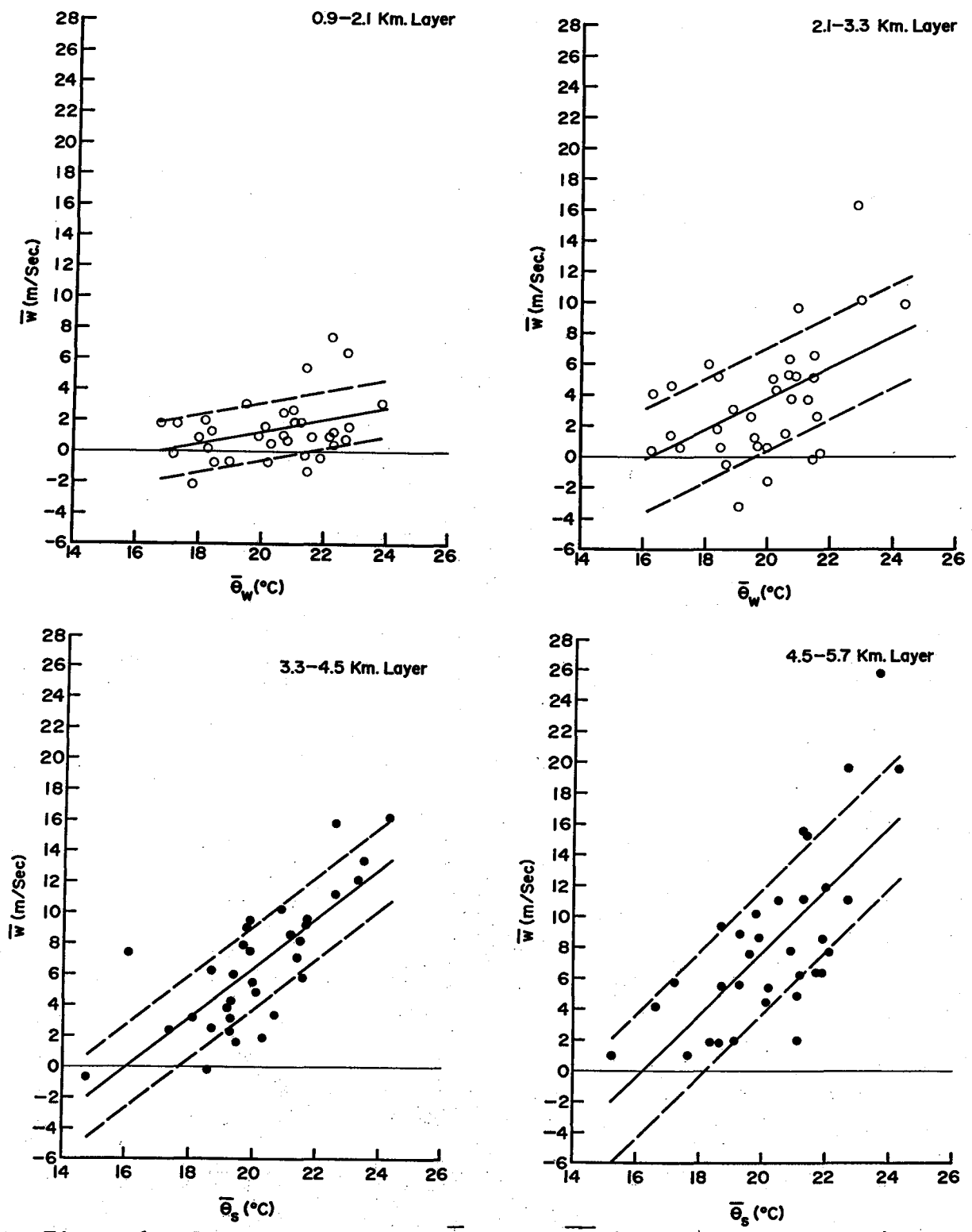


Figure 6. Scatter diagrams of  $\bar{w}$  versus  $\bar{\theta}_w$  (for lower two layers) and  $\bar{\theta}_s$  (for upper six layers). The solid lines are regression lines of  $\bar{w}$  on the abscissa. The dashed envelopes describe the root-mean-squares of the  $\bar{w}$  deviations about the regression lines.

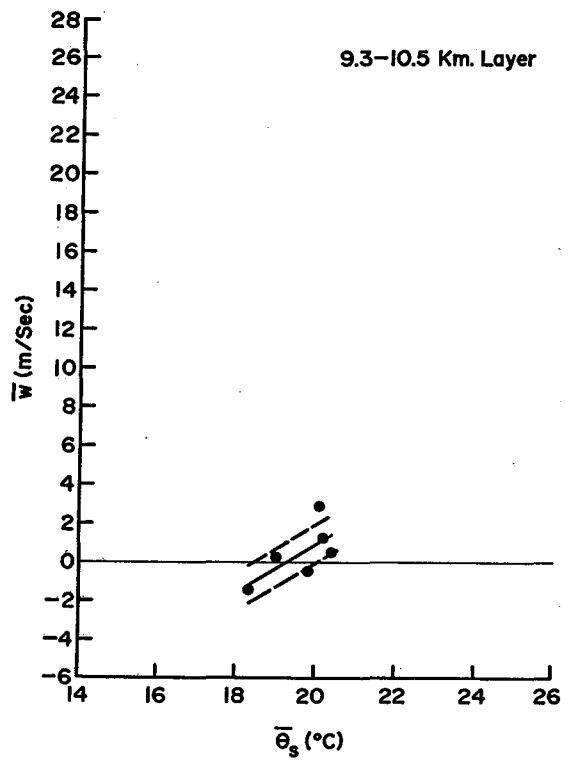
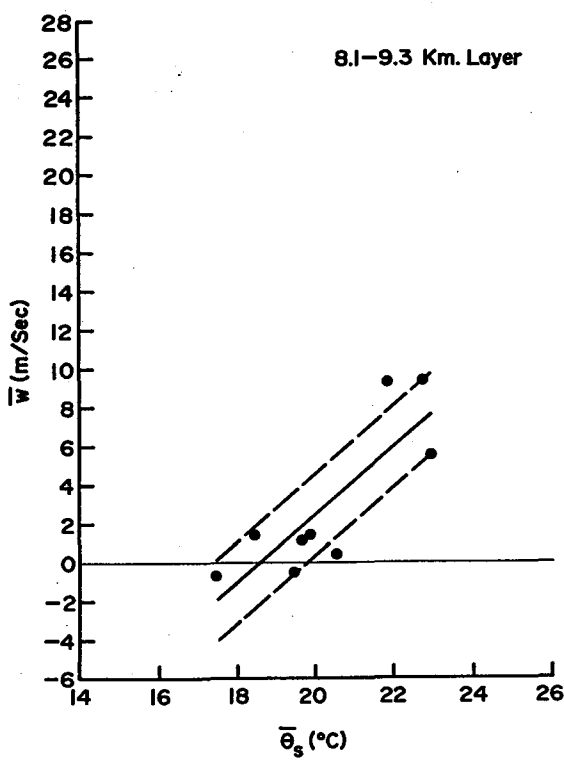
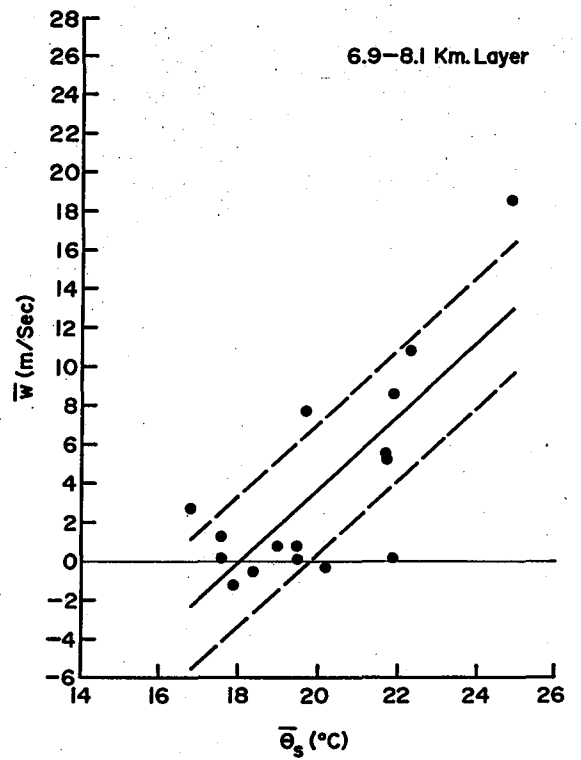
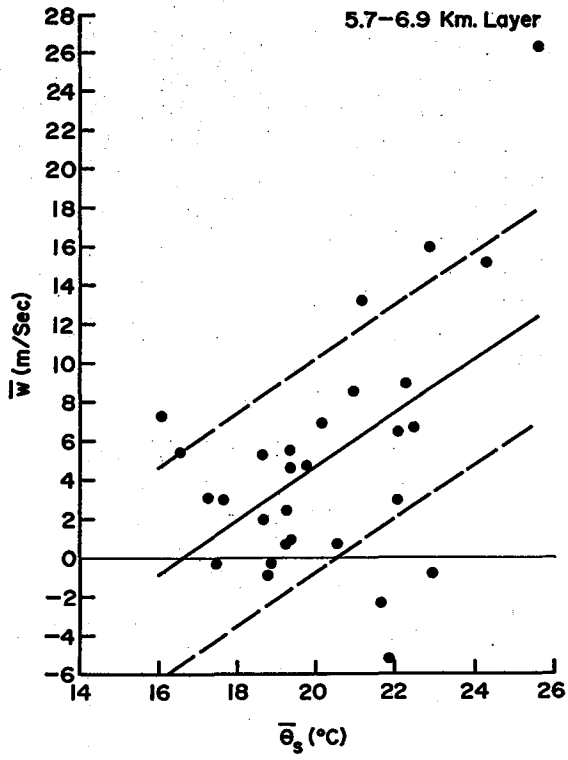


Figure 6. Continued

Table 6. Correlation coefficients between  $\bar{w}$  and  $\bar{\Delta T}_v$ ,  $\bar{\theta}_s$ ,  $\bar{\theta}_w$  for each of eight 1.2 km thick layers. Number of cases as in Table 5. In parentheses are the 95% confidence limits. At very small sample sizes, the method of computing the confidence limits breaks down (Brunk, 1965, p. 221) and the correlations may not be statistically significant at the 5% level.

Layer (km)	No. of cases		Correlation coefficient between $\bar{w}$ and		
	$\bar{\Delta T}_v$	other means	$\bar{\Delta T}_v$	$\bar{\theta}_s$	$\bar{\theta}_w$
0.9 - 2.1	34	34	0.18(-0.17,0.48)	0.27(-0.07,0.56)	0.35(0.01,0.61)
2.1 - 3.3	34	34	0.29(-0.05,0.57)	0.53(0.23,0.73)	0.50(0.20,0.72)
3.3 - 4.5	33	33	0.72(0.50,0.85)	0.77(0.57,0.88)	0.73(0.51,0.86)
4.5 - 5.7	32	33	0.69(0.45,0.84)	0.71(0.48,0.85)	0.67(0.42,0.82)
5.7 - 6.9	28	29	0.65(0.36,0.82)	0.49(0.16,0.73)	0.47(0.12,0.71)
6.9 - 8.1	7	16	0.75	0.76(0.43,0.91)	0.78(0.47,0.92)
8.1 - 9.3	6	9	0.95	0.83(0.36,0.96)	0.83(0.36,0.92)
9.3 - 10.5	6	6	0.87	0.68	0.73

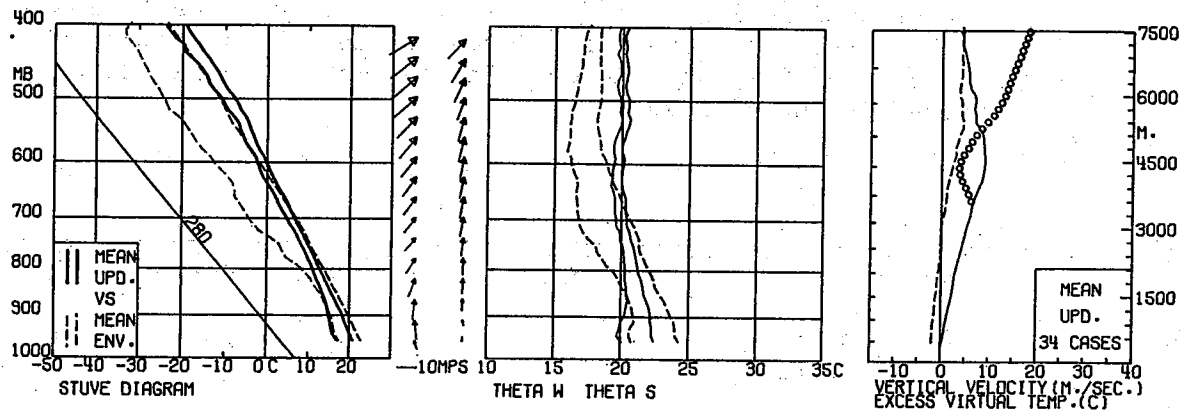


Figure 7. Mean updraft versus mean environment profiles for all 34 storms: (Left) Stüve diagram of mean updraft and environment soundings. The right solid line is the mean updraft temperature profile, the left solid line the mean updraft dewpoint profile, and the dashed lines are similar curves for the mean environment. The 280C dry adiabat is also included. Arrows denote mean horizontal wind speed (proportional to length) and direction. Height of observation is given by position of tip. Updraft winds are to the right of the environment ones. (Center) Mean profiles of  $\theta_w$  and  $\theta_s$  for updraft (both solid) and environment (both dashed).  $\theta_w$  curves are on left of corresponding  $\theta_s$  curves. Pseudo-adiabats are vertical lines on this diagram. (Right) Profiles of mean updraft vertical velocity (solid), mean excess virtual temperature (dashed) and model vertical velocity (circles).

400 mb due to a drastic reduction in sample size above that level. Environmental data above the maximum level of the corresponding updraft sounding are not included in the computations.

The environmental winds are typical for Great Plains thunderstorms, i.e., veering with height from south-southeasterly ( $5 \text{ m sec}^{-1}$ ) at the surface to west-southwesterly ( $17 \text{ m sec}^{-1}$ ) at 400 mb. The updraft winds have lower vector wind shears and more closely resemble the low-level environment; i.e., they are more southerly (except in the cold air outflow) and slower than the environment. This agrees with conceptual thunderstorm models (e.g., Fankhauser, 1971). The rapid veering of the low-level winds from northerly to southerly show that a typical updraft balloon rose through cold air outflow less than 0.5 km deep. At each level, standard deviations of east and north wind components are large ( $\sim 10 \text{ m sec}^{-1}$ ) for both the updraft and the environment soundings, indicating considerable variation between individual cases.

The average updraft sounding has a virtual temperature deficit (relative to the environment) of 2C near the surface and an excess of about 4C between 550 mb and 400 mb. The mean level of free convection (LFC), defined here as the level at which  $\Delta T^* = 0$ , is 700 mb. It is surprising that winds in the updraft layer between 900 m MSL and the LFC are southerly, and yet this layer is negatively buoyant with respect to the environment.

Below 850 mb, the updraft and environment dewpoint profiles are almost identical. Above this level, the dewpoint depression increases in the environment and decreases in the updraft sounding. However, a slight updraft dewpoint depression exists at all levels; this is caused by a combination of instrument error and not all balloons being in updrafts at all levels. The environmental lifted condensation level is 1.2 km MSL.

Figure 8 shows the average updraft and environment soundings for the seven fastest updrafts.<sup>8</sup> The low-level updraft winds back with height from north-northwesterly at the surface to south-southeasterly at 1.2 km MSL. The LFC is roughly 750 mb and virtual temperature differences are large. At the surface and 500 mb,  $\Delta T^*$  equals -3C and +8C, respectively. The environmental LCL is again 1.2 km MSL.

Figure 7 gives the mean  $\theta_w$  and  $\theta_s$  profiles for the 34 environment and updraft soundings. Between 900 and 580 mb, the environment is both potentially ( $\partial \theta_w / \partial z < 0$ ) and conditionally ( $\partial \theta_s / \partial z < 0$ ) unstable.  $\theta_w$  ranges from a maximum of 21.0C near the surface to a minimum of 15.9C at 580 mb. The average updraft profiles are much flatter (as expected since the wet-bulb potential temperature of an air parcel is conservative with respect to reversible adiabatic changes) with characteristic values of 20C. For the

<sup>8</sup>Updrafts were ordered according to average vertical velocity from the surface to 7.5 km MSL (or maximum height if the balloon did not reach this level). The average velocities exceeded  $5 \text{ m sec}^{-1}$  in each of the seven fastest cases (1,2,4,9,22,24,30; appendix A) and were less than  $4 \text{ m sec}^{-1}$  in all other cases.

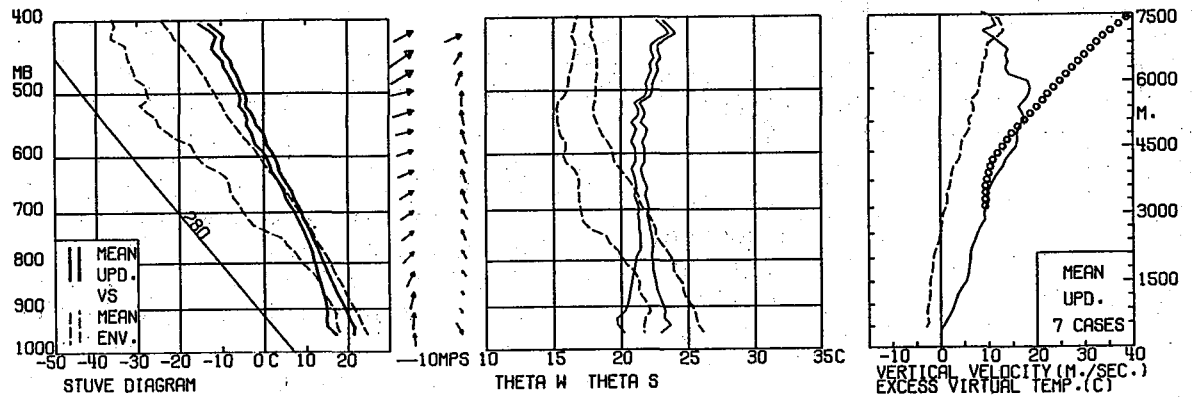


Figure 8. Same as figure 7 except for seven fastest updraft cases.

seven fastest updrafts (fig. 8), the environmental unstable layer extends to 530 mb with  $\theta_w$  ranging from 22.2 to 15.2C, and the mean updraft has  $\theta_w$  values around 21C.

### 3.4 Mean Vertical Velocity Profiles

The average vertical velocity profile for all 34 soundings is shown in figure 7. The peak on the average profile,  $9 \text{ m sec}^{-1}$ , occurs at a height ( $H_{\text{max}}$ ) of 4.8 km MSL, or 3.6 km above mean cloud base. The mean melting level for the updraft soundings is 4.35 km MSL. Since the peak velocity occurs above the freezing level, the low height of the peak may be due to balloon icing. A uniform 0.1 mm ice coating is enough to negate the lift of a rawinsonde balloon. Also, if the updrafts were tilted significantly, buoyant balloons would tend to exit at midlevels. The vertical velocity and temperature data show seven obvious cases of the balloon's coming out of the updraft (at heights between 4.5 and 7 km).

Figure 8 shows the mean velocity profile for the seven fastest updrafts. Here the peak is broader and the maximum velocity of  $19 \text{ m sec}^{-1}$  occurs at 6.15 km. This is about 5 km above mean cloud base and 1.3 km above the mean freezing level.

### 3.5 Dynamical Interpretations

At the average LFC, the average vertical velocity is  $5 \text{ m sec}^{-1}$  upward ( $7 \text{ m sec}^{-1}$  for the seven fastest updrafts). Below the LFC, perturbation pressure<sup>9</sup> gradient forces apparently sometimes force negatively buoyant air to rise. Note that in such cases the vertical perturbation pressure gradient must reverse sign at some fairly low height in the updraft, since its inclusion in one-dimensional numerical models reduces updraft velocity (Lee, 1972; Danielsen et al., 1972) and since it generally opposes the net buoyancy force in two-dimensional models (Soong and Ogura, 1973). Physically, a positive (negative) pressure perturbation at the top (base) of the updraft is required to drive the outflow (inflow).

<sup>9</sup>Perturbation pressure is sometimes referred to as non-hydrostatic pressure. This is a misnomer since the base state is the environmental (not local) hydrostatic pressure.

A simple model is used to predict mean vertical velocity above the LFC. The model is based on buoyancy and adiabatic liquid water loading terms evaluated from the mean sounding at each level (note that this is not strictly applicable since a buoyant balloon does not describe an air parcel trajectory), and on the observed mean vertical velocity at the LFC.<sup>10</sup> Above 6 km the model's vertical velocities, shown in figures 7 and 8, are considerably greater than those observed. They are probably high because the model neglects entrainment drag, adverse perturbation pressure gradient forces, and superadiabatic liquid water loading. On the other hand, the observed vertical velocities may be too low for reasons already cited in section 1.3.

### 3.6 Summary

The data set as a whole indicates that:

(a) Updrafts are warm core at mid- and upper levels.

(b) Local updraft speed is positively correlated at the 95% confidence level with local virtual temperature excess between 3.3 and 6.9 km MSL and with local potential wet-bulb temperature between 0.9 and 9.3 km MSL.

(c) In the mean, there are rising motions below the level of free convection (700 mb).

(d) Adiabatic, i.e., reversible, parcel theory predicts vertical velocities above the LFC that are higher than observed.

(e) The average vertical velocity peaks at 4.8 km MSL. However, balloon icing may be the reason greater vertical velocities generally are not observed at higher levels. The exit of a few balloons from the updraft at midlevels also contributed to this result.

(f) The average horizontal winds in the updraft and environment agree with conceptual Great Plains thunderstorm models (e.g., Fankhauser, 1971).

## 4. DISCUSSION OF MEASUREMENTS INSIDE HIGH SPEED THUNDERSTORM UPDRAFTS<sup>11</sup>

### 4.1 Introduction

The soundings from three of the four fastest updrafts exhibited moist adiabatic lapse rates with wet-bulb potential temperatures ( $\theta_w$ ) in excess of 22.5C.<sup>12</sup> In the fourth,  $\theta_w$  increased with height to values greater than 24C at midlevels. Thus, all four soundings indicated that air originating in surface layers ascends virtually undiluted (at least to midlevels) in strong updraft cores. The existence of undiluted cores has been inferred from

<sup>10</sup>The integrations were actually started just above the LFC because the water loading term prevented parcel "escape" from the LFC.

<sup>11</sup>This section appeared in Journal of Applied Meteorology, 13, 710-17.

<sup>12</sup>Based on 100% humidities in updrafts above cloud base rather than actual measured values, since the humidity element often records low at very high humidities.

analyzing observed cloud tops (Newton, 1966); however, these data probably represent the first direct observational evidence. Therefore, the four soundings are examined in detail in this paper, using a steady state one-dimensional cloud model as a diagnostic tool.

#### 4.2 Data Analysis

The temperature element is unshielded and subject to wetting and icing. Since attention in this section is restricted to below the freezing level, icing effects are not relevant. When the element is completely wetted, it records the wet-bulb temperature or the water temperature. Since high-speed updrafts are presumably saturated and probably contain relatively few large drops, both the above temperatures should, for practical purposes, be the same as the air temperature. The smooth temperature profiles observed in three of the soundings support the conclusion that moisture-induced temperature errors are slight. The humidity element is contained in a duct which makes it less vulnerable than the temperature element to impact by precipitation.

Updrafts were ordered according to average vertical velocity from the surface to 7.5 km MSL (or maximum height if the sounding did not reach this level). The average velocities for the four fastest updrafts were: Watonga (WAT), 5 June 1966, 1822 CST:  $7.6 \text{ m sec}^{-1}$ ; Fort Sill (FSI), 15 June 1966, 2250 CST:  $7.3 \text{ m sec}^{-1}$ ; Dibble (DIB), 24 May 1968, 1700 CST:  $7.7 \text{ m sec}^{-1}$ ; Edmond (EDM), 2 June 1971, 2218 CST:  $8.3 \text{ m sec}^{-1}$ . The next highest value was  $5.8 \text{ m sec}^{-1}$ .

Figures 9 through 12 show Stüve diagrams, profiles of  $\theta_w$  and  $\theta_s$  (defined as  $\theta_w$  with relative humidity set at 100%), vertical velocity profiles, and excess virtual temperature profiles. The Watonga updraft sounding (fig. 9) shows roughly dry adiabatic ascent from the surface to 760 mb, and then pseudo-adiabatic ascent (with  $\theta_w = 24\text{C}$ ) to 590 mb. Above 590 mb, the value of  $\theta_w$  oscillates wildly between 18C and 24C. These gyrations are common in updraft soundings (e.g., fig. 11). They may be (at least partly) caused by spurious instrumental effects arising from the wetting and icing of the unshielded temperature element. The environment sounding (93 km south-southeast) is fairly representative, as it would predict ascent along the 23C pseudo-adiabat above a lifted condensation level (LCL) of 787 mb. Ascent with  $\theta_w = 24\text{C}$  gives a level of free convection (LFC) of 705 mb and a temperature excess at 500 mb ( $\Delta T_{500}$ ) of +8C. The vertical velocity profile shows a fairly smooth increase with height to  $16 \text{ m sec}^{-1}$  at 550 mb and then becomes very jagged. No simple correlation exists between the jagged portions of the vertical velocity and  $\theta_w$  profiles. Even though the environment winds veered with height and showed a low-level jet of  $18 \text{ m sec}^{-1}$  from the south and winds of  $18 \text{ m sec}^{-1}$  from the west at 500 mb, the updraft balloon ascended almost vertically between 700 and 500 mb. Above 500 mb the balloon apparently was in the anvil outflow of the storm. Note that substantial updrafts ( $\sim 10 \text{ m sec}^{-1}$ ) were present in the anvil. The radar echo associated with this storm was almost motionless. The cell was the southernmost in a southwest-northeast oriented squall line, a favored location for tornadic thunderstorms. In fact, a tornado was sighted 11 km northwest of the station 8 min before the balloon was released, so that this updraft may have been rotating.

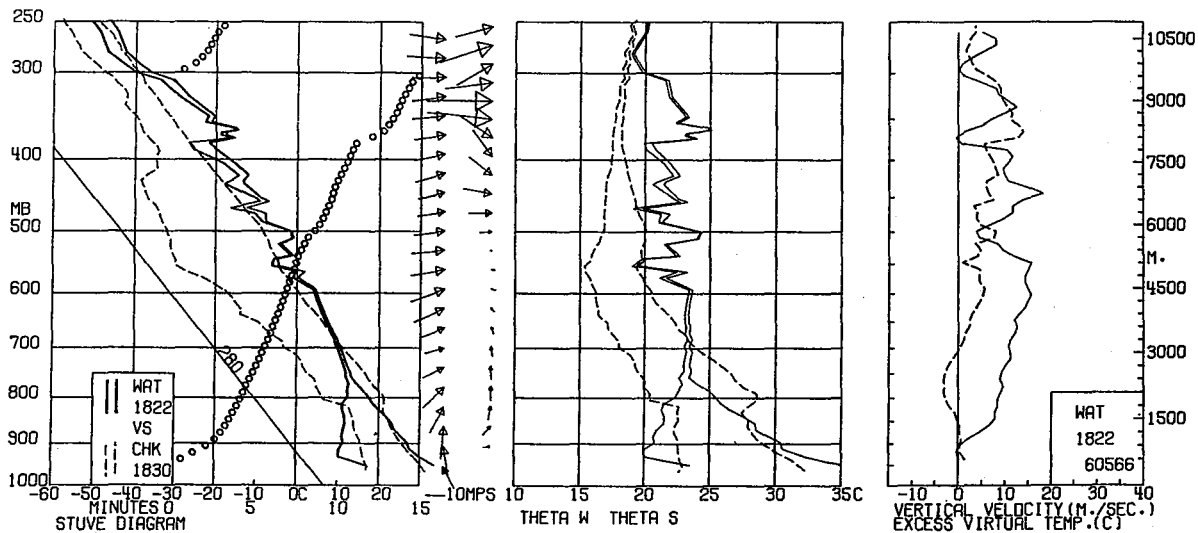


Figure 9. Watonga updraft data: Environment sounding is from Chickasha at 1830 CST: (Left) Stuve diagram of updraft and environment soundings. The right solid line is the updraft temperature profile, the left solid line the updraft dewpoint profile, and the dashed lines are similar curves for the environment. The 280C dry adiabat is also included. Circles designate elapsed time since release versus pressure and reveal balloon ascent rate; curve cycles back to zero every 15 minutes. Arrows denote horizontal wind speed (proportional to length) and direction. Height of observation is given by position of tip. Updraft winds are to the right of the environment ones. (Center) Vertical profiles of  $\theta_w$  and  $\theta_s$  for updraft (both solid) and environment (both dashed).  $\theta_w$  curves are on left of corresponding  $\theta_s$  curves. Pseudo-adiabats are vertical lines on this diagram. (Right) Updraft vertical velocity (solid) and excess virtual temperature (dashed) profiles.

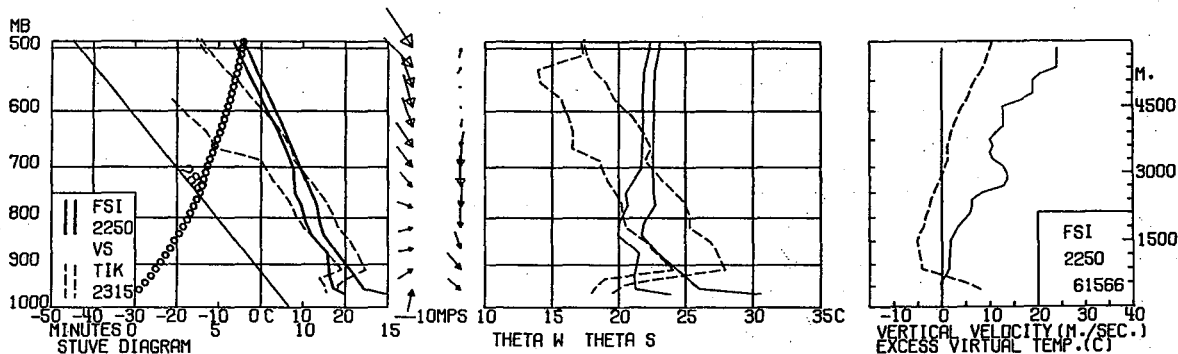


Figure 10. Same as figure 9 for Fort Sill updraft data. 'Environment' sounding is from Tinker Air Force Base at 2315 CST.

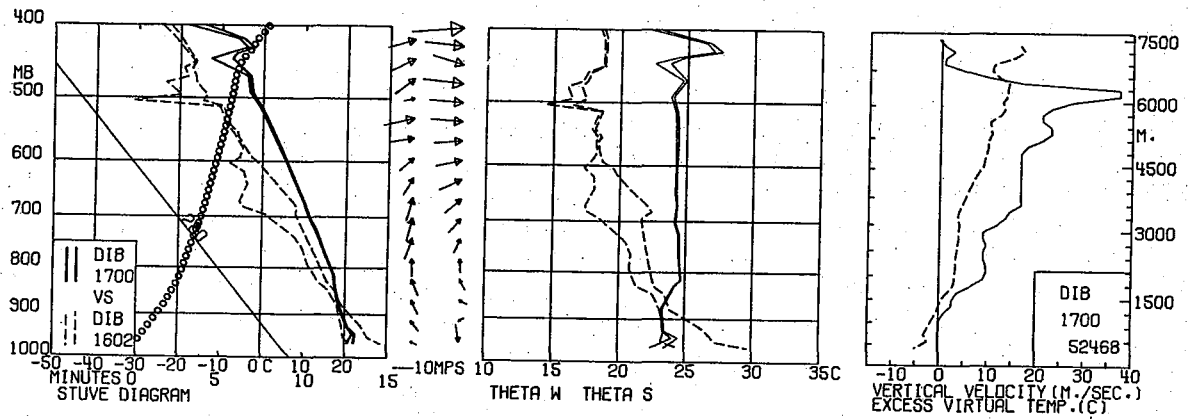


Figure 11. Same as figure 9 for Dibble updraft data. 'Environment' sounding is from Dibble at 1600 CST.

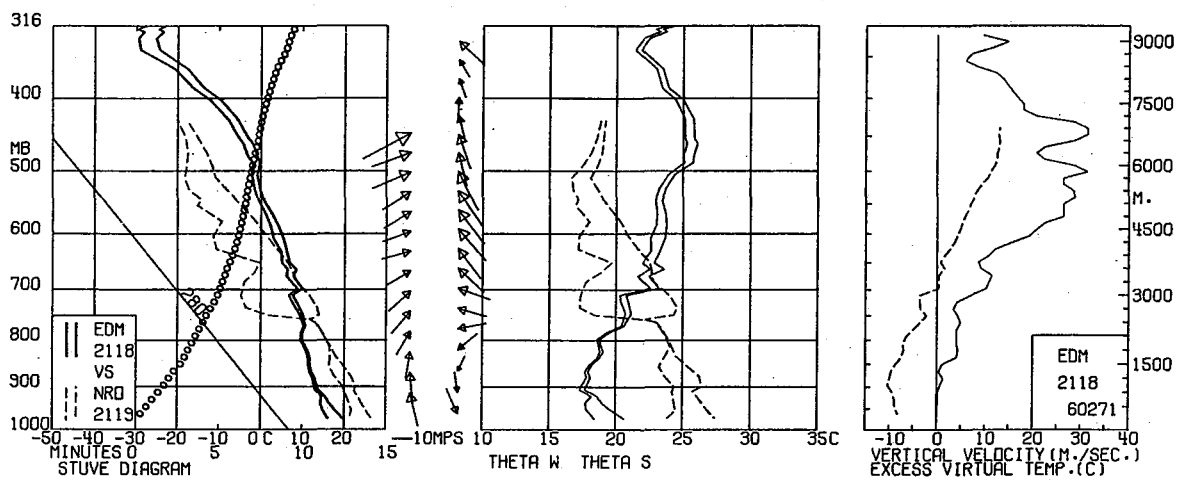


Figure 12. Same as figure 9 for Edmond updraft data. 'Environment' sounding is from Norman at 2219 CST.

The second updraft sounding is a bad example for simulation since no undisturbed "environment" sounding exists. This storm produced  $54 \text{ m sec}^{-1}$  winds in the Lawton-Fort Sill area. It was part of an east-west line that moved southward and had earlier passed over the "environment" station (130 km northeast) modifying the surface layers (see fig. 10). The updraft sounding exhibits pseudo-adiabatic ascent (with  $\theta \sim 23\text{C}$ ) from 770 mb to at least 490 mb (the thermistor broke at this level)<sup>w</sup>. The LFC was 725 mb and  $\Delta T_{500}$  was +10.5C. The vertical velocity reached a peak of  $24 \text{ m sec}^{-1}$  at the termination level.

The third updraft sounding, Dibble, has been discussed previously by Barnes (1970). The associated storm started to move to the right of the mean winds at the time of the sounding and produced severe weather between 1 and 4 hr later. The updraft sounding (fig. 11) closely follows the 24C pseudo-adiabat from 820 to 490 mb. Above the freezing level, the temperature curve again becomes jagged. The environmental sounding<sup>13</sup> is very representative at low levels as the "parcel" method predicts ascent along the 24C pseudo-adiabat. The LCL, LFC, and  $\Delta T_{500}$  were 872 mb, 892 mb, and +9.5C, respectively.<sup>14</sup> The vertical velocity reached a peak of  $37 \text{ m sec}^{-1}$  at 480 mb before falling abruptly to zero, presumably because the balloon left the updraft. However, the temperature did not revert to environmental values until 400 mb.

The fourth sounding, Edmond (fig. 12), was obtained in a squall line that produced straight-line wind damage and funnel clouds. Brown et al. (1971) and Crawford and Brown (1972) discuss the environment and present Doppler radar measurements of this squall line just before the sounding. The balloon entered a developing cell in a strong southward moving, east-west oriented squall line, and rose through a cold air outflow 3 km thick before being entrained into the updraft. Rising motions of roughly  $4 \text{ m sec}^{-1}$  were observed in the rain-cooled air. The environment sounding taken 46 km ahead of the squall line showed that a parcel should ascend along the 24C pseudo-adiabat with a LCL at 907 mb, a LFC at 810 mb, and a  $\Delta T_{500}$  of +9C. Peak vertical velocities of  $32 \text{ m sec}^{-1}$  occurred at 510 and 440 mb, and the balloon was still in the updraft at the sounding termination level (315 mb).

#### 4.3 The Diagnostic Model

To prove that the updraft core is, in fact, virtually undiluted, a one-dimensional cloud model was designed. The model is essentially the same as the entraining plume model applied to cumulonimbi by Squires and Turner (1962). However, a more precise thermodynamic energy equation (appendix B) is used so that the model computes moist adiabatic temperature profiles with high accuracy (to within  $1/4\text{C}$  in potential wet-bulb temperature)

<sup>13</sup>A better choice for environment sounding would have been RSP 1602 CST (as used elsewhere in this study) since the 1602 CST Dibble sounding was itself entrained into a weak updraft at midlevels. However, a glance at case 8 (appendix A) shows that there are only minor differences in virtual temperature between these soundings. Moreover, some humidity data were missing from the RSP sounding.

<sup>14</sup>The LCL is above the LFC because the lowest 160 m of the sounding is super-adiabatic.

in the limit of no entrainment. The model assumptions are that:

- a. The updraft is axisymmetric, vertical, and in a quasi-steady state.
- b. A "proximity" sounding, picked on the low-level inflow side of the storm whenever possible, is representative of the hypothetical, hydrostatic, horizontally homogeneous environment.
- c. The constant pressure surfaces are horizontal planes throughout the updraft-environment region.
- d. The variables (except for radial velocity) have top-hat profiles.
- e. Condensate is not allowed to fall relative to air. This is reasonable since strong updrafts have been associated with low-level weak radar echo regions, indicating a sparsity of large raindrops (having significant fall speeds). Also the updrafts are probably tilted slightly so that precipitation formed at higher elevations does not fall through the lower levels of the updraft.
- f. The formation of ice in the updraft can be neglected. Actually, this assumption is consistent with (e) since we restrict our attention to the portion of the updraft below the freezing level because icing on the balloon and on the temperature element introduces spurious effects into the observations (see figs. 9, 11, and 1).
- g. A cumulonimbus can be modeled as a steady-state jet capped by a bubble (Turner, 1962), and, over a great part of the depth of the cloud, the updraft can be considered as a steady-state jet even while the top of the cloud is developing (Squires and Turner, 1962). Turbulent jets entrain mass at each level at a rate roughly proportional to the local axial velocity and surface area. Thus, vertical stretching of the updraft column (due to vertical accelerations) has an effect on the mixing rate. The model can be run however with the entrainment process "turned off."

Although precipitation is not allowed to fall out of or through the updraft, we use Kessler's (1969) parameterization to divide the liquid water content into two categories, cloud and precipitation, and calculate a radar reflectivity factor.

The following input is required: pressure, environmental temperature, and mixing ratio at each grid level (every 150 m upward from cloud base); updraft temperature ( $T_1$ ), radius ( $b_1$ ), and vertical velocity ( $w_1$ ) at cloud base. A realistic estimate for  $b_1$  is 5 km (Danielsen et al., 1972), and observed values (or downward extrapolations if the balloon entered through the side of the updraft) are used for  $T_1$  and  $w_1$ . The entrainment rate is very sensitive to  $w_1$  and  $b_1$ , but in the limit of no entrainment the results are independent of  $b_1$  and insensitive to  $w_1$ .

## 4.4 Results

### 4.4.1 Dibble Updraft

The Dibble sounding was considered to be the best case to model because (a) the temperature curve closely followed a pseudo-adiabat over a height range of 4 km; (b) the balloon was released into developing cells on the south side of the only storm on the radar within 200 km, so that probably the updraft was not heavily water-loaded and the environment was unmodified;<sup>15</sup> (c) there were many close soundings (within 37 km and 1 hr in time) that could be used to represent the "environment." Runs with three different environment soundings showed only insignificant changes in the results.

Figure 13 shows the effects of entrainment on updraft wet-bulb potential temperature profile for a cloud base vertical velocity,  $w_1$ , of  $2.5 \text{ m sec}^{-1}$  and varying cloud base radii,  $b_1$ . The measured saturated wet-bulb potential temperature ( $\theta_s$ ) is included for comparison. (We assume that the updraft is saturated even though the humidity element recorded slightly less than 100%.) Increasing  $b_1$  (decreasing the entrainment) results in smaller lapse rates. However, even the lapse rate for  $b_1 \leq 20 \text{ km}$  (an unrealistically high value) is steep compared with the observed values. Changing  $w_1$  to  $5 \text{ m sec}^{-1}$  decreases the lapse rates (as indicated by the crosses in the figure), but they are still too steep for  $b_1 \leq 20 \text{ km}$ . We conclude that the cores of strong updrafts are virtually undiluted to midlevels. This result is important because it supports the ideas of Morton (1967) and Marwitz et al. (1970) that mixing occurs relatively slowly, not instantaneously and uniformly across the cloud as assumed in one-dimensional entraining cloud models.

Since the observed lapse rates were practically pseudo-adiabatic, further runs of the model were made without entrainment. Soong and Ogura (1973) concluded from numerical models that the vertical pressure perturbation gradient force in the vertical momentum equation, customarily excluded in one-dimensional models, opposes the net buoyancy force and is of the same order of magnitude as the thermal buoyancy force in the core of the cloud. This term is parameterized here in two alternative ways. First, a virtual mass is used (although this concept is more rigorously applicable to bubbles than to jets). Second, the entrainment term in the vertical velocity equation is retained, and the entrainment drag term multiplied by a constant  $K$  ( $\sim 5$  or  $10$ ). This is the approach adopted by Danielson et al. (1972). Note that both parameterizations reduce the model's vertical velocities and that the second also reduces cloud top.

Figure 14 compares the actually observed vertical velocity profile with model curves generated with different virtual mass coefficients ( $\gamma = 1$  signifies a 100% increase in inertia, etc). The  $\gamma = 1$  curve is probably the best fit to the observed profile. Figure 15 is a similar comparison showing the effects of varying  $K$  (with  $b_1 = 5 \text{ km}$ ). The  $K = 5.5$  curve, one-half the value adopted by Danielson et al. (1972), is the best fit.

<sup>15</sup> Especially since the first echoes had appeared just an hour before.

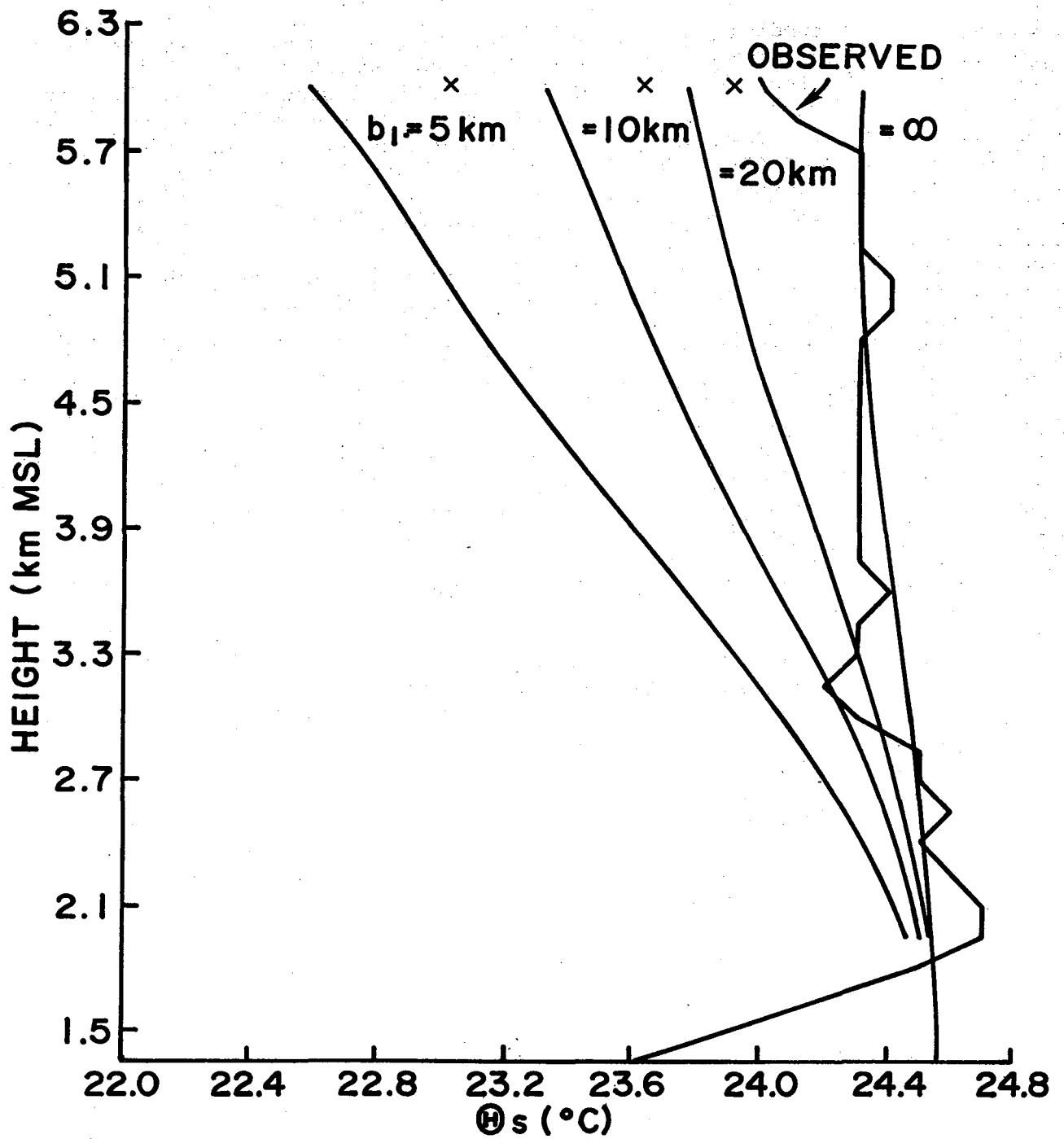


Figure 13. Observed  $\theta_s$  profile and model profiles for various values of  $b_1$  ( $b_1 = \infty$  signifies no entrainment) and  $w_1 = 2.5 \text{ m sec}^{-1}$  for Dibble updraft, X denotes top of curves for  $b_1 = 5, 10, 20 \text{ km}$  when  $w_1$  is changed to  $5 \text{ m sec}^{-1}$ .

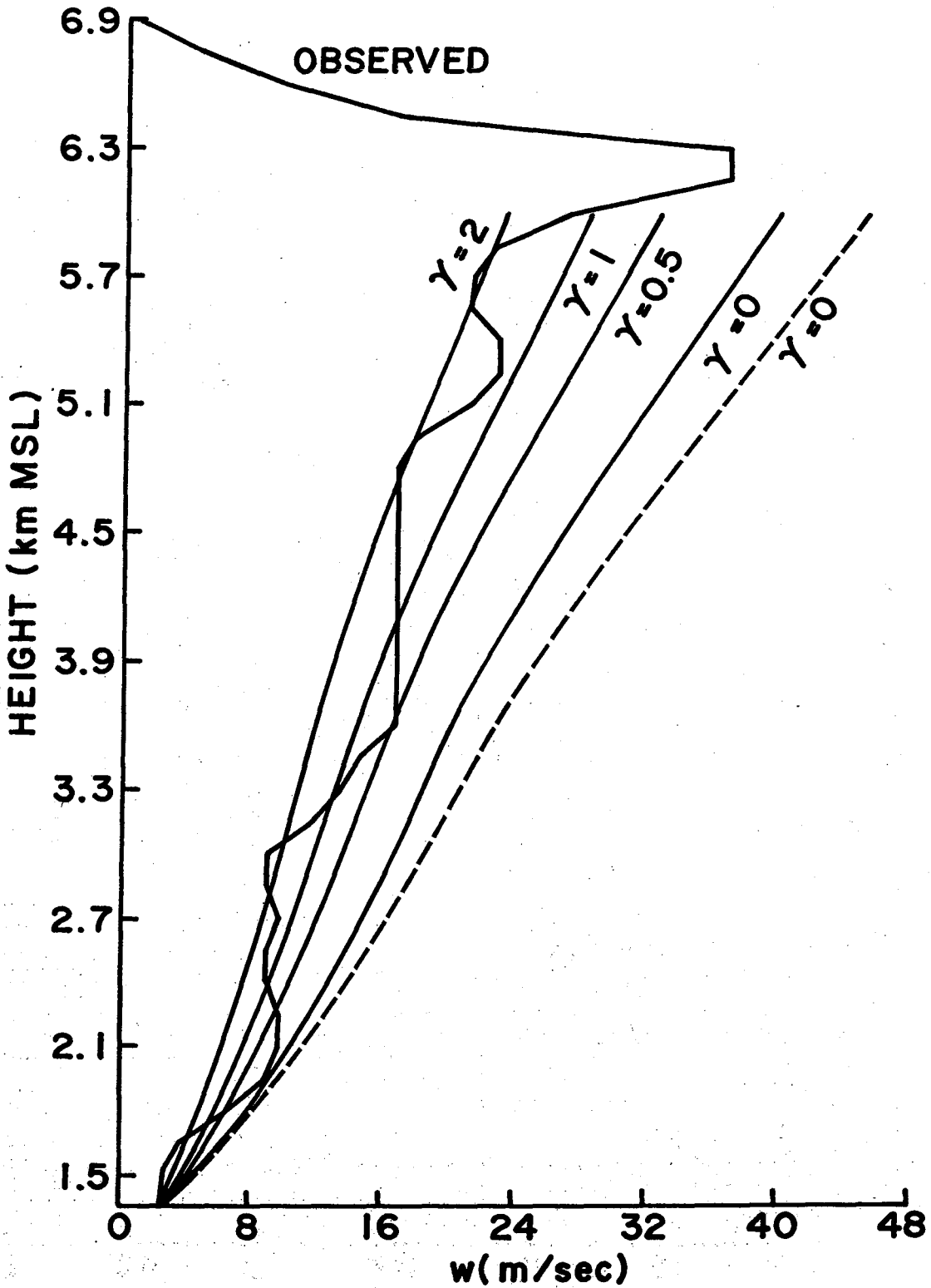


Figure 14. Observed vertical velocity profile and model profiles with different virtual mass coefficients for Dibble updraft. Dashed curve shows effect of neglecting water loading term in  $\gamma = 0$  case.

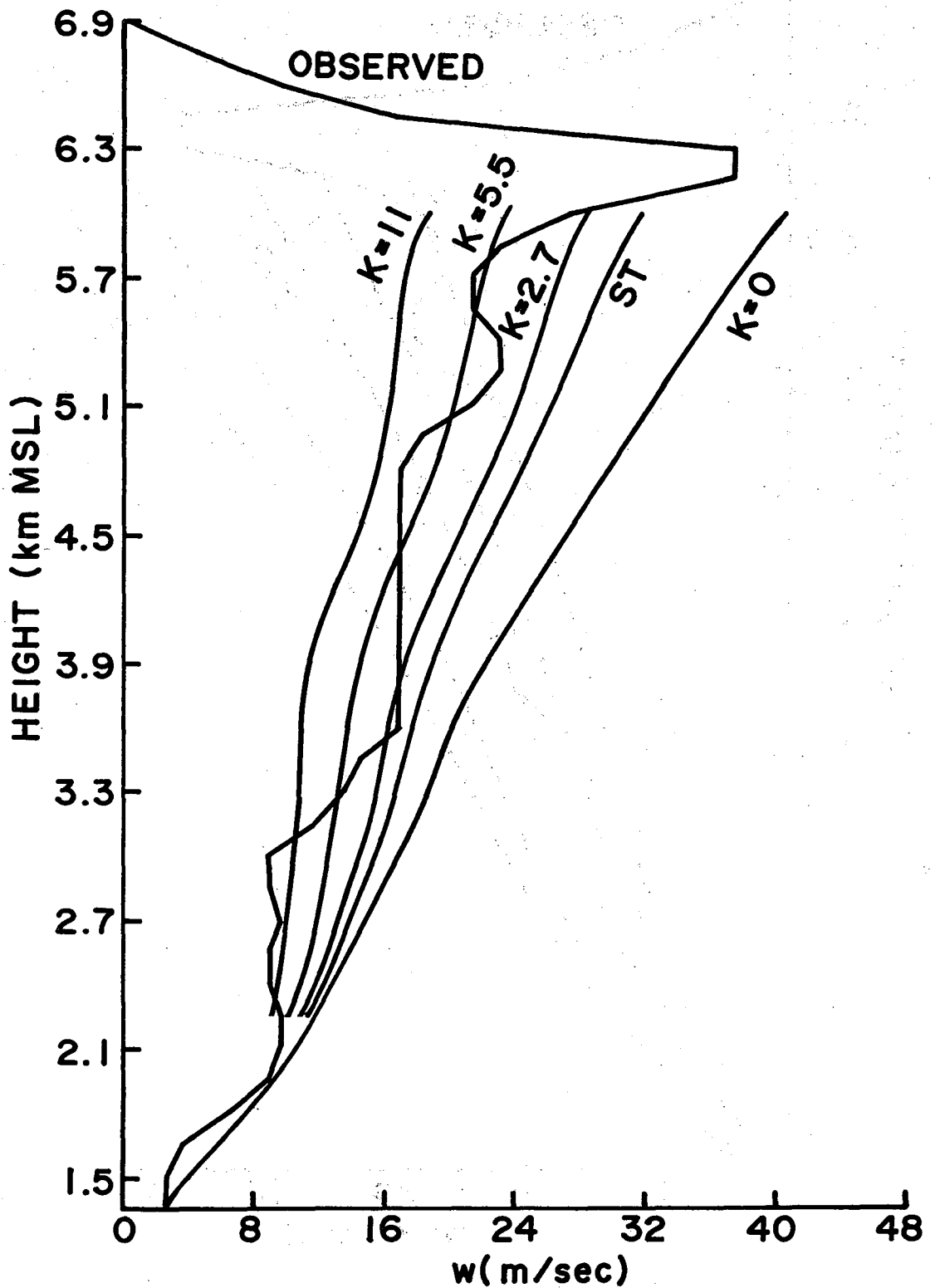


Figure 15. Observed vertical velocity profile versus model profiles with different values of  $K$  for Dibble updraft.  $b_1$  is 5 km. ST denotes profile obtained from unmodified Squires-Turner model.

The updraft radius as a function of height in the non-entraining case is shown in figure 16. The radius decreases with height to conserve mass flux since vertical velocity increases greatly with height. This shape is characteristic of the lower halves of cumulonimbi. For  $b_1 = 5$  km the mass flux is  $2.0 \times 10^8$  kg sec<sup>-1</sup>. Figure 17 shows model profiles of virtual temperature excess, liquid water and precipitation mixing ratios, and radar reflectivity. These appear to be reasonable for the vault region of a developing thunderstorm.

#### 4.4.2 Other Updrafts

Figures 18, 19, and 20 show observed and model profiles for the three other high-speed updrafts. In all cases the presence of high  $\theta_w$  air at midlevels indicates the existence of virtually undiluted updraft cores. Since the Edmond balloon rose through a cold air outflow layer 3 km thick before being entrained into the updraft, a sounding believed representative of the updraft core was constructed as shown in figure 18(a) and used as input to the model. Figure 18(b) shows the observed vertical velocity profile (remember that the balloon was not in the updraft core at low levels) and the theoretical velocity profile (computed without pressure drag). Reasonable agreement is obtained.

Neither of the other two updraft soundings is good for simulation by the model. Both soundings indicate high cloud bases and even higher levels of free convection with considerable upward velocities observed at each LFC. The Watonga sounding remained on a pseudo-adiabat for only 170 mb. The environment sounding was only moderately close (93 km away). In the Fort Sill case, a squall line had passed over the "environment" station (130 km northeast) prior to the sounding. The simulations are included for completeness (figs. 19 and 20) although definitive conclusions cannot be drawn from them.

#### 4.5 Conclusions

Strong updrafts have been shown to have cores that extend at least to midlevels and are virtually undiluted by environmental air. This casts doubt on how applicable one-dimensional cloud models that assume instantaneous mixing are for modeling cumulonimbi (e.g., Squires and Turner, 1962; Danielsen et al., 1972). Turner (1973, p. 196) has raised other doubts about the validity of such models.

The Dibble sounding, the best case for simulation, indicates (subject to the assumptions made) that the updraft velocity is reduced considerably by adverse pressure gradient forces. However, data from the other updrafts were insufficient to verify this hypothesis.

### 5. CONCLUSIONS

The conclusions for this study are contained in sections 2.6, 3.6, and 4.5. Even though the data are not of high quality, our findings confirm previous knowledge and speculations (see sect. 1.1), in particular the existence of undiluted updraft cores, the warm core nature of the storms at mid- and upper levels, and the weak vector wind shear in updrafts. In

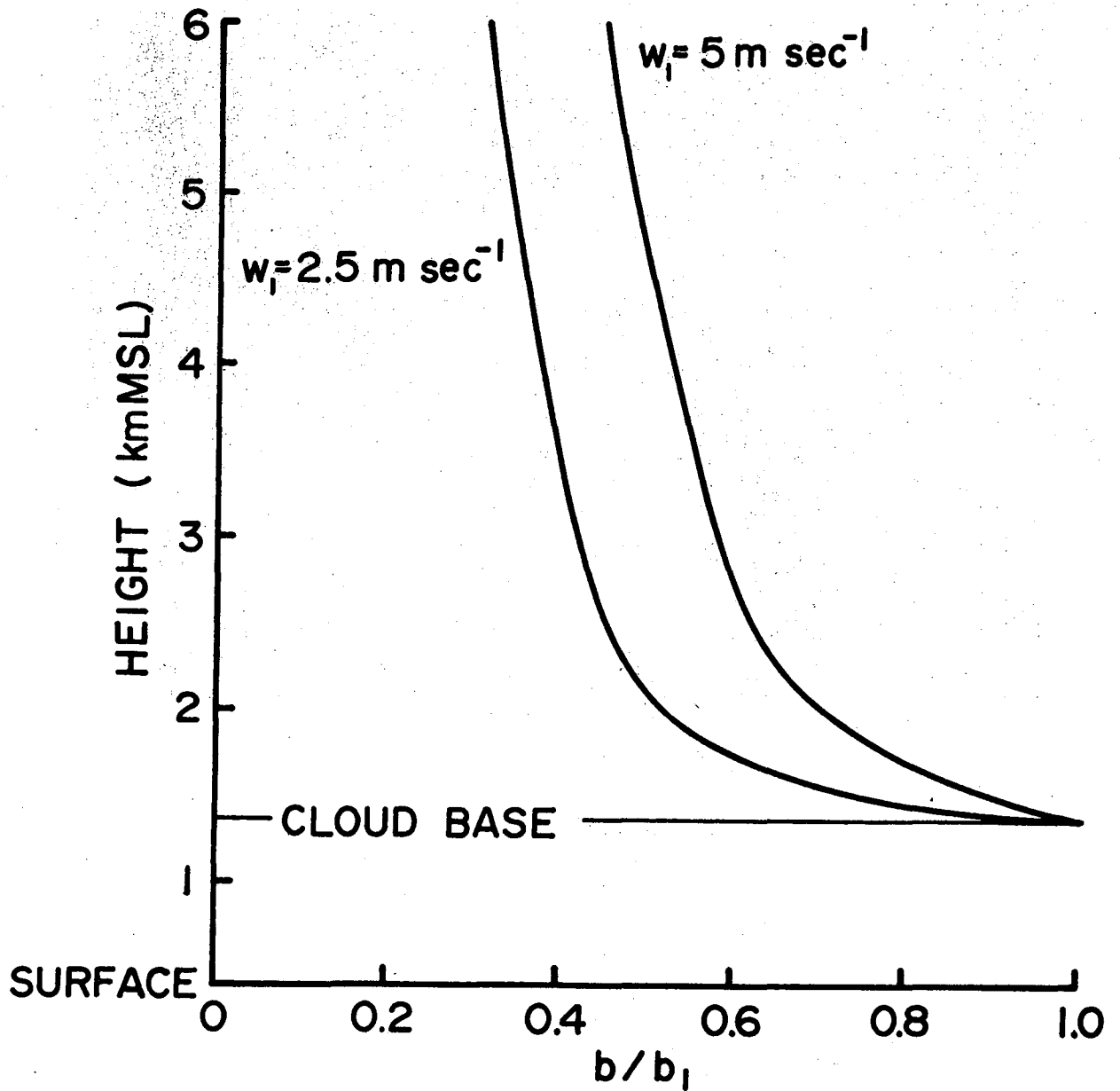


Figure 16. Updraft radius, normalized by cloud radius, as function of height in non-entraining case for  $w_1 = 2.5$  and  $5 \text{ m sec}^{-1}$ . This is actual (undistorted) updraft shape when  $b_1 = 5 \text{ km}$ .

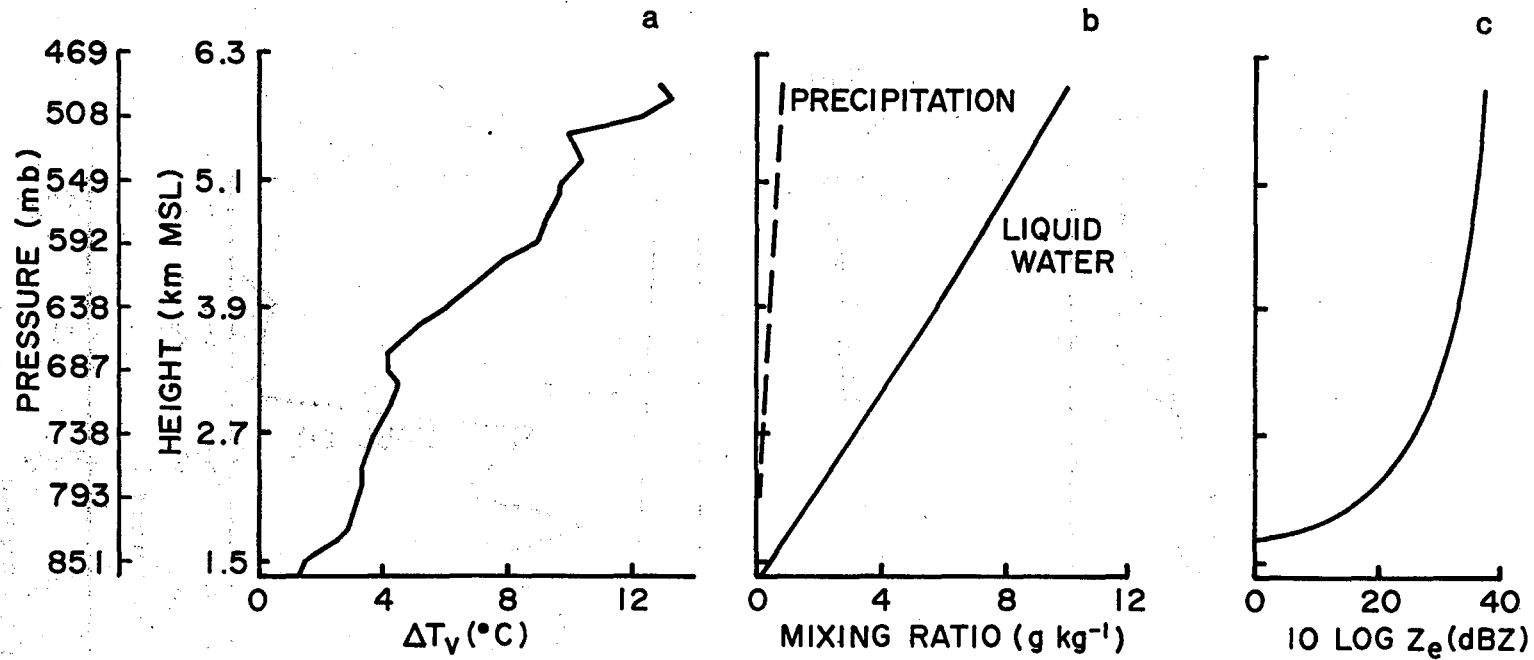


Figure 17. Dibble updraft: model profiles of (a) virtual temperature excess,  $\Delta T_v$ , (b) liquid water and precipitation mixing ratios, (c) radar reflectivity,  $10 \log Z_e$ , in non-entraining case.

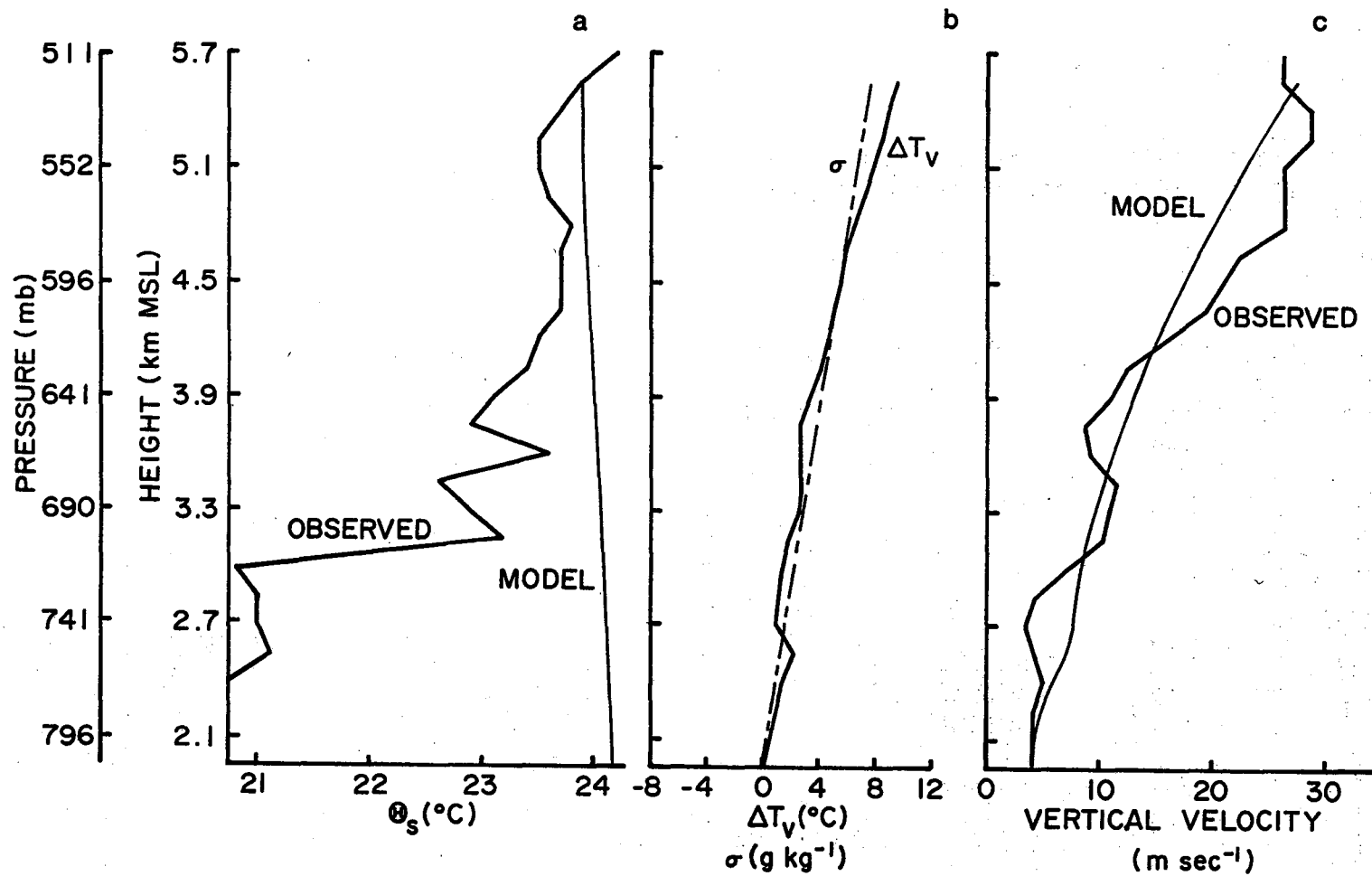


Figure 18. Edmond updraft: (a) observed and model  $\theta_s$  profiles (b) model virtual temperature excess ( $\Delta T_v$ ) and liquid water mixing ratio ( $\sigma$ ) profiles (c) observed and model vertical velocity profiles. Model runs were made with zero entrainment and  $\gamma = K = 0$ .

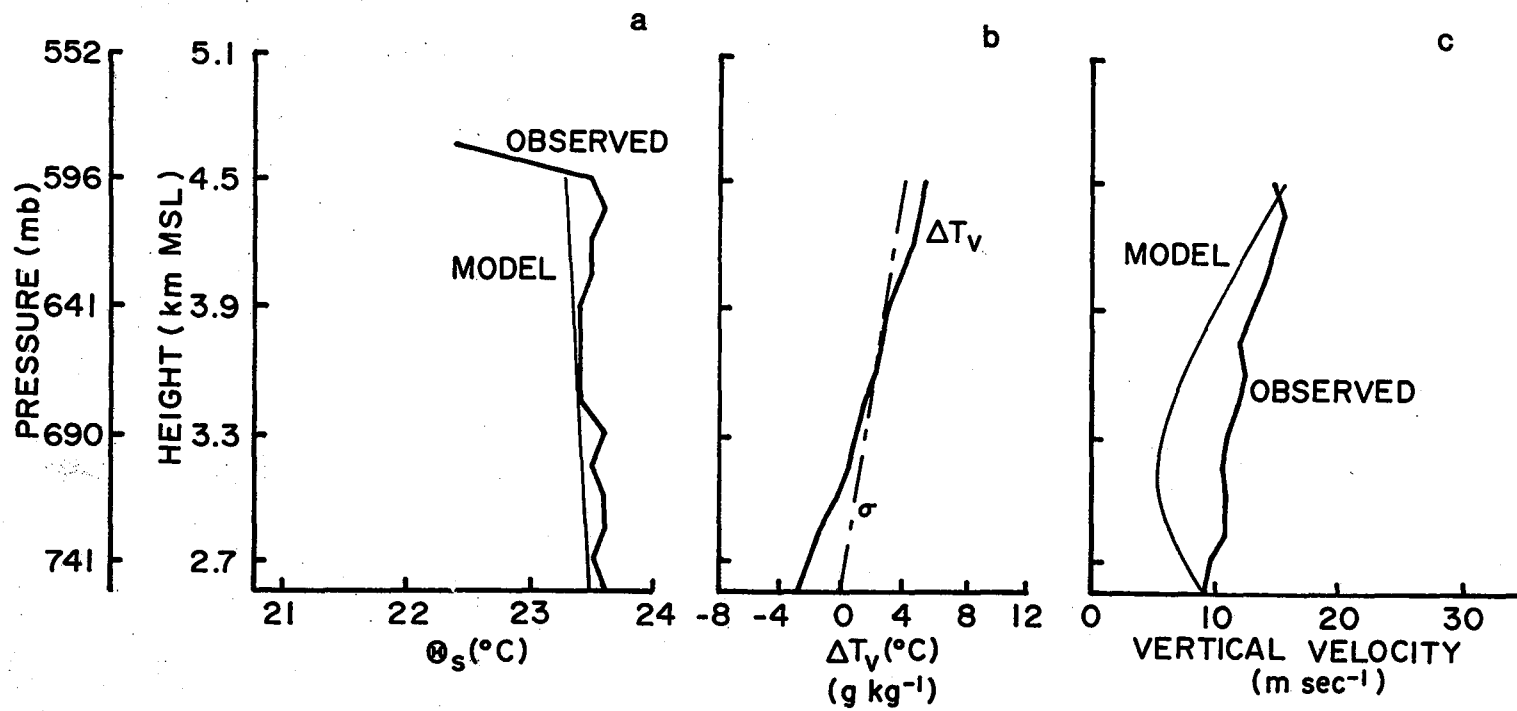


Figure 19. Same as figure 18 but for Watonga updraft.

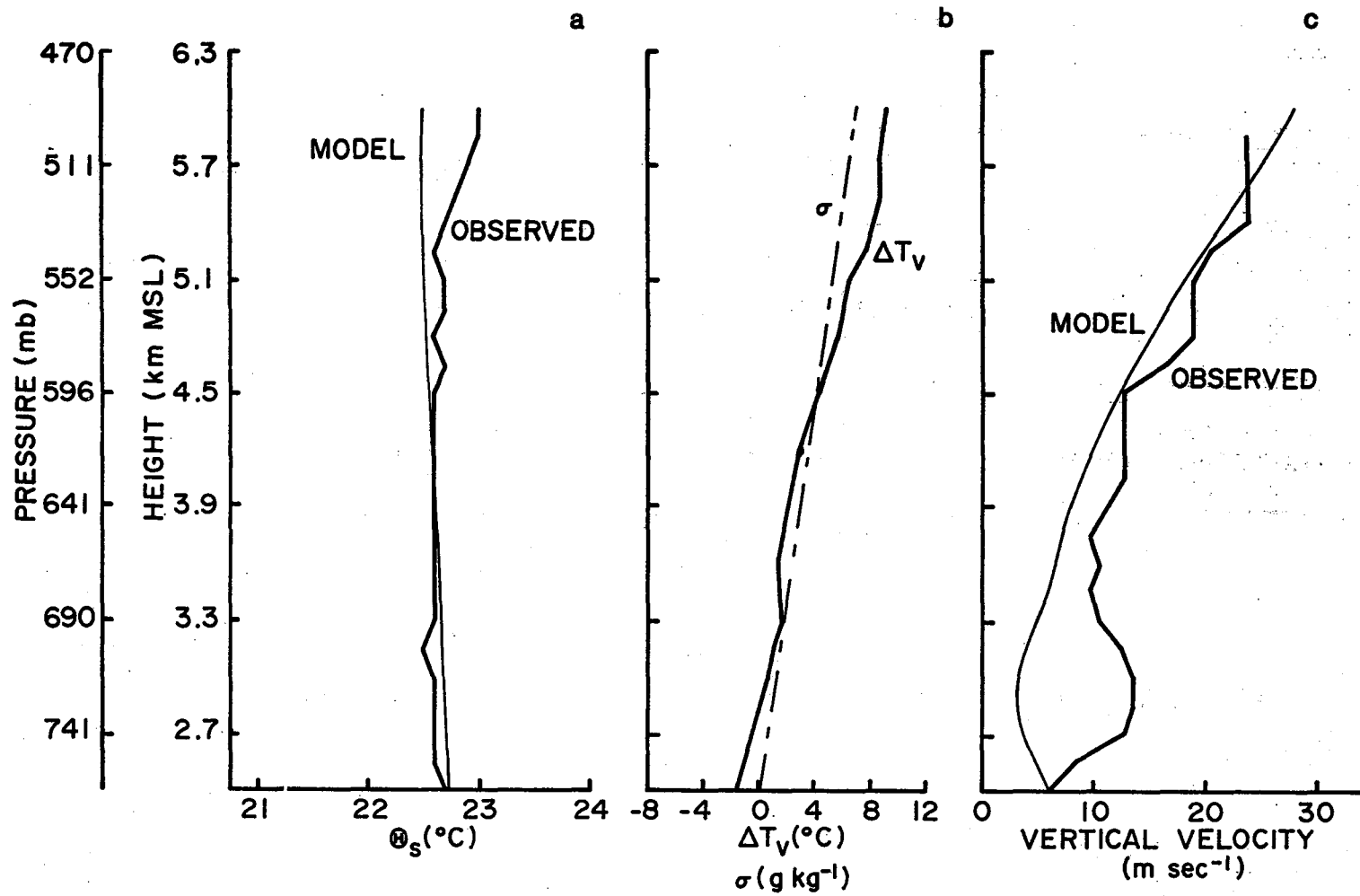


Figure 20. Same as figure 18 but for Fort Sill updraft.

addition, our results agree with Marwitz's (1973) findings that air comprising the updraft below and immediately above cloud base is generally cold relative to the environment and must be rising under the influence of perturbation pressure gradient forces. Higher up in the storm, these forces probably reverse sign and retard the updraft. The controversy about the height of the maximum vertical velocity in the updraft remains. Our finding that the maximum vertical velocity occurs within 5 km of cloud base apparently confirms those of other experiments that tracked objects released below cloud base. However, this result may be strongly influenced by several factors such as flight train icing, balloons prematurely leaving tilted updrafts due to their own buoyancy, and the extent to which the updrafts are water loaded.

Aircraft, surface mesonet, and detailed radar data were not used in this study because we felt that improvements in our results would be slight and would not justify the effort involved.

We close by giving the following recommendations for future investigations of this type:

(a) Prior to release the free lift of the balloon should be measured so that the rawinsonde's ascent rate with respect to still air can be computed more accurately.

(b) The upper air network should be outside the ground clutter of the radar.

(c) The instrument package should be modified to reduce moisture induced errors. In particular, the temperature element should be shielded.

(d) Wind tunnel tests should be conducted to determine both the mass of ice that can accumulate on the radiosonde and the magnitude of temperature errors due to ice and liquid water.

(e) Sky photography at each raob station would provide useful additional information in some cases.

In addition, operational rawinsonde teams should report abnormally high ascent rates, since soundings with such ascent rates should be excluded from synoptic-scale analyses. Copies of these updraft sounding strip charts might be saved for future analysis.

## 6. ACKNOWLEDGMENTS

The authors thank their colleagues Dr. J. Schaefer for a critical review of this report, and Mr. S. Nelson and Dr. J. McCarthy for discussions on the instrumental effects of hydrometeor impact. Dr. Mary Hodge of the NOAA NWS Test and Evaluation Laboratory was also consulted on the types of radiosonde error that commonly occur in deep convective clouds. Mr. R. Ketchum assisted this investigation in several ways. We are also indebted to Mr. Ray Crooks, MIC Oklahoma City WSFO, for quickly providing missing RAREPS.

The soundings were taken by personnel from the 6th Weather Squadron (Mobile), Tinker Air Force Base, and from the 3rd Target Acquisition Battalion, Ft. Sill.

## 7. REFERENCES

- Auer, A. H., Jr. and W. Sand, 1966: Updraft measurements beneath the base of cumulus and cumulonimbus clouds. J. Appl. Meteor., 5, 461-466.
- Barnes, S. L., 1970: Some aspects of a severe right-moving thunderstorm deduced from mesonetwork rawinsonde observations. J. Atmos. Sci., 27, 634-648.
- Barnes, S. L., 1971: Reply. J. Atmos. Sci., 28, 653-654.
- Barnes, S. L., J. H. Henderson and R. J. Ketchum, 1971: Rawinsonde observation and processing techniques at the National Severe Storms Laboratory. NOAA Tech. Memo ERL NSSL-53, 246 pp.
- Bates, F. C., 1961: The Great Plains squall-line thunderstorm - a model. Ph.D. Thesis, St. Louis University, Mo., 164 pp.
- Battan, L. J. and J. B. Theiss, 1966: Observations of vertical motions and particle sizes in a thunderstorm. J. Atmos. Sci., 23, 78-87.
- Brown, R. A., W. C. Bumgarner, K. C. Crawford and D. Sirmans, 1971: Preliminary Doppler velocity measurements in a developing radar hook echo. Bull. Amer. Meteor. Soc., 52, 1186-1188.
- Browning, K. A., 1964: Airflow and precipitation trajectories within severe local storms which travel to the right of the winds. J. Atmos. Sci., 21, 634-639.
- Brunk, H. D., 1965: An Introduction to Mathematical Statistics. Blaisdell, Waltham, Mass. (Second Edition), 429 pp.
- Bushnell, R. H., 1973: Vertical winds in thunderstorms measured by dropsondes. Preprints, Eighth Conf. Severe Local Storms, Denver, Co., Amer. Meteor. Soc., 10-13.
- Byers, H. R., 1965: Elements of Cloud Physics. University of Chicago Press, Chicago, 191 pp.
- Byers, H. R. and R. R. Braham, 1949: The thunderstorm: Report of the thunderstorm project (a joint project of U. S. Air Force, U. S. Navy, NACA and U. S. Weather Bureau), U. S. Government Printing Office, Washington, D. C., 287 pp.
- Caplan, P. M., 1966: On the evaporation of raindrops in the presence of vertical gradients of temperature and relative humidity. J. Atmos. Sci., 23, 614-617.
- Crawford, K. C. and R. A. Brown, 1972: Doppler velocity measurements in an approaching squall line. Preprints, 15th Radar Meteor. Conf., Champaign-Urbana, Ill., Amer. Meteor. Soc., 27-34.

- Danielsen, E. F., R. Bleck and D. A. Morris, 1972: Hail growth by stochastic collection in a cumulus model. J. Atmos. Sci., 29, 135-155.
- Davies-Jones, R. P., 1974: Discussion of measurements inside high speed thunderstorm updrafts. J. Appl. Meteor., 13, 710-717.
- Davies-Jones, R. P., and J. H. Henderson, 1973: Characteristics of thunderstorm updraft soundings. Preprints, Eighth Conf. Severe Local Storms, Denver, Co., Amer. Meteor. Soc., 1-5.
- Davies-Jones, R. P., and N. B. Ward, 1971: Comments on "Some aspects of a severe right moving thunderstorm deduced from mesonet network rawinsonde observations." J. Atmos. Sci., 28, 652-653.
- Donaldson, R. J., 1967: A preliminary report on Doppler radar observation of turbulence in a thunderstorm. Air Force Cambridge Research Laboratories Report AFCRL-67-0015.
- Fankhauser, J. C., 1971: Thunderstorm-environment interactions deduced from aircraft and radar observations. Mon. Wea. Rev., 99, 171-192.
- Fawbush, E. J. and R. C. Miller, 1954: The types of air masses in which North American tornadoes form. Bull. Amer. Meteor. Soc., 35, 154-165.
- Fujita, T. T. and H. Grandoso, 1968: Split of a thunderstorm into anti-cyclonic and cyclonic storms and their motion as determined from numerical model experiments. J. Atmos. Sci., 25, 416-439.
- Garrett, A. J., 1974: Applications of a plume model and other synoptic parameters to prediction of thunderstorms. M. S. Thesis, Massachusetts Institute of Technology, Cambridge, Mass., 97 pp.
- Grandia, K. L., 1973: Aircraft observations in the weak echo region of a thunderstorm. Preprints, Eighth Conf. Severe Local Storms, Denver, Co., Amer. Meteor. Soc., 6-9.
- Hart, H. E., and L. W. Cooper, 1968: Thunderstorm airflow studies using radar transponders and superpressure balloons. Preprints, Thirteenth Radar Meteor. Conf., Montreal, Canada, Amer. Meteor. Soc., 196-201.
- Henderson, J. H., 1971: The internal structure of a thunderstorm as revealed by  $\Theta_w$  surfaces. Preprints, Seventh Conf. Severe Local Storms, Kansas City, Mo., Amer. Meteor. Soc., 234-239.
- Henderson, J. H., 1972: A detailed description of the internal structure of a thunderstorm. Preprints, Fifteenth Radar Meteor. Conf., Champaign, Ill., Amer. Meteor. Soc., 53-56.
- Hodge, M. W., 1958: Superadiabatic lapse rates of temperature in radiosonde observations. Mon. Wea. Rev., 86, 103-106.

- Hodge, M. W. and C. Harmantas, 1965: Compatibility of United States rawinsondes. Mon. Wea. Rev., 93, 253-266.
- Kessler, E., 1969: On the distribution and continuity of water substance in atmospheric circulations. Meteorological Monographs, 10, No. 32, Amer. Meteor. Soc., 84 pp.
- Kyle, T. C. and W. R. Sand, 1973: Water content in convective storms. Science, 180, 1274-1276.
- Lee, J. L., 1972: A numerical study of shallow convection. Report No. 19, Dept. of Meteor., Pennsylvania State Univ., 93 pp.
- Ludlam, F. H., 1959: Hailstorm Studies. Nubila, Anno II, 38-50.
- Ludlam, F. H., 1966: Cumulus and cumulonimbus convection. Tellus, 18, 687-698.
- MacCready, P. B., and D. M. Takeuchi, 1968: Precipitation initiation mechanisms and droplet characteristics of some convective cloud cores. J. Appl. Meteor., 7, 591-602.
- Marwitz, J. D., 1972: The structure and motion of severe hailstorms. Part III: Severely sheared storms. J. Appl. Meteor., 11, 189-201.
- Marwitz, J. D., 1973: Trajectories within the weak echo regions of hailstorms. J. Appl. Meteor., 12, 1174-1182.
- Marwitz, J. D., A. H. Auer, Jr. and D. L. Veal, 1972: Locating the organized updraft on severe thunderstorms. J. Appl. Meteor., 11, 236-238.
- Marwitz, J. D., J. R. Middleton, A. H. Auer and D. L. Veal, 1970: The dynamics of updraft vaults in hailstorms as inferred from the entraining jet model. J. Atmos. Sci., 27, 1099-1102.
- McComb, H. C. and R. G. Beebe, 1956: A thunderstorm sounding. Mon. Wea. Rev., 84, 107.
- Morton, B. R., 1967: On the formulation of convective plume models. Thermal Convection: A Colloquium. NCAR-TN-24. National Center for Atmospheric Research, Boulder, Co., 305-322.
- Nelson, S. P., 1973: Radiosonde altitude measurements using double radiotheodolite techniques. NOAA Tech. Memo. ERL NSSL-65, 20 pp.
- Newton, C. W., 1966: Circulations in large sheared cumulonimbus. Tellus, 18, 699-713.
- Roach, W. T., 1967: On the nature of the summit areas of severe storms in Oklahoma. Quart. J. Roy. Meteor. Soc., 93, 318-336.

- Roys, G. P. and E. Kessler, 1966: Measurements by aircraft of condensed water in Great Plains thunderstorms. ESSA Technical Note 49-NSSP-19, 17 pp.
- Saunders, P. M., 1962: Penetrative convection in stably stratified fluids. Tellus, 14, 177-194.
- Severin, B. P., 1971: Comparative meteorological testing of the AMT-13 dropsonde and JOOX-series rawinsonde in an environmental wind tunnel. Air Weather Service Technical Report 222.
- Sinclair, P. C., 1973: Severe storm air velocity and temperature structure deduced from penetrating aircraft. Preprints, Eighth Conf. Severe Local Storms, Denver, Co., Amer. Meteor. Soc., 25-32.
- Smithsonian Meteorological Tables, 1958: The Smithsonian Institution, Washington, D. C. (Sixth Revised Edition), 527 pp.
- Soong, S. and Y. Ogura, 1973: A comparison between axisymmetric and slab symmetric cumulus cloud models. J. Atmos. Sci., 30, 879-893.
- Squires, P. and J. S. Turner, 1962: An entraining jet model for cumulonimbus updrafts. Tellus, 14, 422-434.
- Steiner, R. and R. H. Rhyne, 1962: Some measured characteristics of severe storm turbulence. U. S. Weather Bureau, National Severe Storms Project Report No. 10, 17 pp.
- Sulakvelidze, G. K., H. S. Bibilashvili and O. F. Lapcheva, 1967: Formation of precipitation and modification of hail processes. Translated from Russian. Israel Program for Scientific Translation, 208 pp.
- Turner, J. S., 1962: The "starting plume" in neutral surroundings. J. Fluid Mech., 13, 356-368.
- Turner, J. S., 1973: Buoyancy Effects in Fluids. Cambridge University Press, England, 367 pp.
- U. S. Environmental Data, 1966: Storm Data, 8, 57-59.
- U. S. Environmental Data, 1971: Storm Data, 13, 104.
- Vonnegut, B. and C. B. Moore, 1958: Giant electrical storms. Recent Advances in Atmospheric Electricity ed. L. G. Smith. Pergamon Press, New York, 399-411.
- Warner, C., 1972: Calculations of updraft shapes in storms. J. Atmos. Sci., 29, 1516-1519.
- Weather Radar Manual, 1967: United States Government Printing Office, Washington, D. C.

Wichmann, M., 1951: Über das Vorkommen und Verhalten des Hagels in Gewitterwolken. Ann. Meteor., 4, 218-225.

Wilk, K. E. and K. C. Gray, 1970: Processing and analysis used with the NSSL weather radar system. Preprints, Fourteenth Radar Meteor. Conf., Tucson, Az., Amer. Meteor. Soc., 369-374.

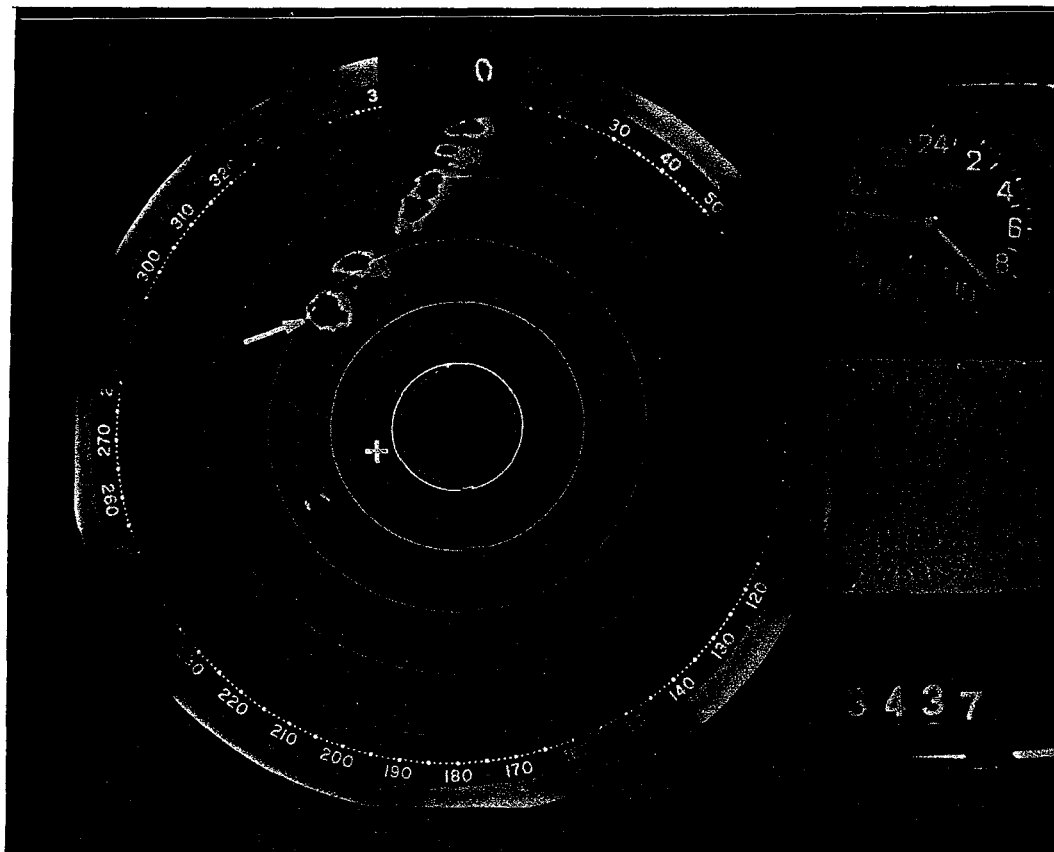
## APPENDIX A

### DATA BASE

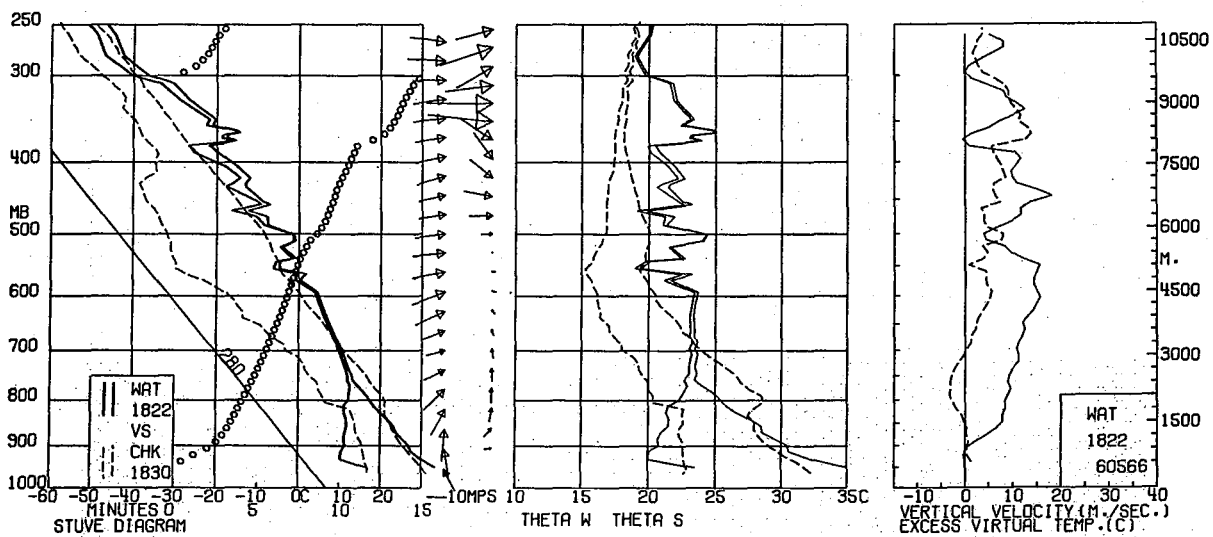
The following pages contain NSSL WSR-57 whole-scope photographs (with 20 n mile range marks) of the radar echoes very close to the time that the updraft soundings were released, the individual sounding data (see figure legend below), synoptic weather descriptions, RAREPS from Oklahoma City Weather Service Forecast Office (corrected so that the azimuth and range are from Norman), descriptions of updraft locations relative to radar echoes, and surface weather observations at release time (for both updraft and environment soundings). Underlined RAREPS indicate those portions of the reports which refer to the areas of interest. Operational radar observations are started at approximately thirty minutes after the hour, and transmitted at forty five minutes after the hour. Listed RAREPS are those closest in time to updraft soundings.

### FIGURE LEGEND

- (Above) NSSL WSR-57 whole-scope photographs (with 20 n mile (37 km) range marks) of the radar echoes very close to the time the updraft soundings were released. Arrow and cross mark positions of updraft and environment stations, respectively.
- (Left) Stuve diagram of updraft and environment soundings. The right solid line is the updraft temperature profile; the left solid line is the updraft dewpoint profile; the dashed lines are similar curves for the environment. The 280C dry adiabat is also included. Circles designate elapsed time since release versus pressure and reveal balloon ascent rate; curve cycles back to zero every 15 min. Arrows denote horizontal wind speed (proportional to length) and direction. Height of observations is given by position of tip. Updraft winds are to the right of the environment winds.
- (Center) Vertical Profiles of  $\theta_w$  (wet-bulb potential temperature) and  $\theta_s$  ( $\theta_w$  with relative humidity set to 100%) for updraft (both solid) and environment (both dashed).  $\theta_w$  curves are left of corresponding  $\theta_s$  curves. Pseudo-adiabats are vertical lines on this diagram.
- (Right) Updraft vertical velocity (solid) and excess virtual temperature (dashed) profiles.



CASE 1

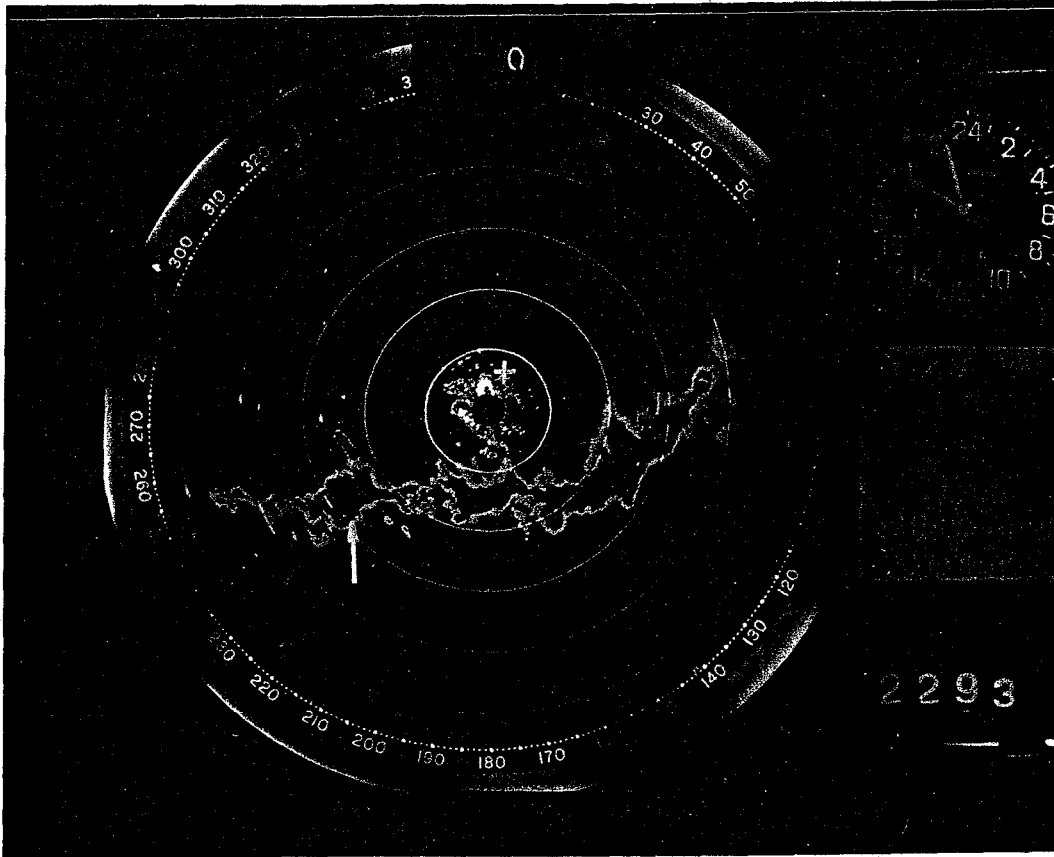


SYNOPSIS - Thunderstorms formed ahead of a cP front and near the intersection of the front and a dryline in the mT air mass. Upper level flow continued westerly with a moderate trough approaching from the west.

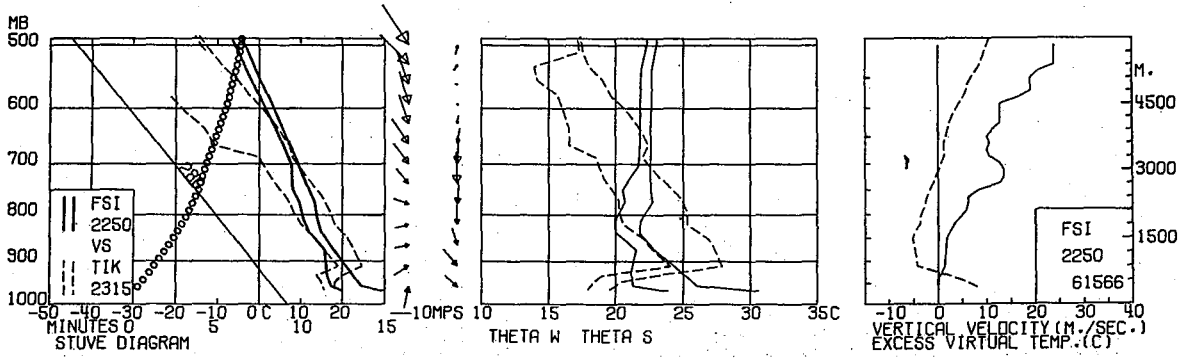
RADAR - 1745 CST - LN BRKN TRW/+ 17/184 311/63 W10 2820 TOPS 480 AREA  
WDLY SCTD TRW-/+ 88/124 90/159 173/147 174/112 D4 2720 1845 CST - LN  
BRKN TRW/TRW+/+ 20/159 309/56 W15 2815 TOPS 550-560

Balloon - Entered on rt. rear of echo, there is a tight reflectivity gradient associated with echo.

SFC WX AT RLS TIME - CLDS - 5/10 CB 3/10 CUMAM, WX - TSTM - TORNADO  
6 NW 1814 CST - T OVHD MOVG E-SE OCNL RW - LTGCCCCG NE LTGCG OVHD  
AP B1835 - ENVIRONMENT WX - 4/10 CB



CASE 2

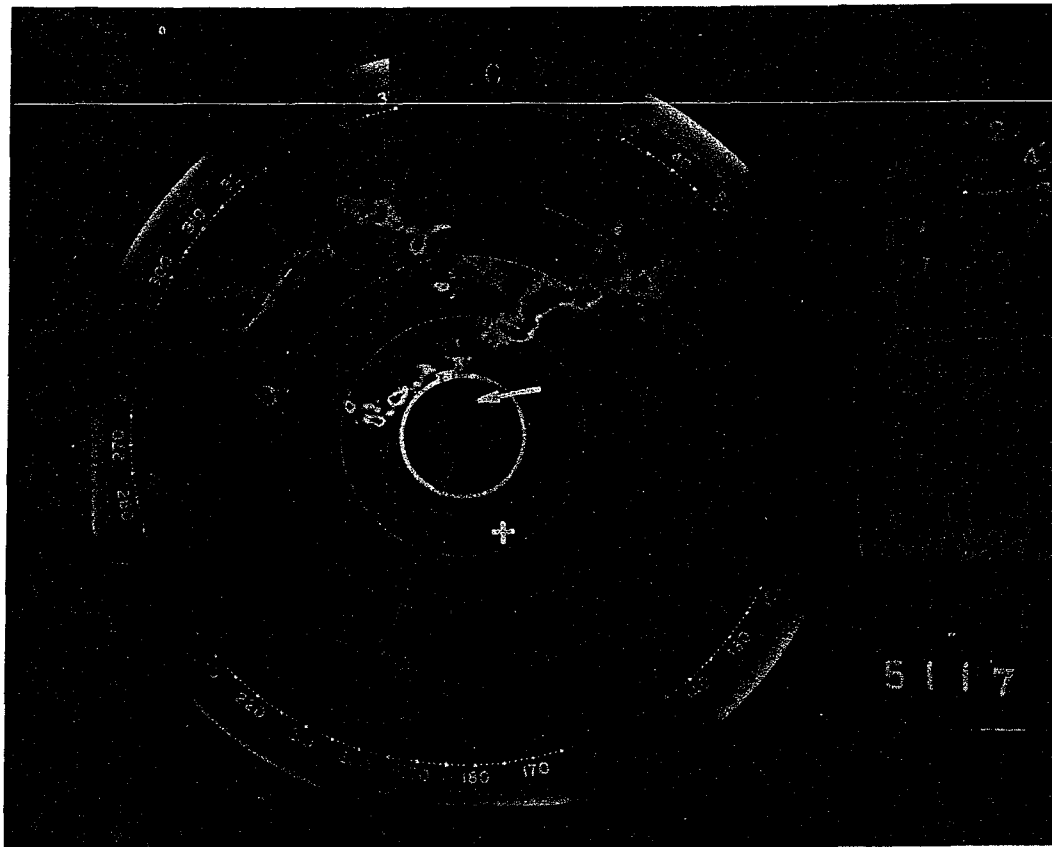


SYNOP - Strong cP front swept across Oklahoma at midnight. Lines of severe thunderstorms developed in mT air ahead of front. At 500 mb northerly flow continued.

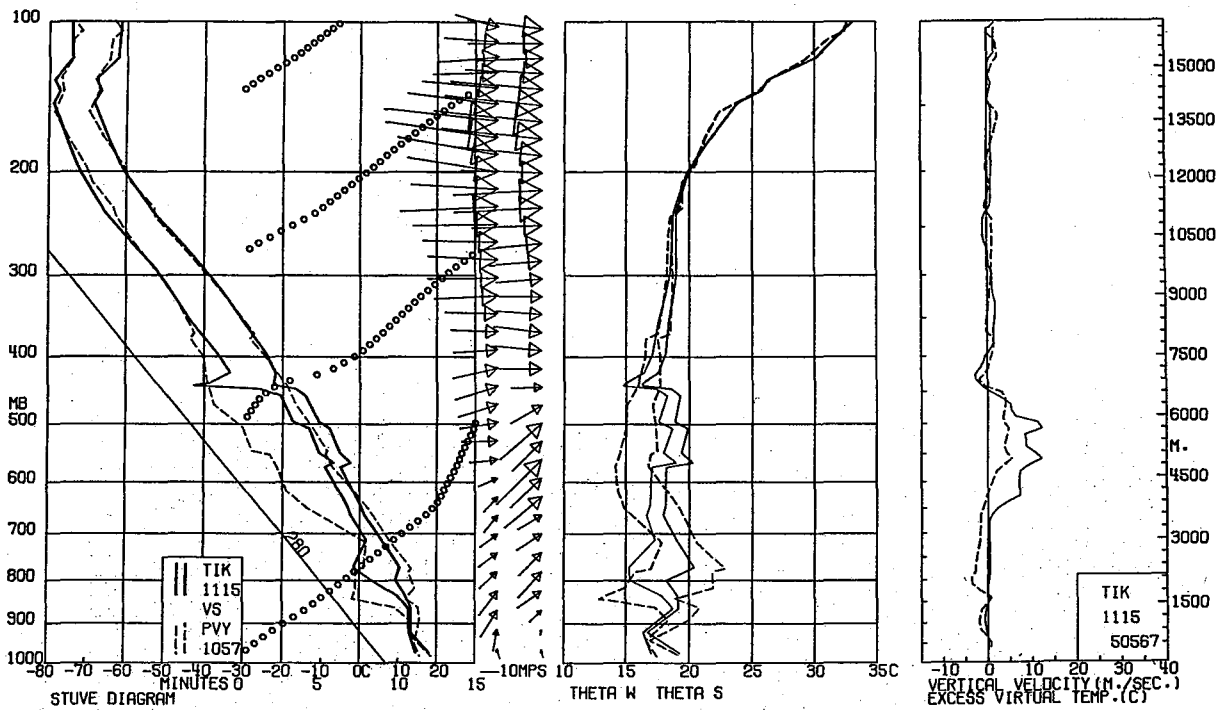
RADAR - 2245 CST - LN BRKN TRW TRW+/NC 73/162 97/41 256/103 271/142  
W30 3425 TOPS 300-400 W60 EXTRM E END INCLDS LN BRKN TRW+ 90/58 129/37  
240/32 253/62 240/60 W12 TOPS 500-550 LN BRKN TRWU 309/153 271/167  
W10-15 2920

Balloon entered echo on rt. front near the tight reflectivity gradient. Echo had an associated indentation. This echo produced 120 mph gust and 3/4 inch hail in Lawton area.

SFC WX AT RLS TIME - UPDRAFT - 2256 CST AFT-RLS - WINDS APPROXIMATELY 60-65 KTS. A LOT OF LIGHTNING - HVY RAIN WITH SML HAIL - ENVIRONMENT  
WX - 10/10 CB



CASE 3



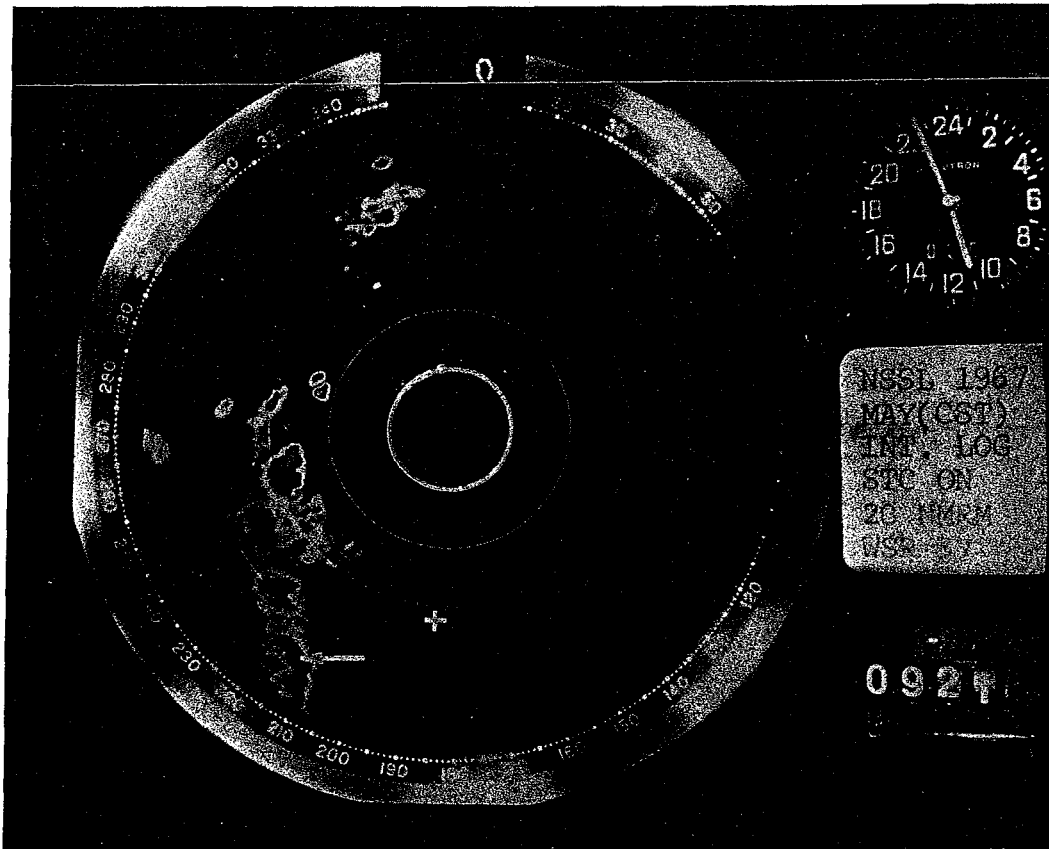
SYNOP - Complex low and frontal systems dominated the surface weather in Oklahoma. Most of the activity developed along and to the north of a mP stationary front across north central Oklahoma. At 500 mb moderate southwesterly flow was occurring.

RADAR - 1405 CST TRW-/NEW 300/62 D8 TOP 360. LN BRNK TRW TRW+/NC 3/76  
313/83 288/166 W18 2725 TOPS 350/400 INCLDS TRW+ 313/83 TOP 500 HAIL  
INDCD AREA BRKN TRW NC 67/118 26/18 359/62 24/108 45/129 MOVMT 2725 TOPS  
300

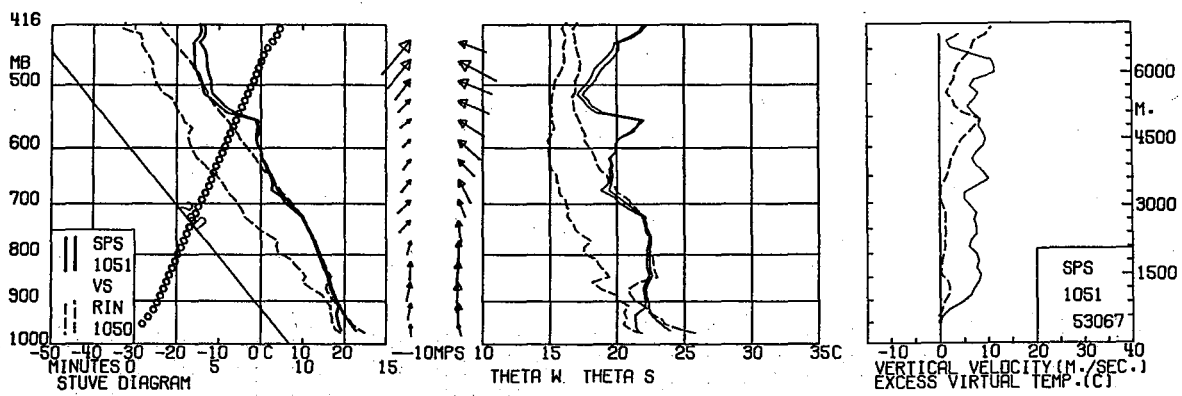
Radar echo that balloon penetrated in ground clutter.\* Believe balloon was overrun by dissipating squall line.

SFC WX AT RLS TIME - 10/10 STRATUS - ENVIRONMENT WX - 10/10 STRATUS

\*Note: The radar ground return is not visible since the first range gate is electronically delayed out to a range of 20 n mi.



CASE 4

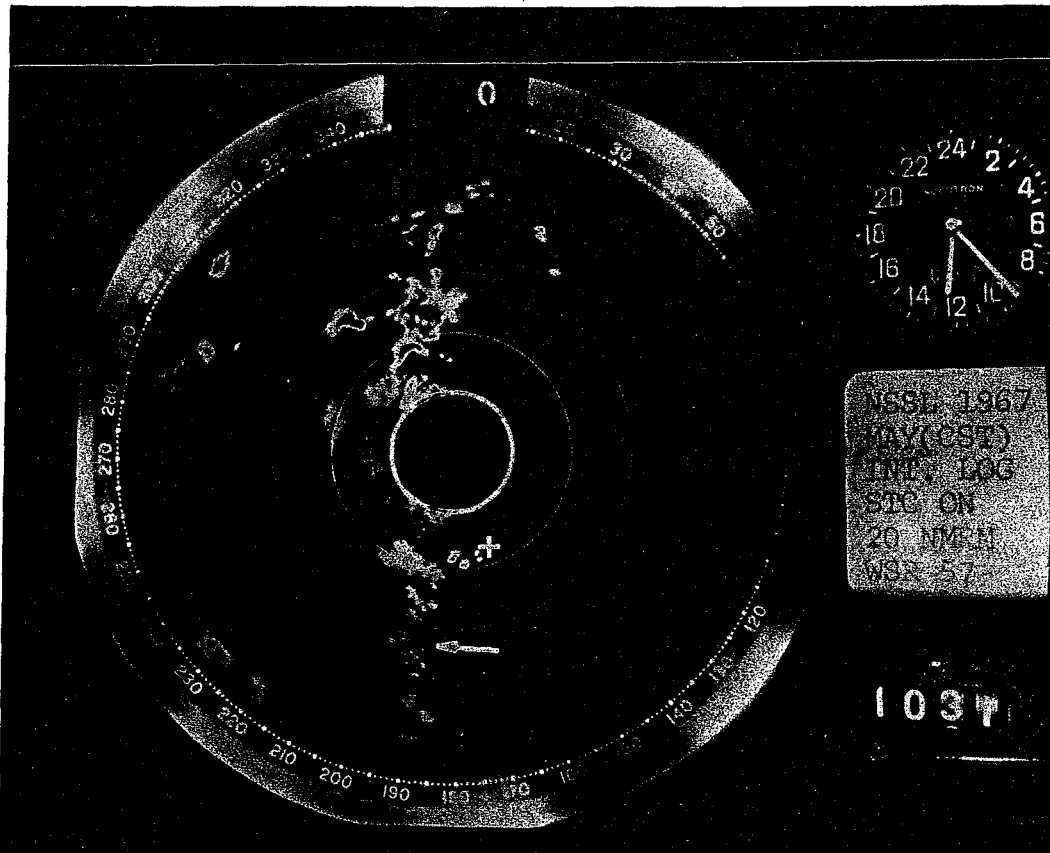


SYNOP - The surface pattern was complex with a developing low pressure trough across western Oklahoma. Thunderstorms developed east of troughing in mT air. Flow at 500 mb remained strong southwesterly as the axis of a long wave trough moved into the Texas Panhandle by midnight.

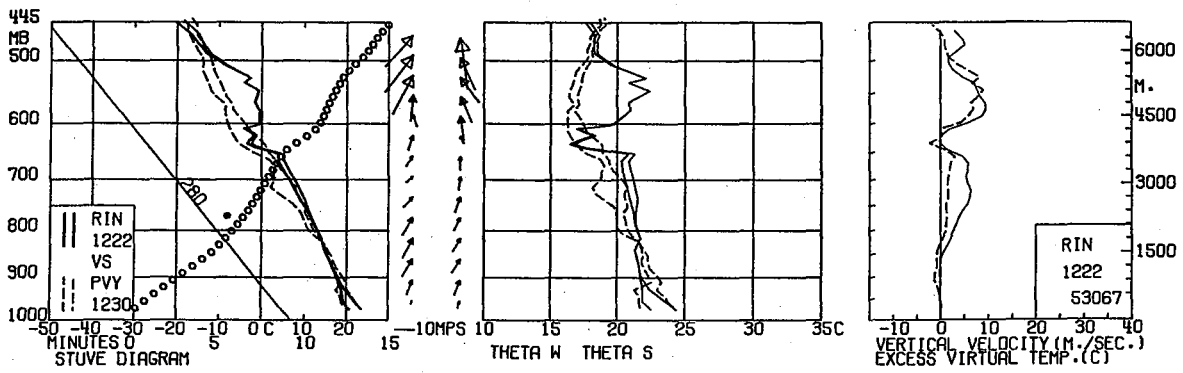
RADAR - 1045 CST - AREA BRKN TRW/+ 343/84 D20 2425 TOP 450 LN BRKN TRW/+  
280/68 250/66 223/85 221/140 W25 CELLS 2335 TOP 550 CELL TRW/NEW 267/101  
D10 TOP 440

Balloon entered on rt. front of radar echo near the tight reflectivity gradient.

SFC WX AT RLS TIME - 10/10 STRATUS WITH R - ENVIRONMENT WX - 10/10 STRATUS



CASE 5

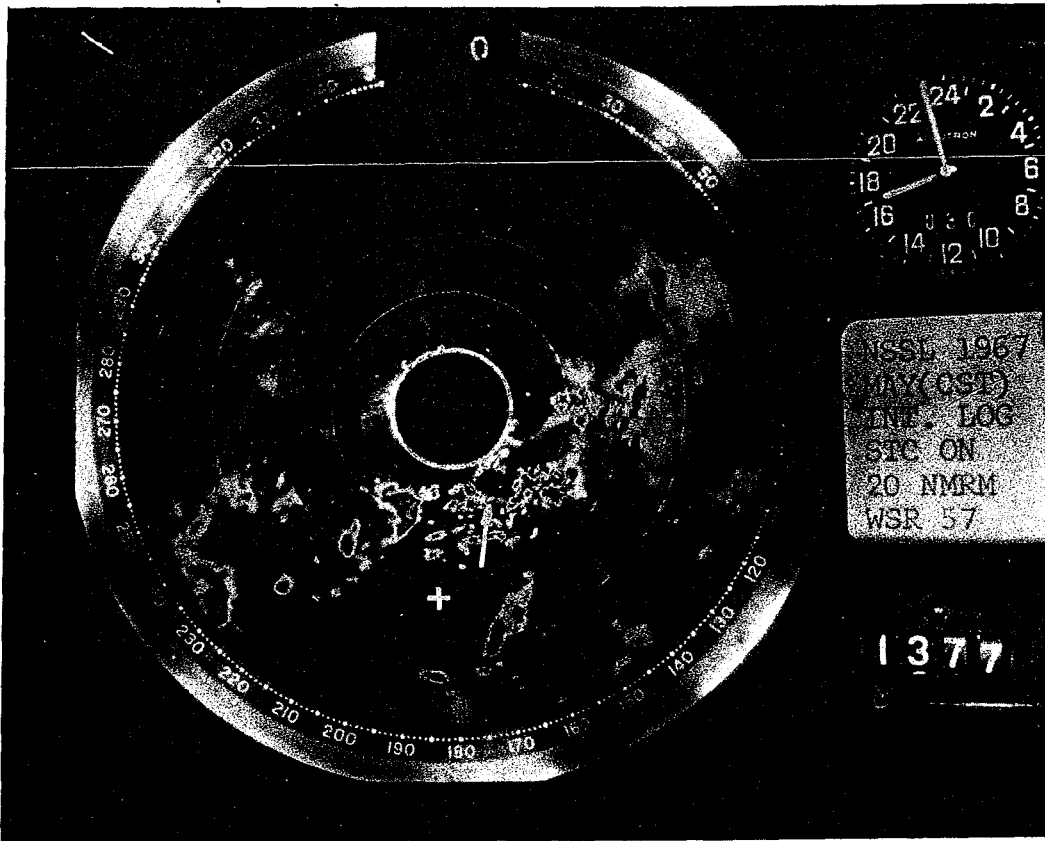


SYNOP - The surface pattern was complex with a developing low pressure trough across western Oklahoma. Thunderstorms developed east of troughing in mT air. Flow at 500 mb remained strong southwesterly as the axis of a long wave trough moved into the Texas Panhandle by midnight.

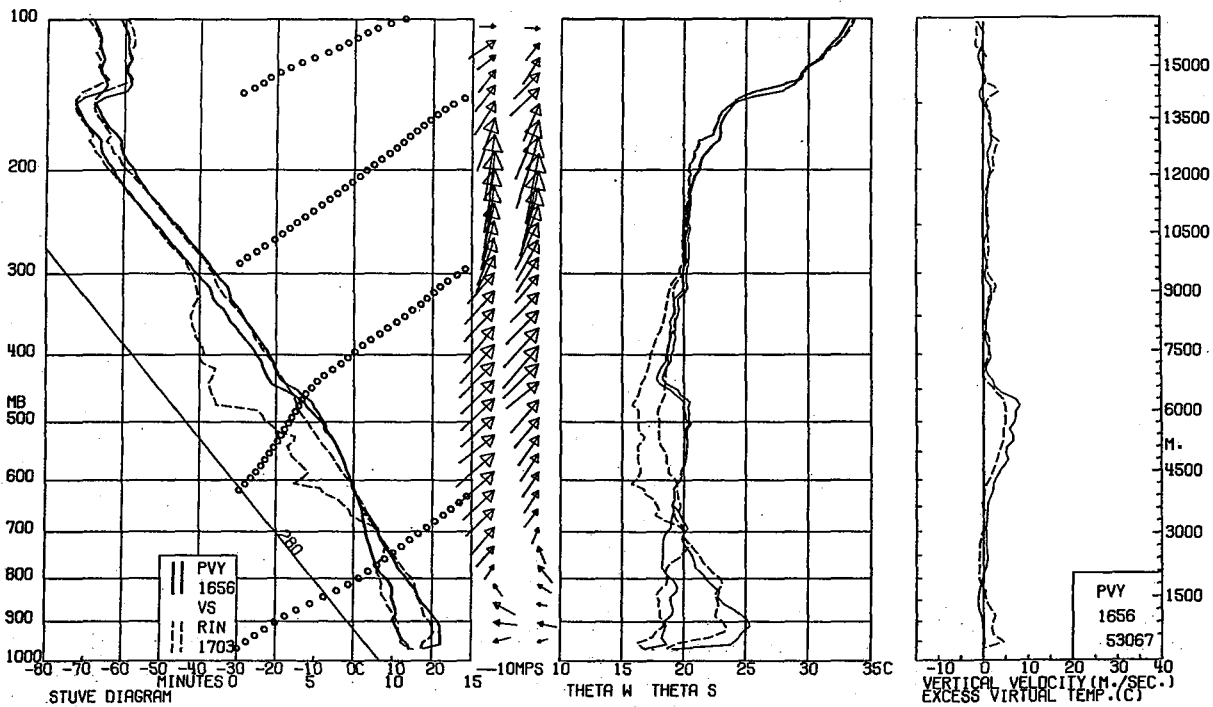
RADAR - 1245 CST - AREA BRKN TRW TRW+/NC 16/99 144/36 182/98 207/132  
242/100 315/124 MOVMT 2335 TOPS 350/450 LN SCTD TRWU 246/212 235/209

Radar reflectivity data looks doubtful.

SFC WX AT RLS TIME - 10/10 CB WITH TRW--, A TERRIFIC STORM HIT RLS SITE  
AFTER LAUNCH OF BALLOON - ENVIRONMENT WX - 2/10 CB, 8/10 STRATUS THUNDER  
HEARD



CASE 6

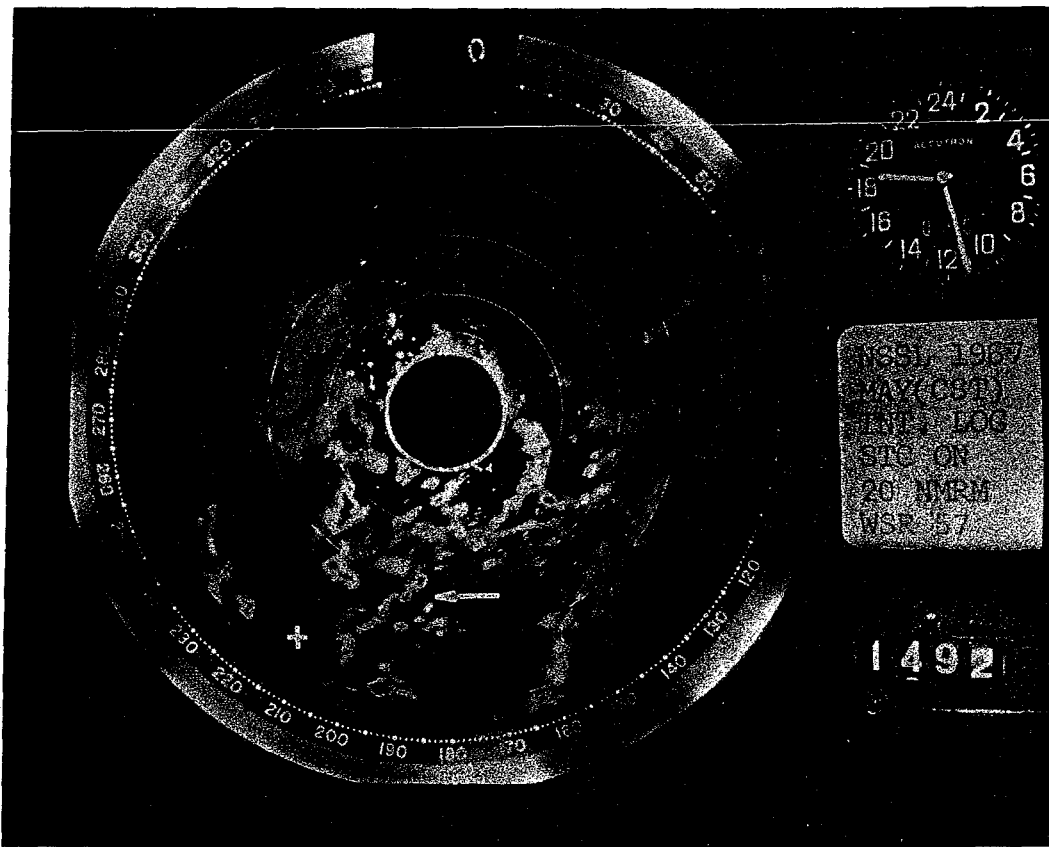


SYNOP - The surface pattern was complex with a developing low pressure trough across western Oklahoma. Thunderstorms developed east of troughing in mT air. Flow at 500 mb remained strong southwesterly as the axis of a long wave trough moved into the Texas Panhandle by midnight.

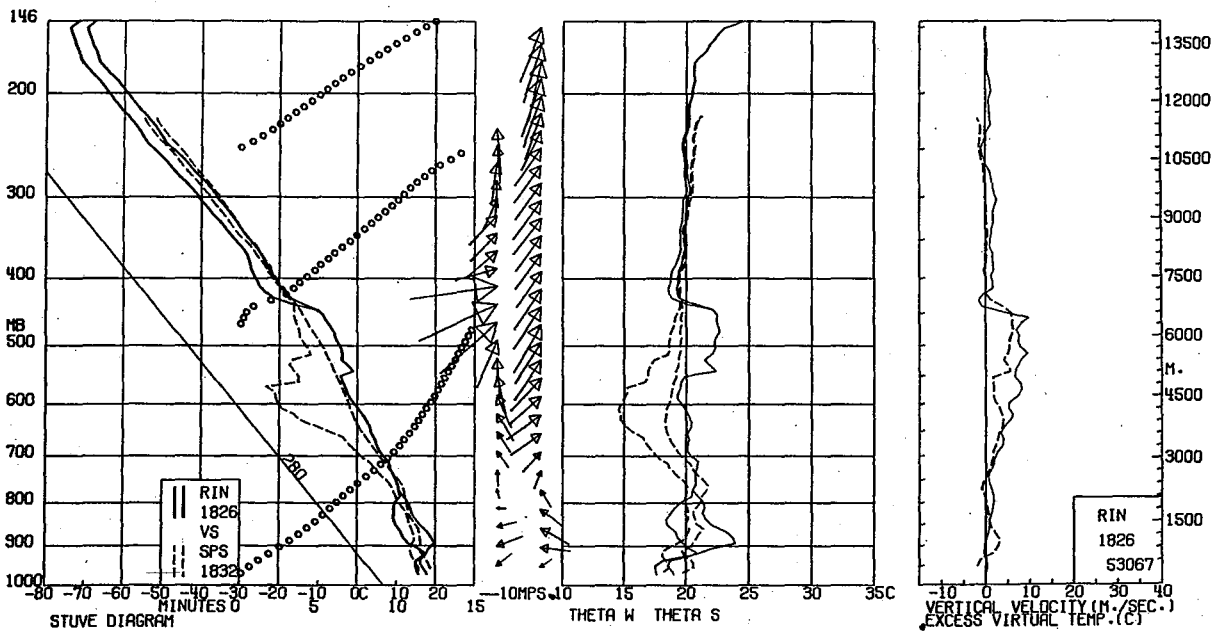
RADAR - 1645 CST - CELLS TRWU 33/181 341/190 308/148 284/190 288/236 D4  
AREA BRKN TRW- TRW/NC 32/131 45/154 96/117 155/142 215/164 253/143  
292/121 275/36 70/25 2330 TOP 300/350 STRNGST 214/47 TOP 450 TRW- 150/106  
234/113 CELL TRW/NC 335/114 D4 2520 TOP 360

Balloon entered echo on rt. front near area of tight reflectivity gradient.

SFC WX AT RLS TIME - 4/10 CB, 6/10 STRATUS, WITH TRW- ENVIRONMENT WX -  
5/10 CB 5/10 ALTOSTRATUS



CASE 7

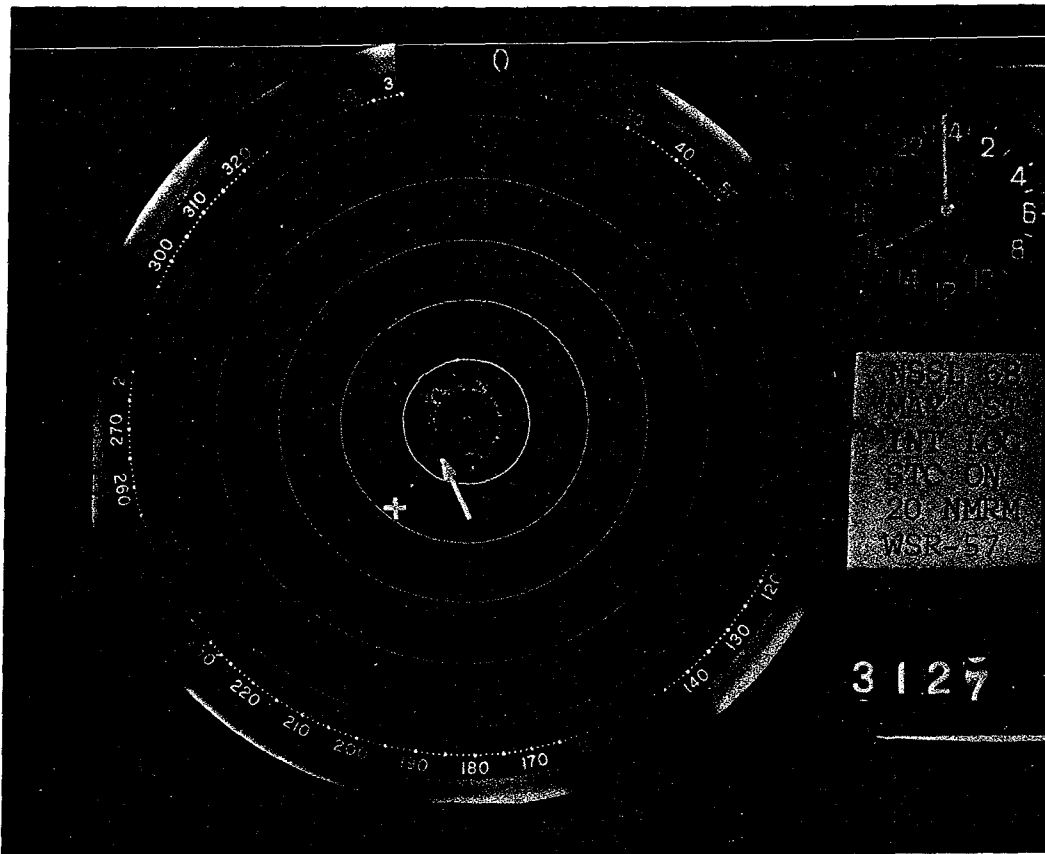


SYNOP - The surface pattern was complex with a developing low pressure trough across western Oklahoma. Thunderstorms developed east of troughing in mT air. Flow at 500 mb remained strong southwesterly as the axis of a long wave trough moved into the Texas Panhandle by midnight.

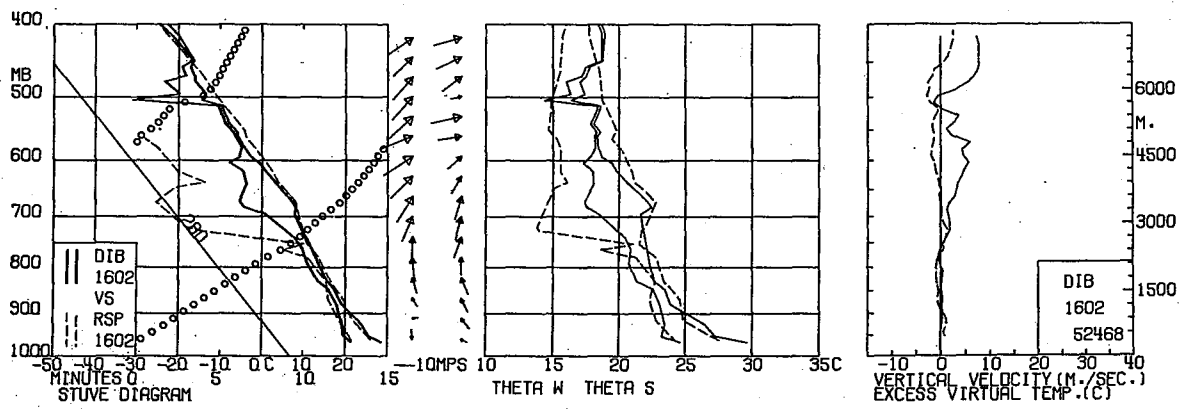
RADAR - 1845 CST - AREA BRKN TRW- TRW/NC 70/72 68/128 97/152 150/146  
206/157 300/211 2330 TOPS 200/300 ISOLD TRW+ TOPS 450 CELL TRWU 204/191  
D15 CELL TRWU 18/189 D5

Balloon was overrun by echo at 3 km and entered the rt. front near a tight reflectivity gradient.

SFC WX AT RLS TIME - 8/10 CB 2/10 ALTOSTRATUS - ENVIRONMENT WX - 10/10  
STRATUS WITH MODERATE RAIN



CASE 8

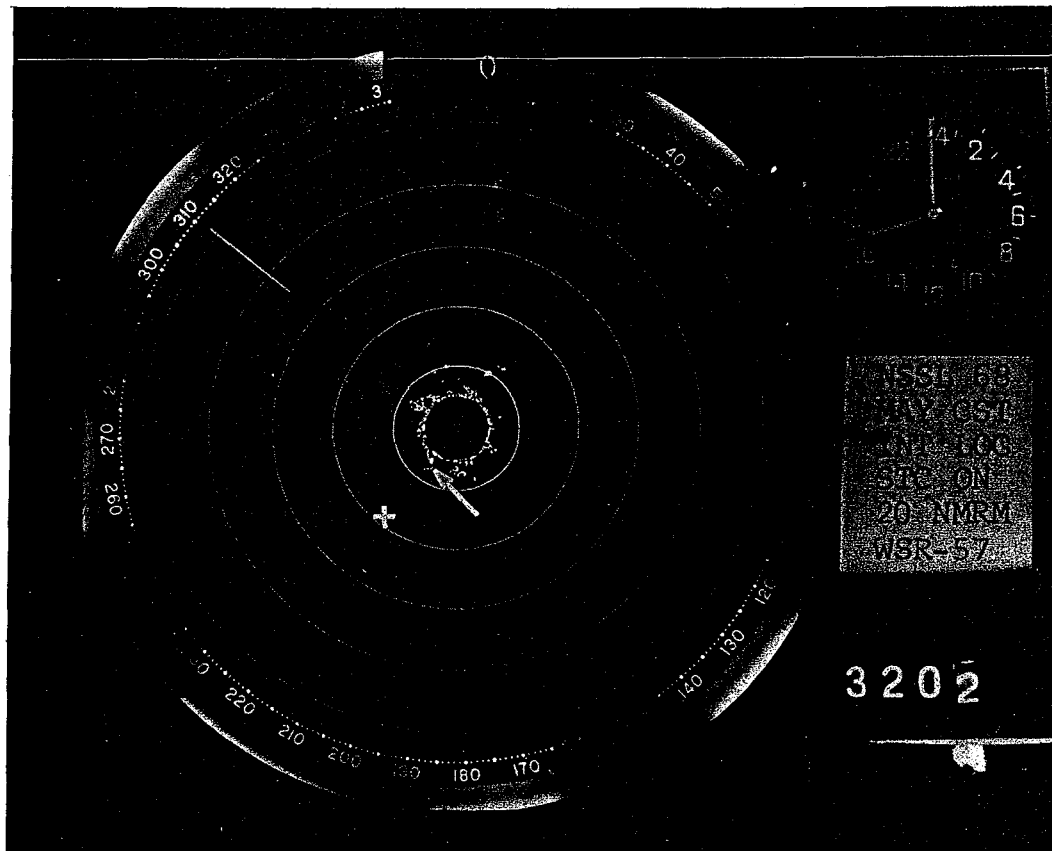


SYNOP - Thunderstorms developed along a quasi-stationary cP front in the mT air. At 500 mb a short wave moved in strong southwesterly flow across central Oklahoma.

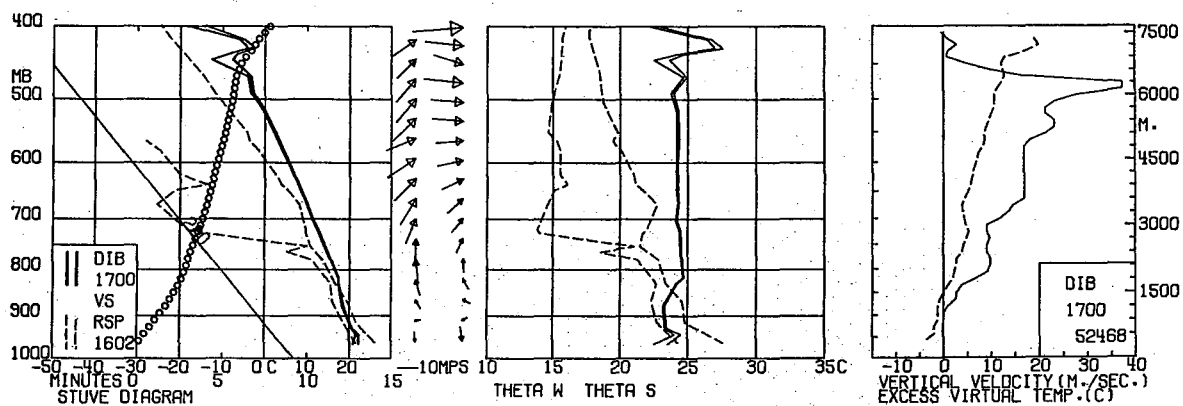
RADAR - 1545 CST CELL TRW/NEW 221/130 D4 TOP 300 CELLS TRWU 231/223  
240/242 D4

Balloon was overrun by echo at 3 km. Balloon entered rt. front quadrant of echo. At time of entry echo had developed a tight reflectivity gradient and contained an indentation indicative of a weak echo region.

SFC WX AT RLS TIME - 3/10 CB 3/10 TCU 3/10 CU WITH TRW IN PROGRESS -  
ENVIRONMENT WX - 10/10 CU



CASE 9

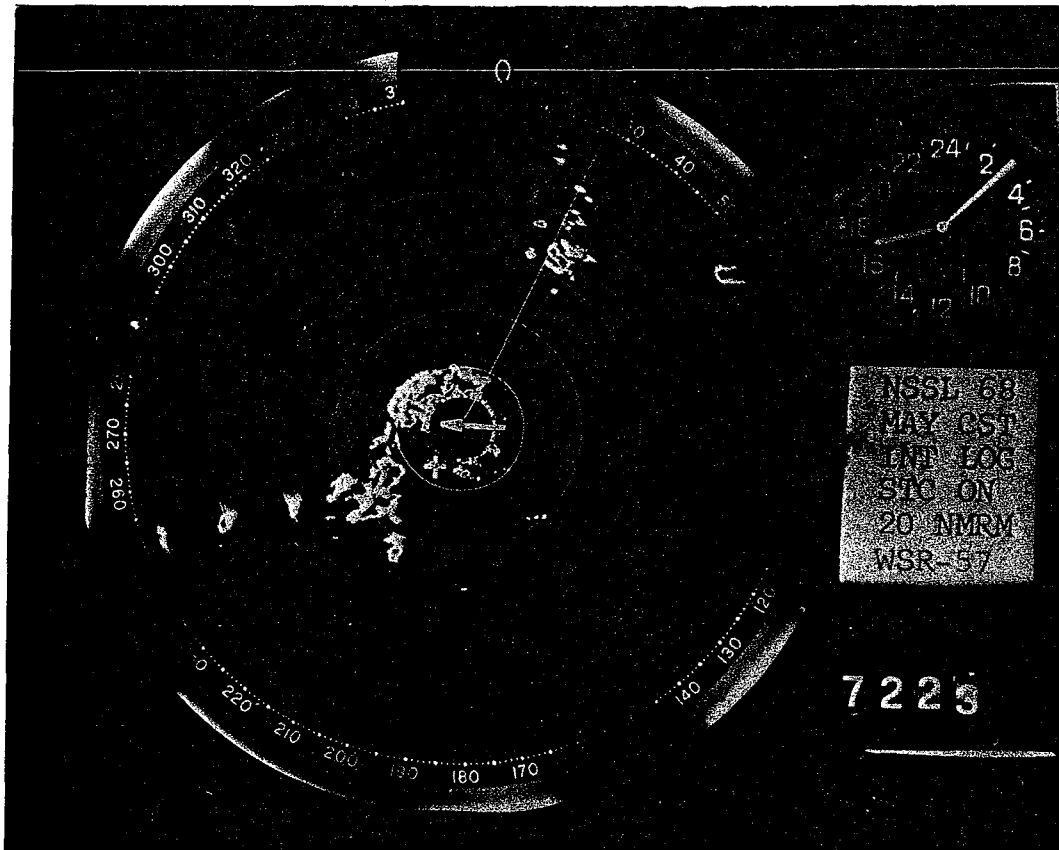


SYNOP - Thunderstorms developed along a quasi-stationary cP front in the mT air. At 500 mb a short wave moved in strong southwesterly flow across central Oklahoma.

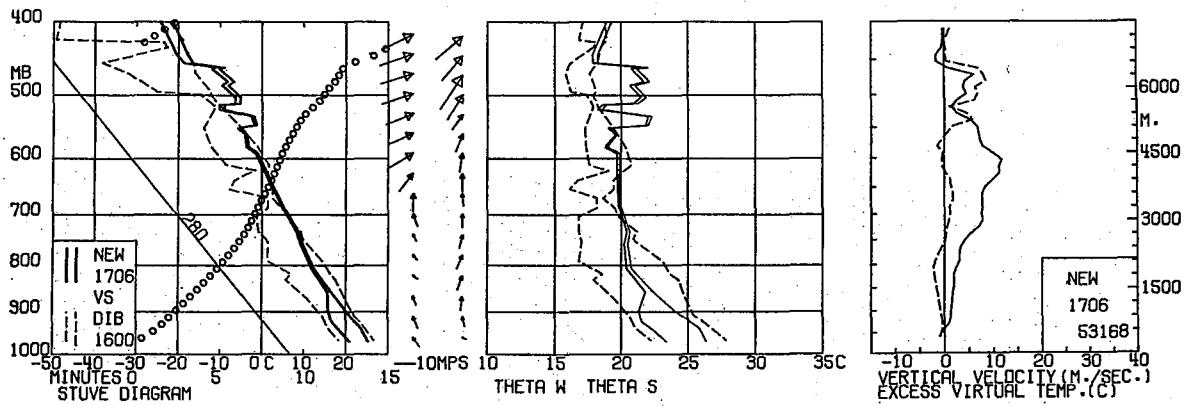
RADAR - 1645 CST AREA SCTD TRW/+ 132/8 240/21 W12 2515 MAX TOP 400 AT  
210/11 CELLS TRWU 226/151 225/176 228/222 237/224 D10 2720

Balloon entered rt. rear of radar echo. This echo became severe and was associated with numerous reports of hail and funnels from 1800-2100 CST.

SFC WX AT RLS TIME - 4/10 CB 4/10 TCU 2/10 ALTOCU WITH TRW- IN PROGRESS -  
ENVIRONMENT WX - 10/10 CUMULUS



CASE 10

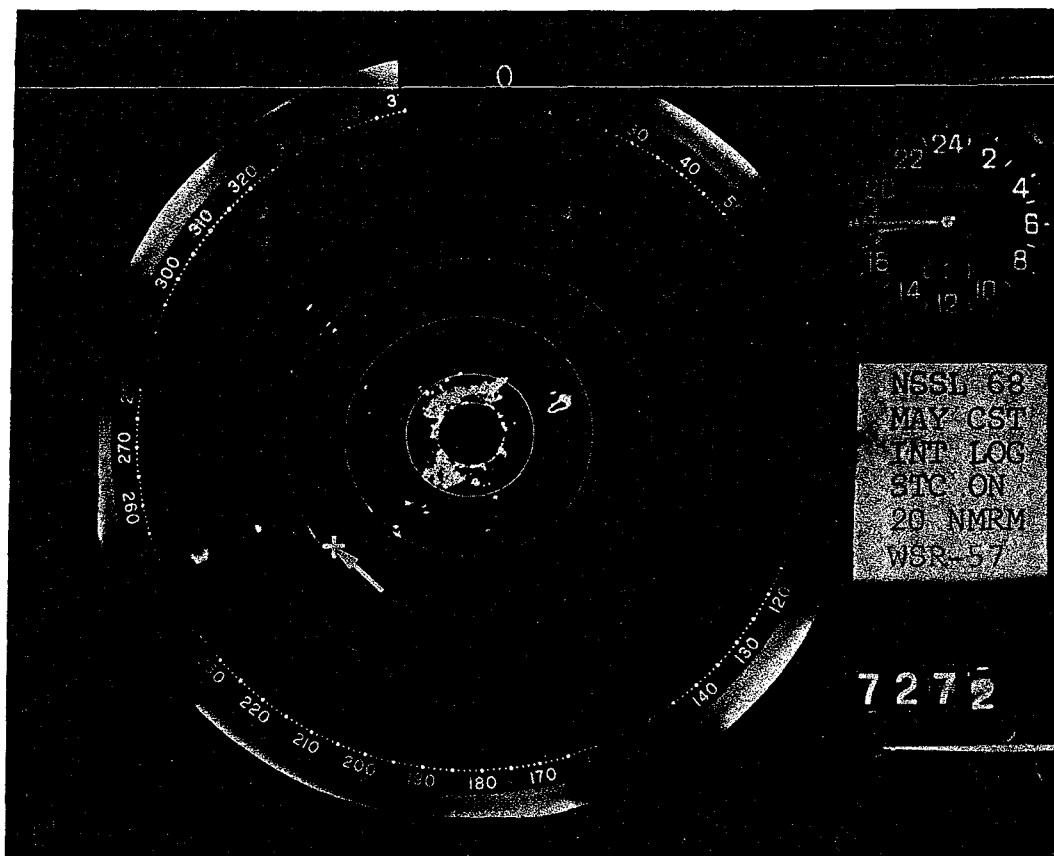


SYNOPSIS - A line of thunderstorms developed out ahead of an advancing cP front in the mT air. Flow at 500 mb was southwesterly.

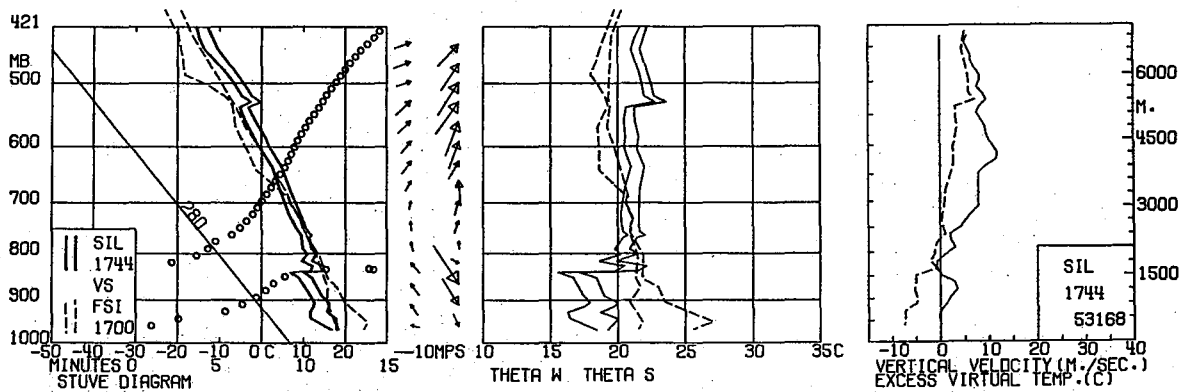
RADAR - LN BRKN TRW+/NC 335/24 261/43 257/103 W25 CELLS 2830 LN BRKN TRW/NEW 245/44 222/59 W15 RHINO SHORT PULSE ONLY

Balloon entered echo in ground clutter pattern.

SFC WX AT RLS TIME - 10/10 CB WITH TRW-- IN PROGRESS - ENVIRONMENT WX - 3/10 CB 4/10 ALTOCU WITH THUNDER HEARD



CASE 11

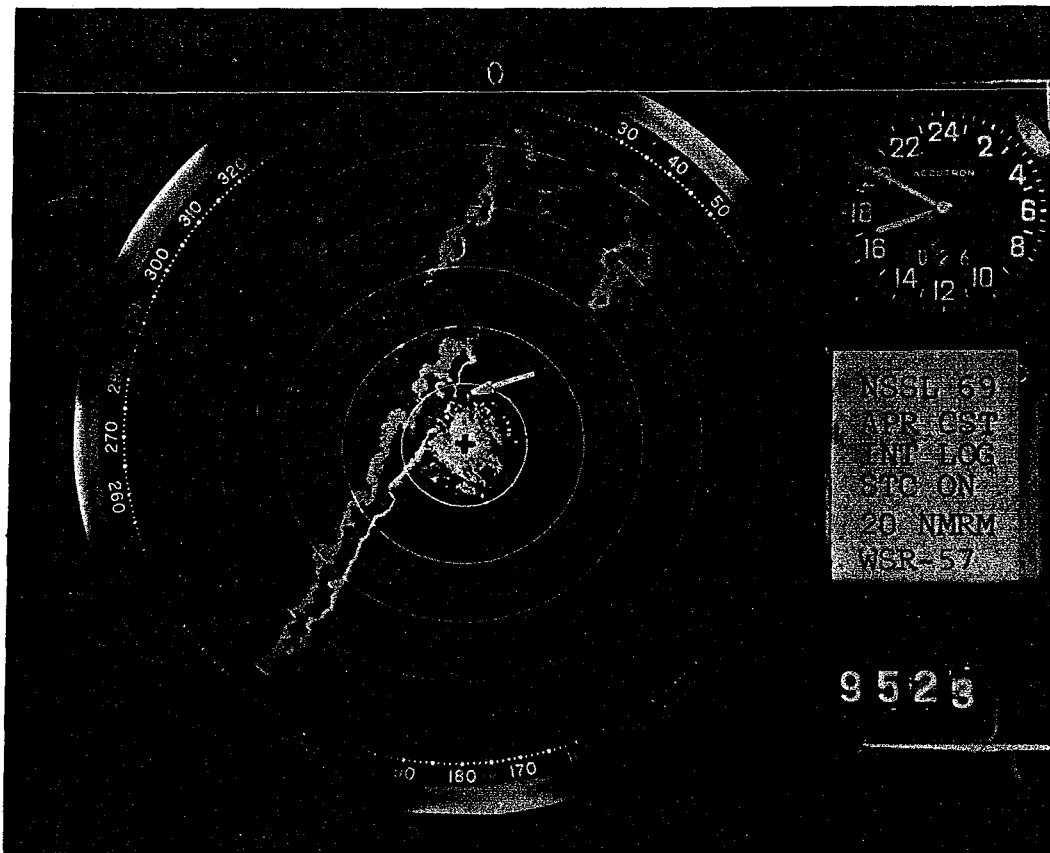


SYNOP - A line of thunderstorms developed out ahead of an advancing cP front in the mT air. Flow at 500 mb was southwesterly.

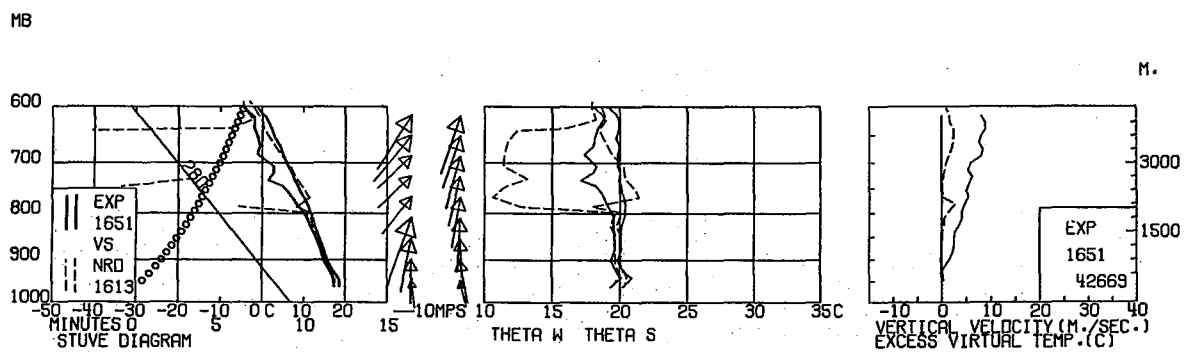
RADAR - LN BRKN TRW+/NC 33/45 241/48 260/145 W30 2830 MAX TOP 500 AT 228/45 CELLS TRWU 273/188 262/125 CELLS TRW/NEW 64/119 36/49 67/174 D5 0000

Radar data doubtful.

SFC WX AT RLS TIME - WX FOR RLS SITE AND ENVIRONMENT SITE MISSING



CASE 12

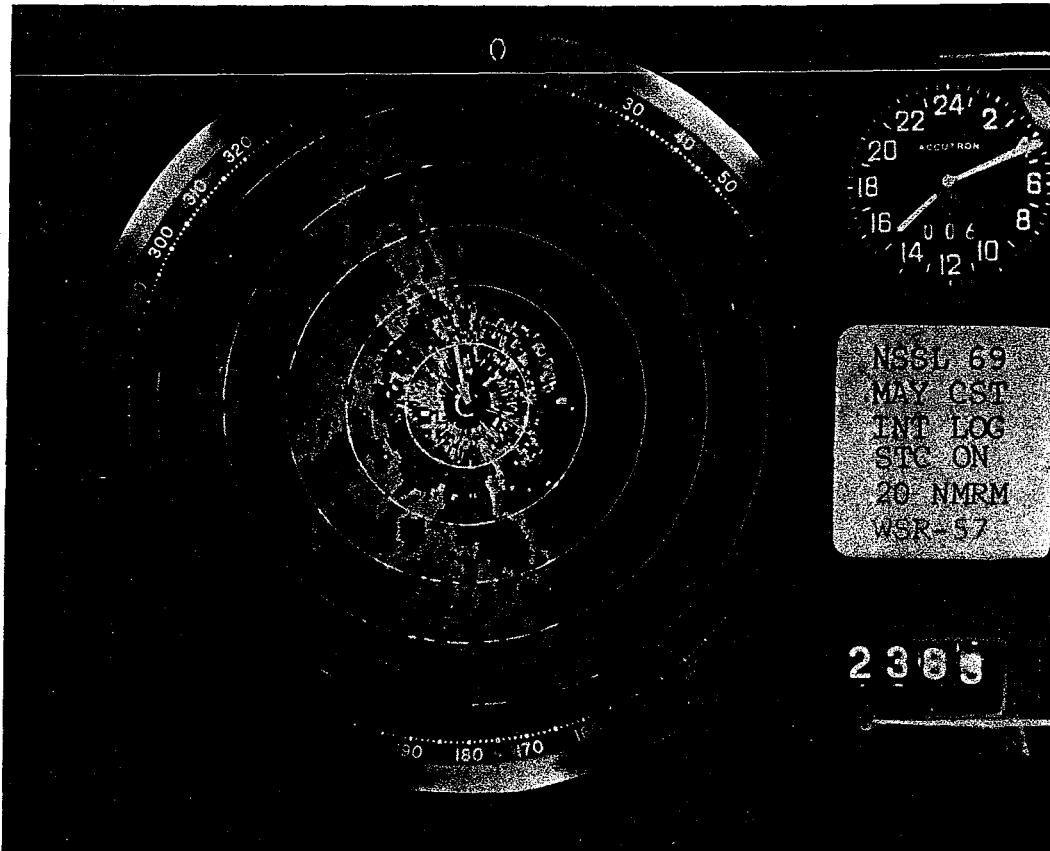


SYNOP - Thunderstorms formed ahead of a slow moving mP front in northwestern Oklahoma in the mT air. A short wave moved in southwesterly flow at 500 mb.

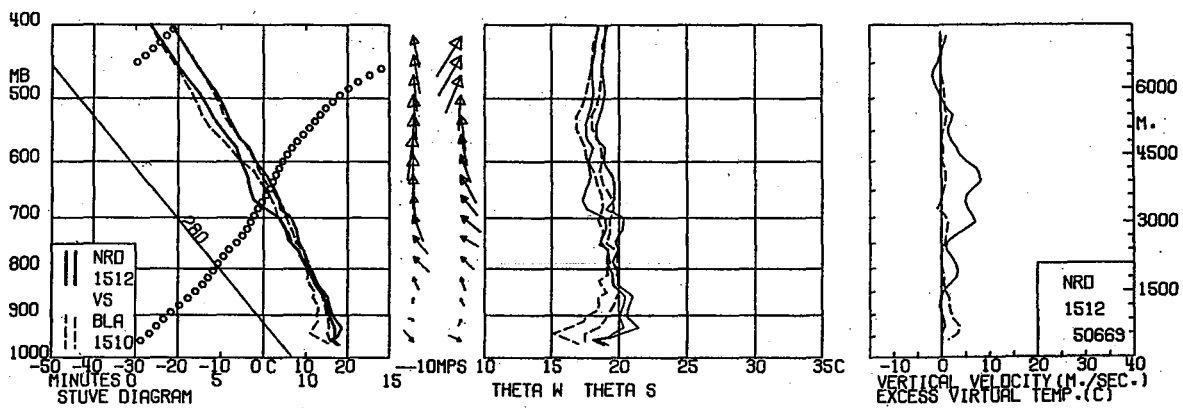
RADAR - LN OVC TRW+/NC 11/150 349/63 265/27 227/106 18W 2530 CELLS 2235  
MAX TOPS 480 AT 286/25 FUNNEL AT 284/27 AT 1625 CST. LN BRKN TRW+/+  
24/138 47/72 48/46 10W 2530 MAX TOPS 460 AT 46/68

Balloon entered the rt. rear of the radar echo near a tight reflectivity gradient. Much severe weather along squall line.

SFC WX AT RLS TIME - 10/10 STRATUS - ENVIRONMENT WX - 10/10 STRATUS WITH  
RW- IN PROGRESS



CASE 13

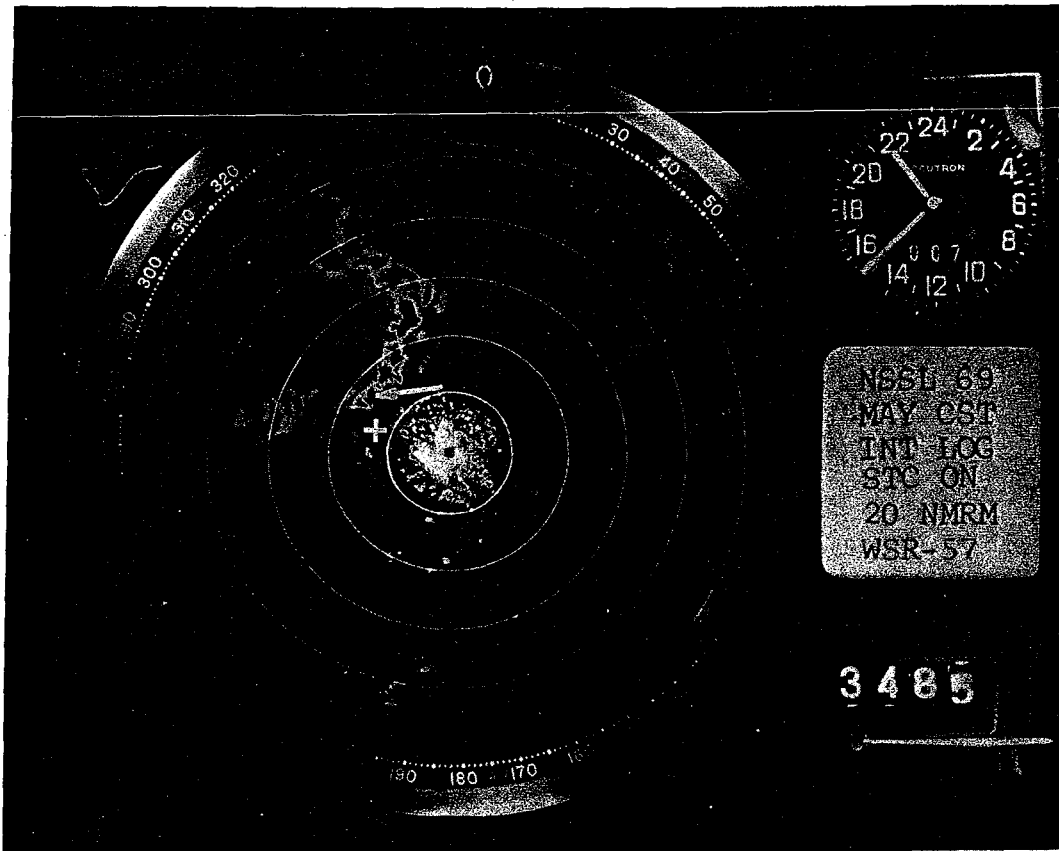


SYNOP - A weak mP front located in northwest Oklahoma during the morning moved through Oklahoma during the day. Thunderstorms formed in the mT air mass. At 500 mb a cut-off low over the Arizona-New Mexico border began filling and moved northeastward.

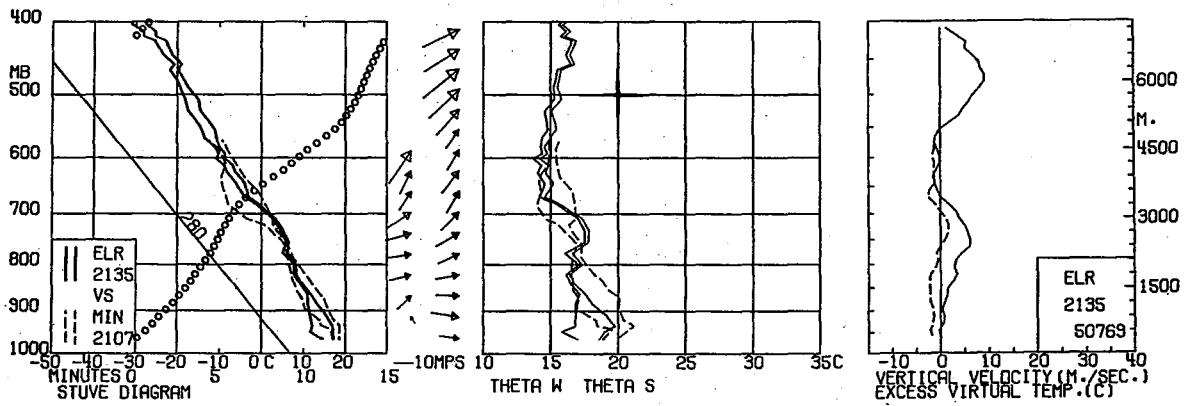
RADAR - AREA BRKN TRW+/NC 310/133 350/63 156/56 243/130 2330 MAX TOPS  
390 AT 223/13 AND 370 AT 334/35

Balloon entered radar echo within 1 km of radar site.

SFC WX AT RLS TIME - 10/10 CB WITH TRW- IN PROGRESS - ENVIRONMENT WX MISSING



CASE 14

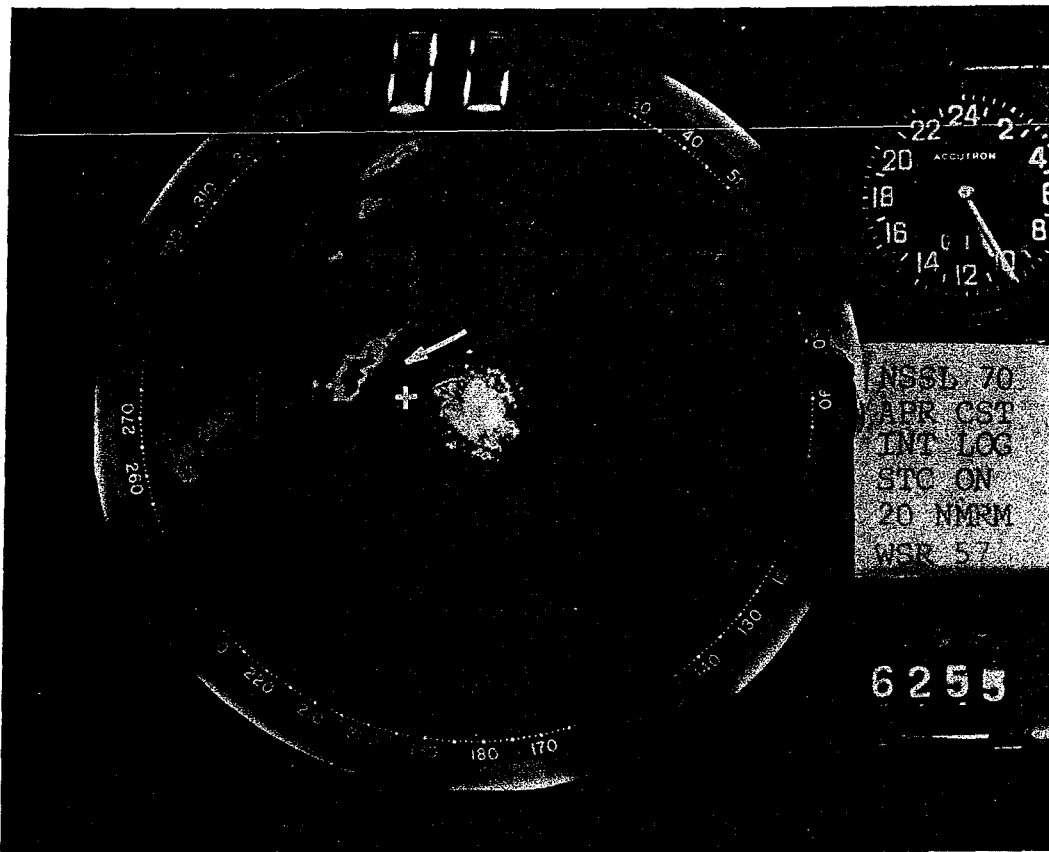


SYNOP - Thunderstorms formed in the mP air mass, as a low at 500 mb opened into a trough and a short wave impulse moved across Oklahoma. A vigorous cP front swept into northwestern Oklahoma by midnight.

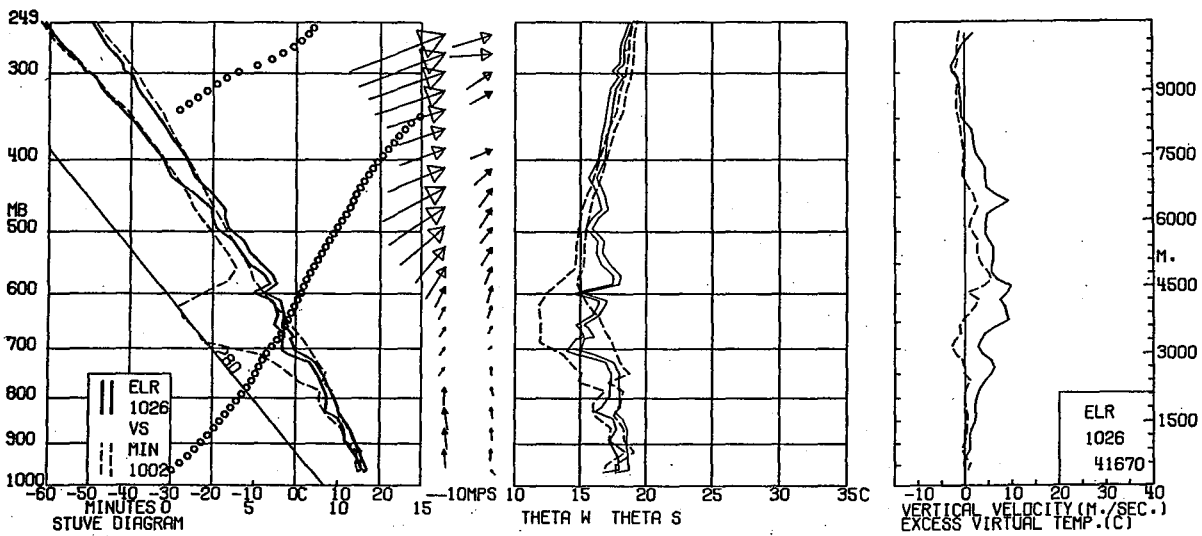
RADAR - LN BRKN TRW+/NC 332/104 337/54 296/41 277/80 25W 2225 MAX TOP  
440 AT 339/64 LN BRKN TRW/+ 8/134 351/138 332/134 10W 2225 AREA SCTD  
TRW-/NEW 122/98 125/138 147/141 195/135 210/87 D3 MAX TOP 260

Balloon entered the rt. rear of the radar echo that had an associated tight reflectivity gradient and an indentation.

SFC WX AT RLS TIME - 8/10 CB WITH RW IN PROGRESS - ENVIRONMENT WX -  
2/10 CB 2/10 CU 4/10 ALTOSTRATUS



CASE 15

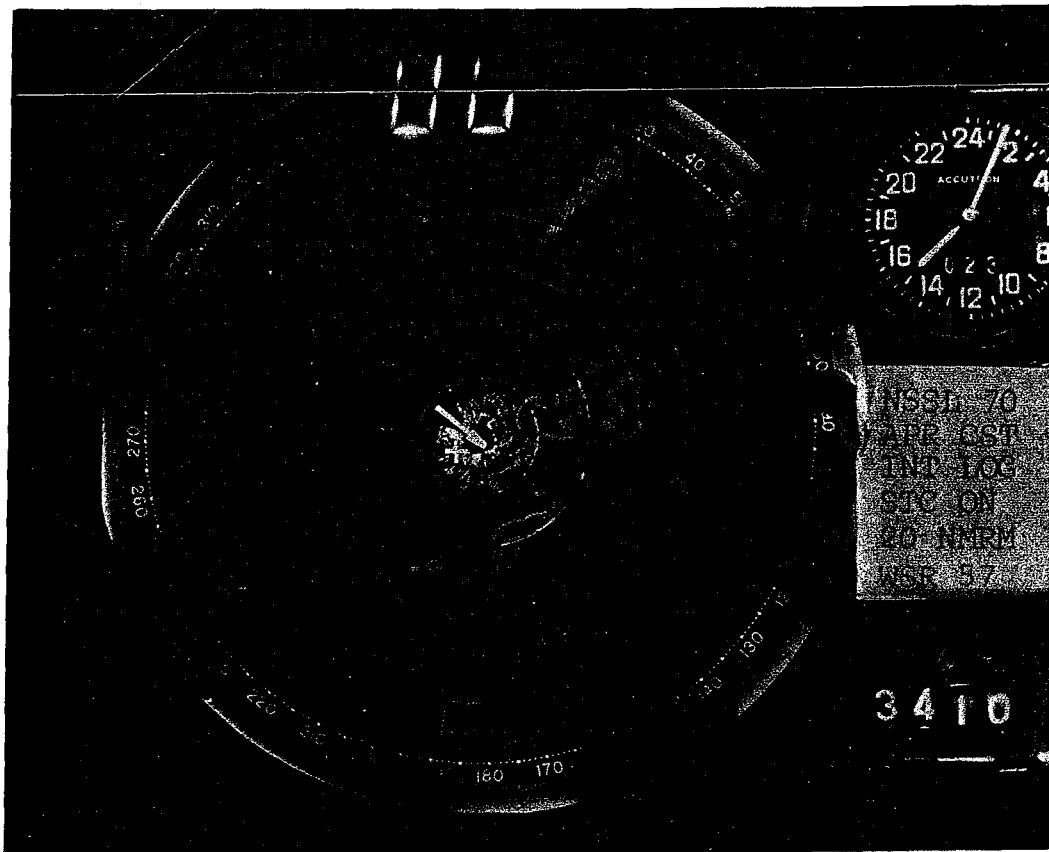


SYNOP - Thunderstorms developed in the mT air mass ahead of a slow moving mP front. Most of the early morning activity moved northeastward in association with a short wave at 500 mb. Activity redeveloped later in the day as overrunning thunderstorms in the mP air.

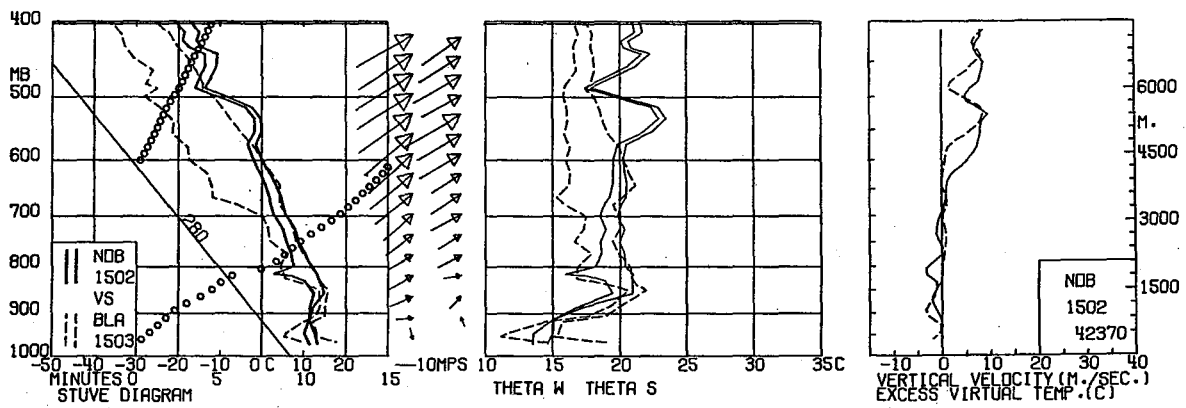
RADAR - AREA SCTD TRW/NC 358/155 344/38 242/117 277/116 D4 CELLS 2430  
MAX TOP 380 307/28 TOPS 370 AT 342/89 AND 350 AT 333/71

Balloon entered rt. front of radar echo near indentation.

SFC WX AT RLS TIME - 10/10 CB WITH TRW- IN PROGRESS - ENVIRONMENT WX -  
SKY TOTALLY OBSCURED IN FOG



CASE 16

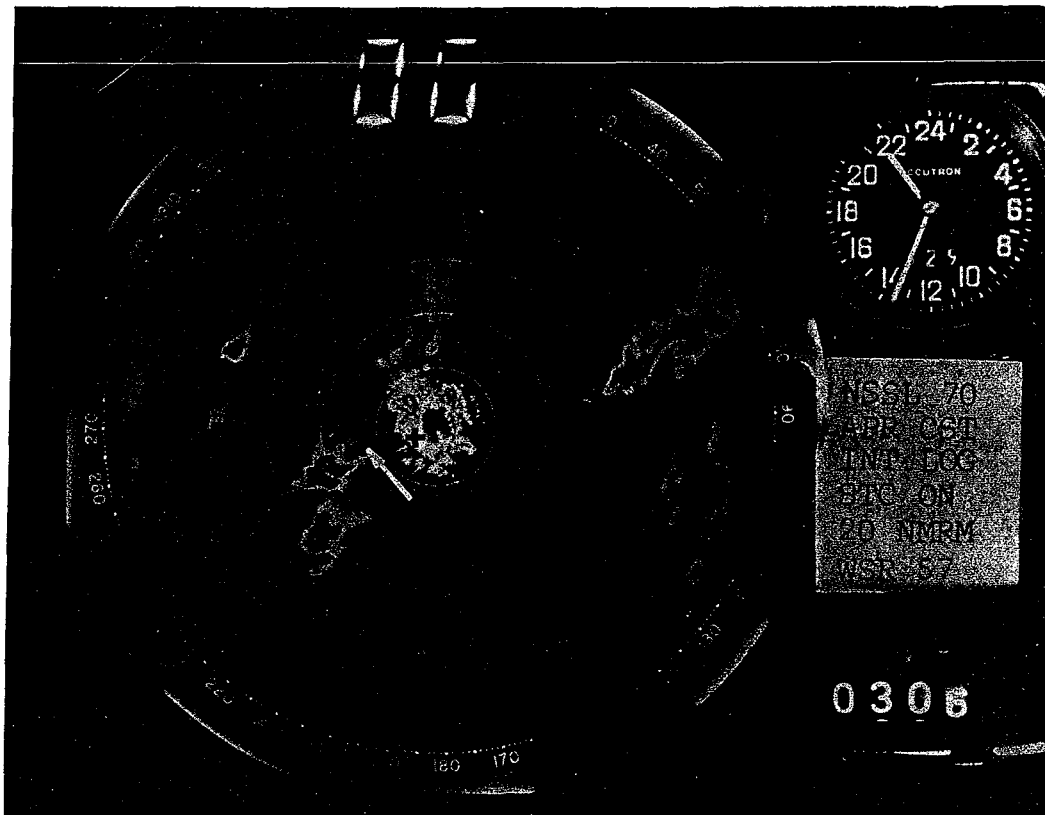


SYNOPSIS - Overrunning thunderstorms developed across central Oklahoma in the mP air mass north of the quasi-stationary mP front in southern Oklahoma. This front drifted slowly southward during the day and on into northern Texas. At 500 mb, the flow remained moderate westerly.

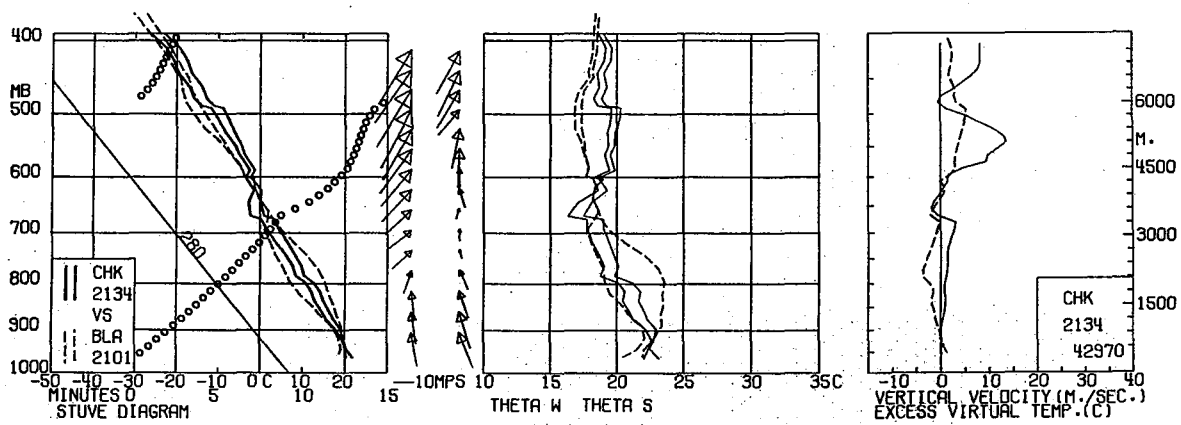
RADAR - LN BRKN TRW/NC 37/165 33/106 11W CELLS 2440 MAX TOP 460 AT 38/130  
AREA BRKN TRW+/NC 59/110 93/93 212/76 27/24 CELLS 2440 MAX TOP 550 130/34  
LN SCTD/NC 159/102 190/107 208/157 15W CELLS 2440 MAX TOP 350 AT 184/105

The balloon entered the left rear of the radar echo.

SFC WX AT RLS TIME - 4/10 CUFRA 6/10 CU WITH RW- IN PROGRESS - ENVIRONMENT  
WX - 5/10 CU 2/10 STRATUS



CASE 17

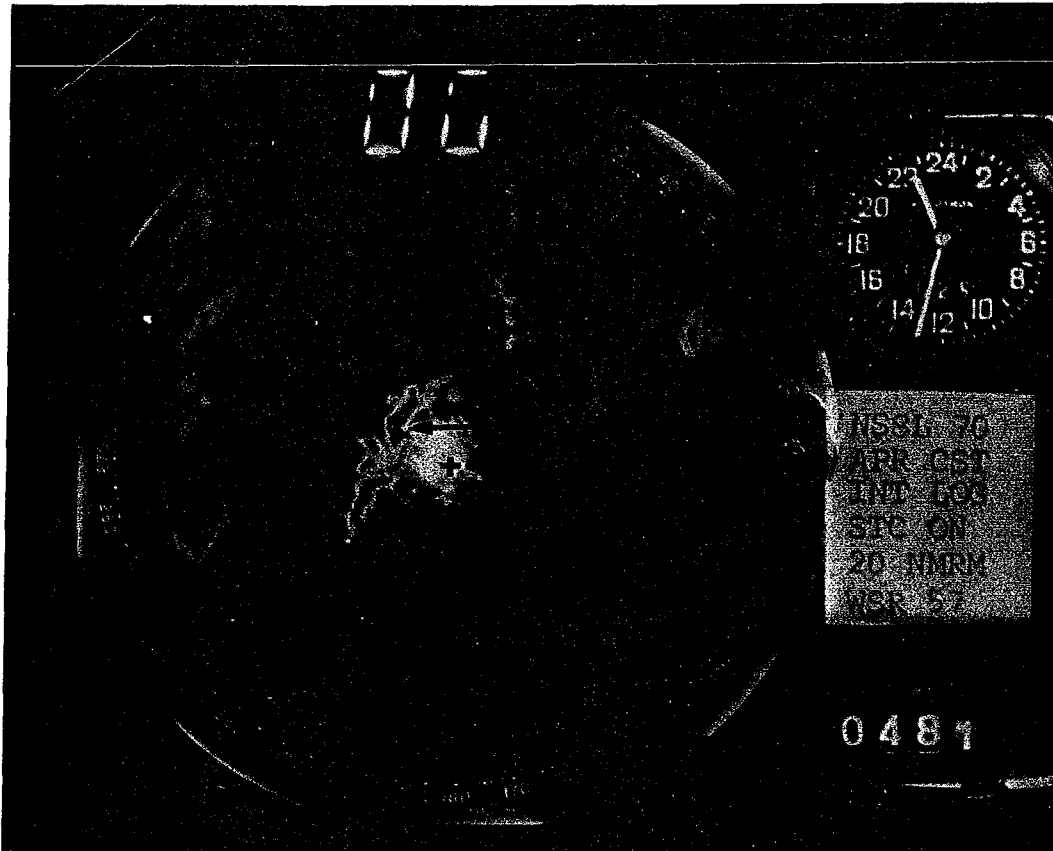


SYNOP - A sharp 500 mb trough line was oriented NNE-SSW across eastern New Mexico. An old cP front, coincident with a dry line, was located in western Oklahoma. Thunderstorms developed in the mT air as an open wave developed along the front in western Oklahoma.

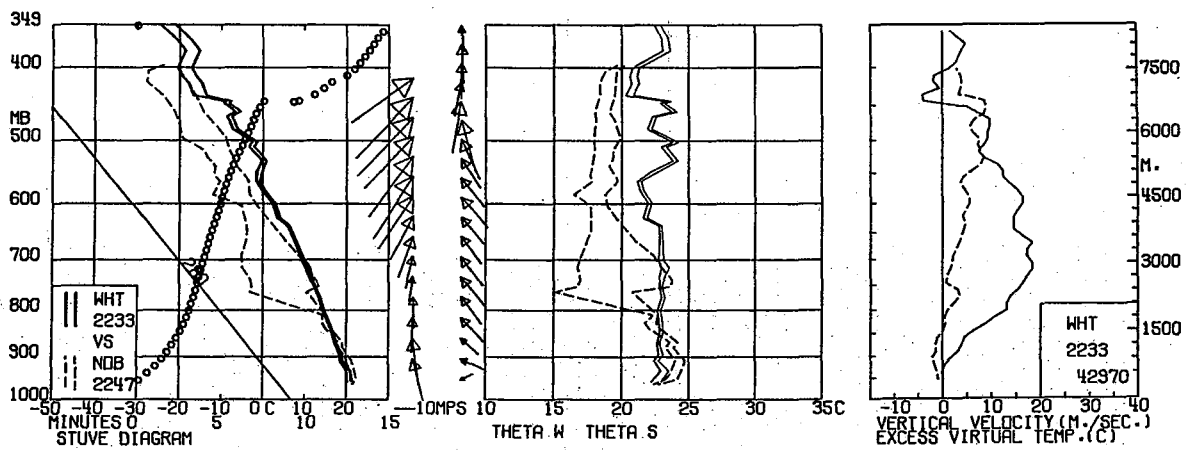
RADAR - AREA SCTD TRW+/NC 67/128 144/136 256/154 303/112 CELLS 2240 MAX  
TOP 560 AT 251/122 AND TOP 490 AT 234/49

Balloon entered radar echo on left front near an indentation.

SFC WX AT RLS TIME - 10/10 CB WITH TRW- IN PROGRESS FQT LTGICCCCG -  
ENVIRONMENT WX - 10/10 CU



CASE 18

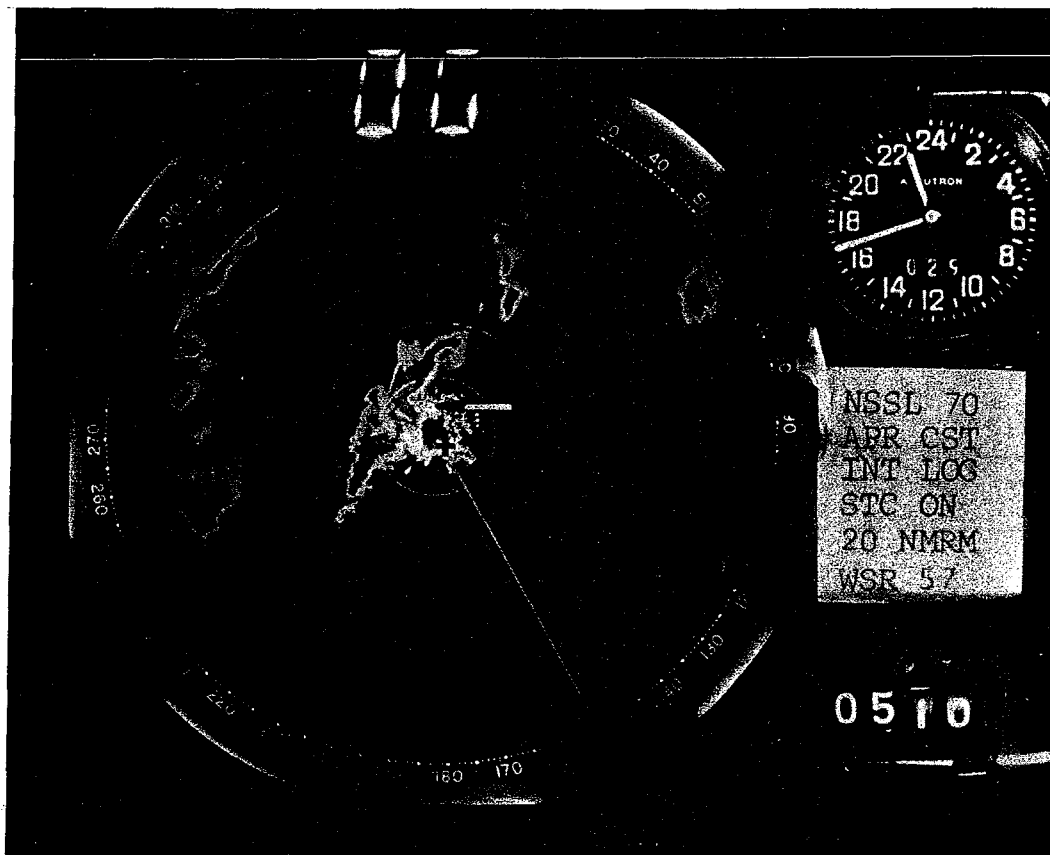


SYNOPSIS - A sharp 500 mb trough line was oriented NNE-SSW across eastern New Mexico. An old cP front, coincident with a dry line, was located in western Oklahoma. Thunderstorms developed in the mT air as an open wave developed along the front in western Oklahoma.

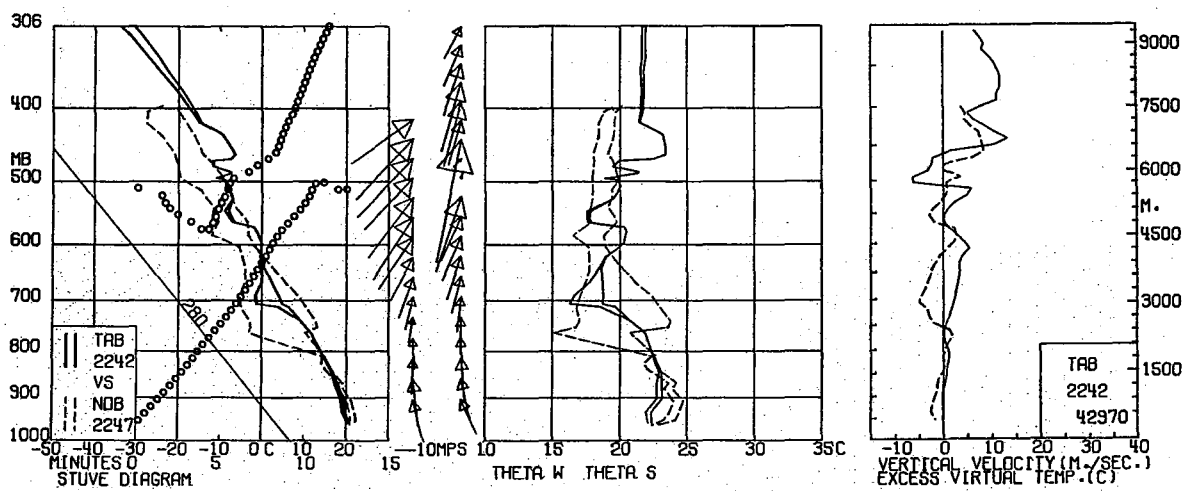
RADAR - AREA BRKN TRW/NC 70/123 D50 CELLS 2235 MAX TOP 540 AT 71/107  
AREA BRKN TRW/NC 27/82 231/46 25W CELLS 2235 MAX TOP 460 AT 247/28 AREA  
BRKN TRW+A/NC 339/129 250/76 235/209 288/135 D15 CELLS 2335 MAX TOP 620  
AT 257/92 GOLF BALL SIZE HAIL CELL AT 257/92

Balloon entered radar echo to rt. rear in hook shaped indentation near tight reflectivity gradient.

SFC WX AT RLS TIME - 10/10 STRATUS WITH RW- IN PROGRESS - ENVIRONMENT  
WX - 3/10 CB 7/10 CU



CASE 19

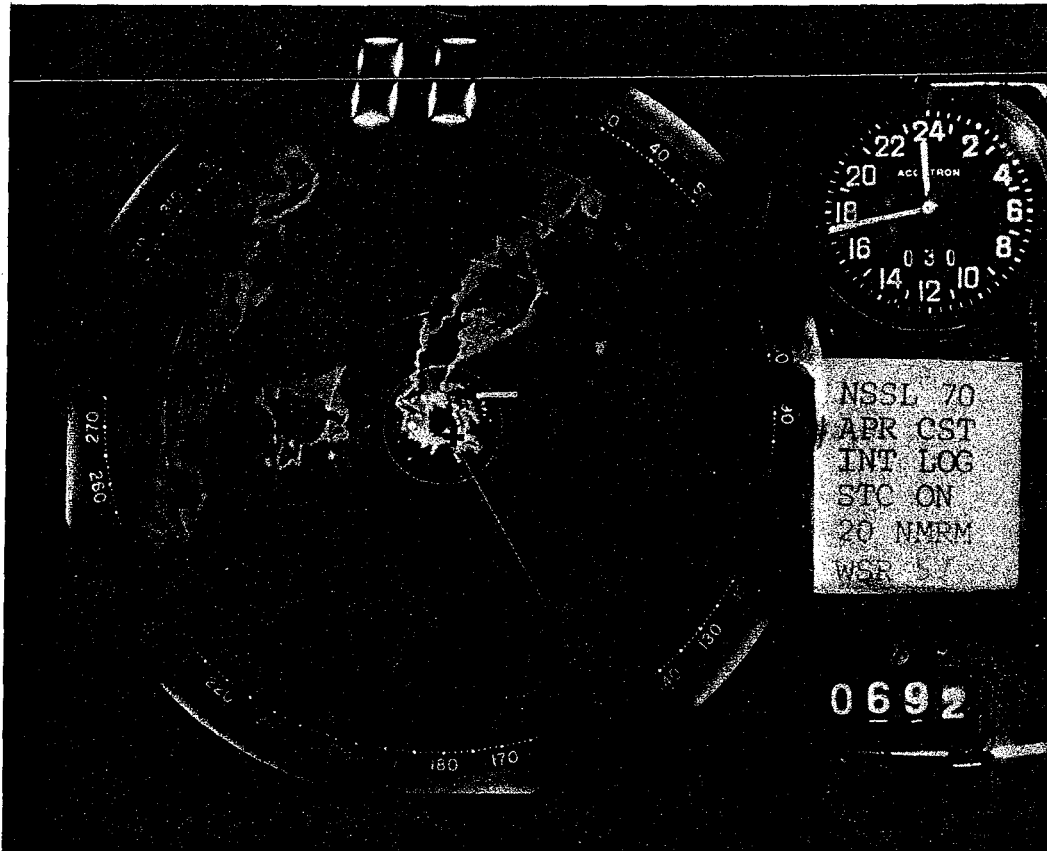


SYNOPSIS - A sharp 500 mb trough line was oriented NNE-SSW across eastern New Mexico. An old cP front, coincident with a dry line, was located in western Oklahoma. Thunderstorms developed in the mT air as an open wave developed along the front in western Oklahoma.

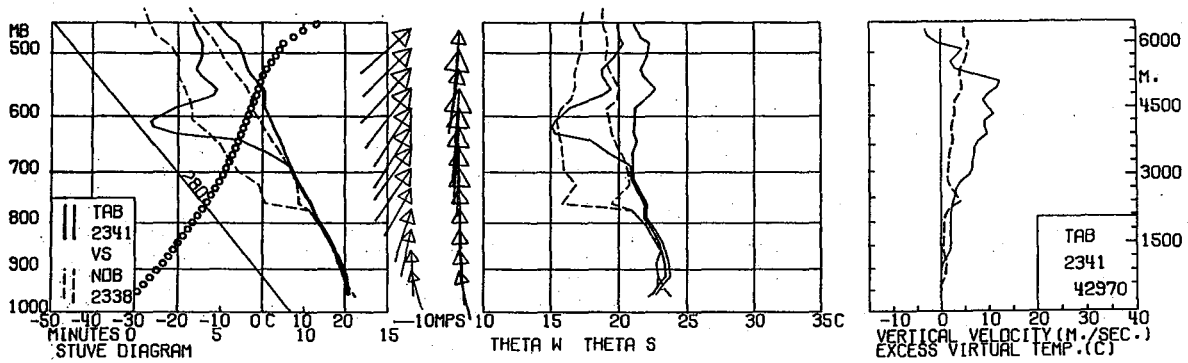
RADAR - AREA BRKN TRW/NC 70/123 D50 CELLS 2235 MAX TOP 540 AT 71/107 AREA BRKN TRW/NC 27/82 231/46 25W CELLS 2235 MAX TOP 460 AT 247/28 AREA BRKN TRW+A/NC 339/129 250/76 235/209 288/135 D15 CELLS 2335 MAX TOP 620 AT 257/92 GOLF BALL SIZE HAIL CELL AT 257/92

Balloon was overrun by echo and entered the rt. front quadrant near a tight reflectivity gradient.

SFC WX AT RLS TIME - 6/10 CB 3/10 STRATUS - ENVIRONMENT WX - 3/10 CB 7/10 CU



CASE 20

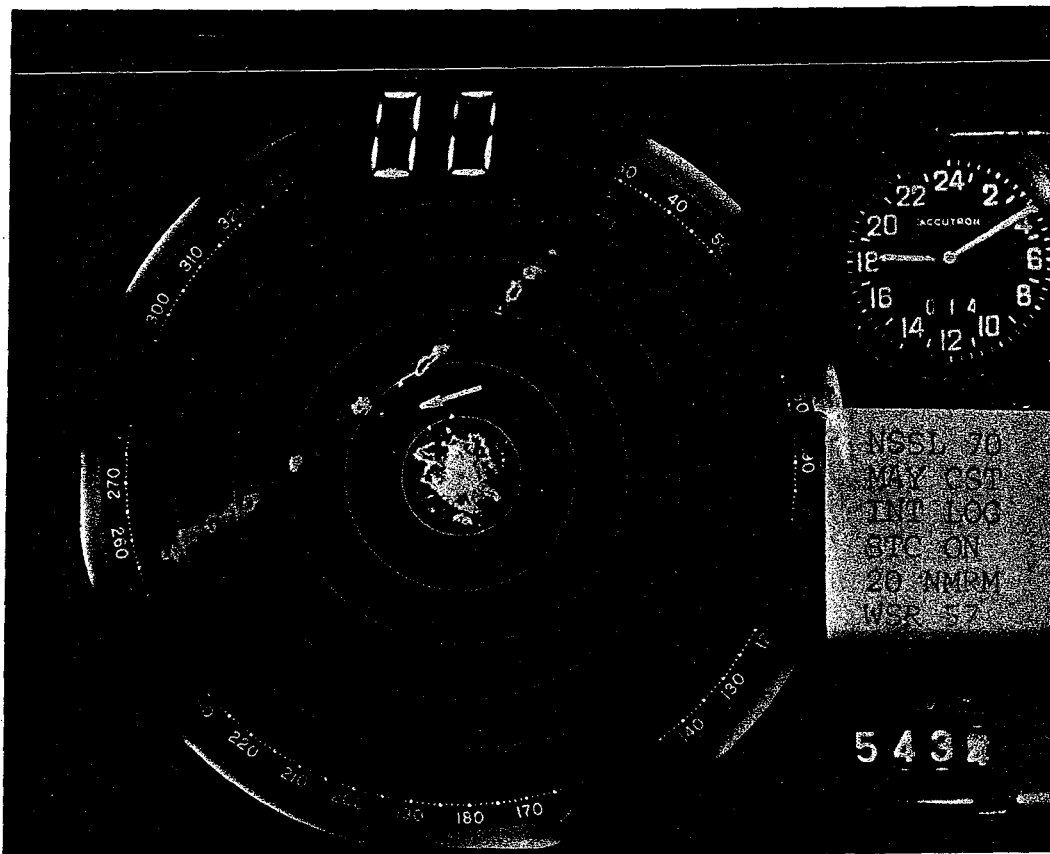


SYNOP - A sharp 500 mb trough line was oriented NNE-SSW across eastern New Mexico. An old cP front, coincident with a dry line was located in western Oklahoma. Thunderstorms developed in the mT air as an open wave developed along the front in western Oklahoma.

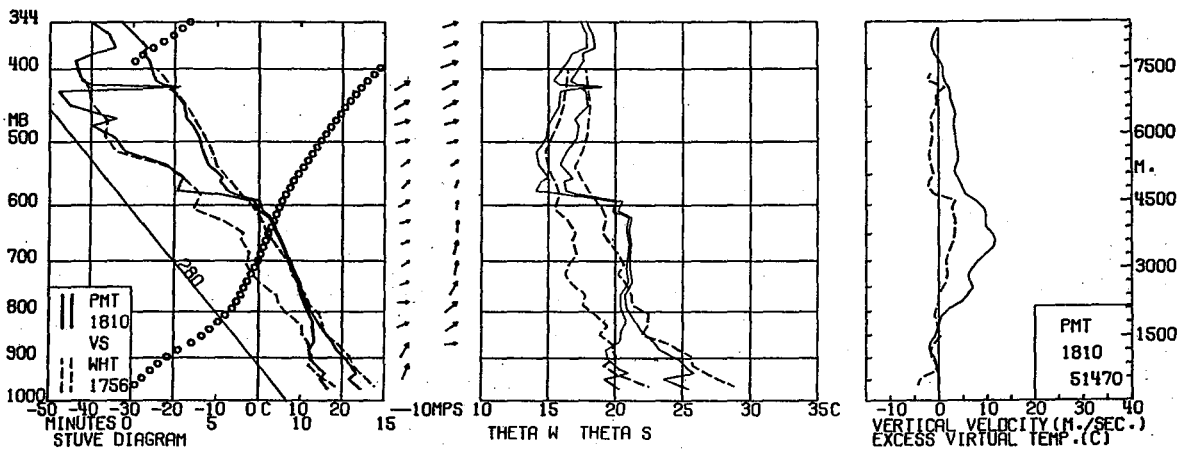
RADAR - AREA SCTD TRW/NC 64/159 D30 CELLS 2235 LN BRKN TRW+/+ 29/97  
259/20 30W CELLS 2235 CELL TRW+/+ 273/56 D30 CELLS 2235 TOP 700 AREA  
BRKN TRW+/NC 347/163 239/170 55W CELLS 2235 POWER FAILURE BEFORE OBSER-  
VATION COMPLETED.

Balloon entered echo on rt. front near indentation. Echo still maintained tight reflectivity gradient near indentation.

SFC WX AT RLS TIME - 3/10 CB 7/10 STRATUS - ENVIRONMENT WX - 5/10 CB  
5/10 CU



CASE 21

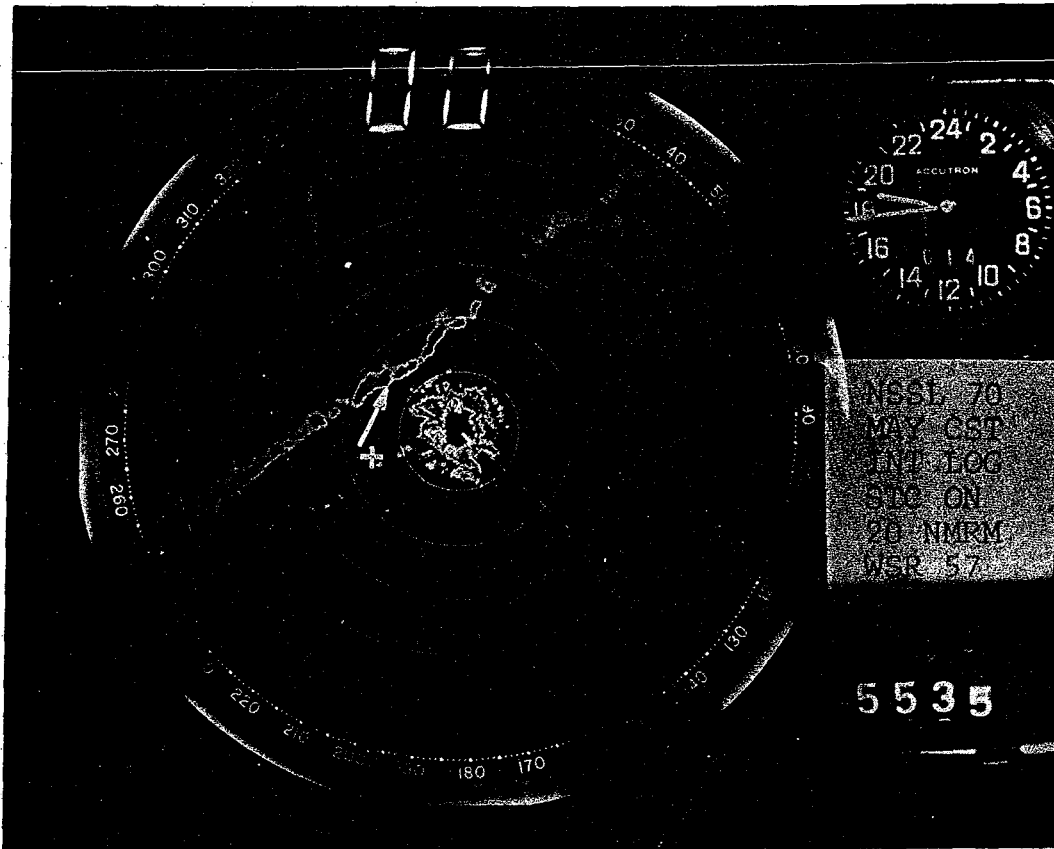


SYNOPSIS - A line of activity developed in the mT air mass ahead of a slow-moving mP front. The mP front moved southeastward across the state during the day and out of state by midnight. At 500 mb, a short wave trough moved across northwestern Oklahoma.

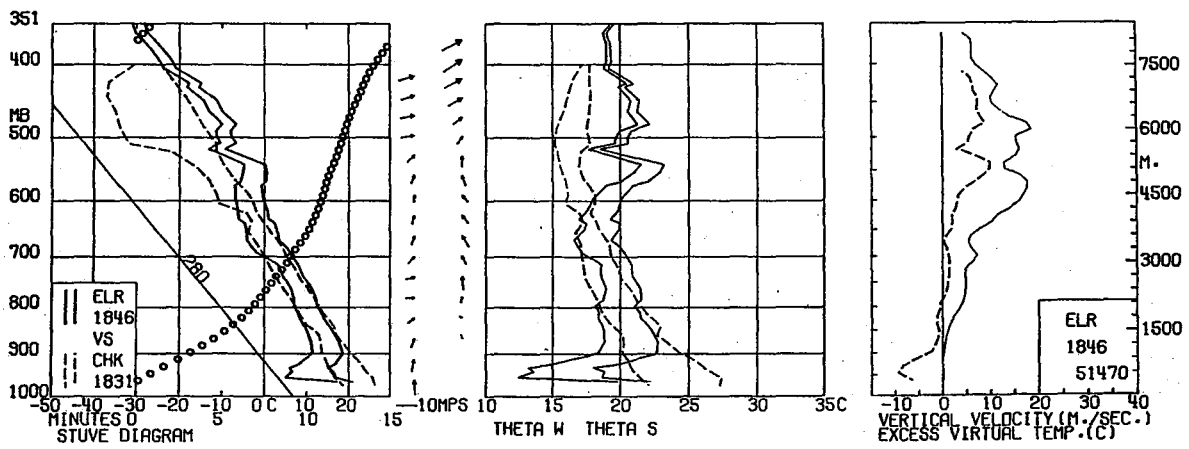
RADAR - AREA BRKN TRWU 39/193 56/171 50/137 34/156 CELLS 2615 LN BRKN TRW/NC 22/88 304/52 254/178 5W 2910 CELLS 2615 MAX TOP 470 343/51 TOP 460 AT 307/50 CELLS TRW-/NC 359/120 356/114 D3 2615 TOPS 300

Balloon apparently got into a developing echo approximately 15 km ahead of squall line pictured above.

SFC WX AT RLS TIME - 3/10 CB 4/10 STRATOCU 1/10 CIRROSTRATUS - ENVIRONMENT WX - 3/10 CB 4/10 CIRROSTRATUS



CASE 22

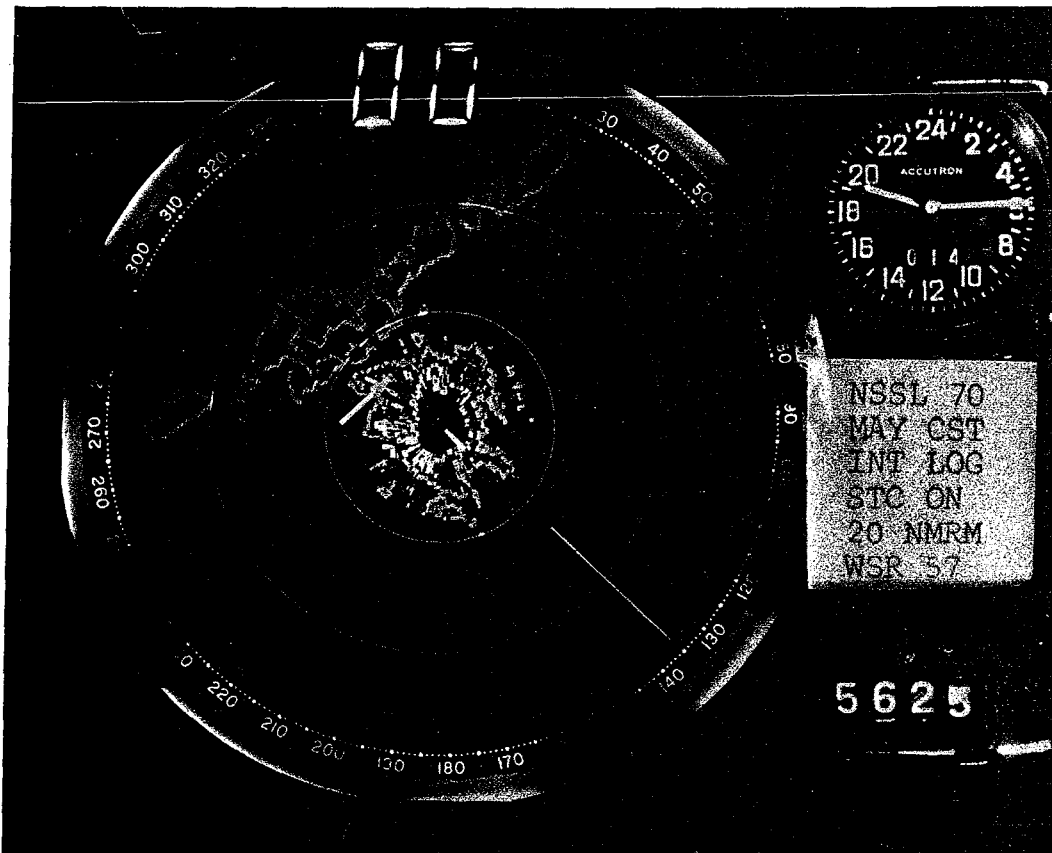


SYNOP - A line of activity developed in the mT air mass ahead of a slow-moving mP front. The mP front moved southeastward across the state during the day and out of the state by midnight. At 500 mb a short wave trough moved across northwestern Oklahoma.

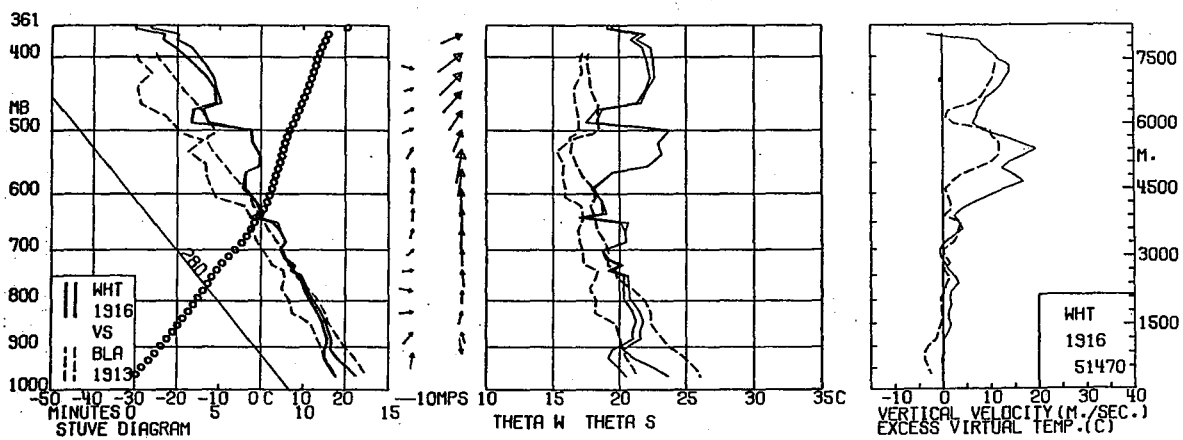
RADAR - LN BRKN TRW/NC 46/173 357/50 328/31 250/172 5W 2910 CELLS 2515  
MAX TOP 440 AT 302/40 LN SCTD TRW-/NEW 264/18 244/70 2W MAX TOP 320 AT  
262/20

Balloon entered radar echo with tight reflectivity gradient on rt. front near indentation in echo.

SFC WX AT RLS TIME - 10/10 CB WITH TRW+ IN PROGRESS CB ALQDS AND OVERHEAD  
ENVIRONMENT WX - 1/10 CB 1/10 CU 8/10 CS LN CB SW-NW-NE



CASE 23



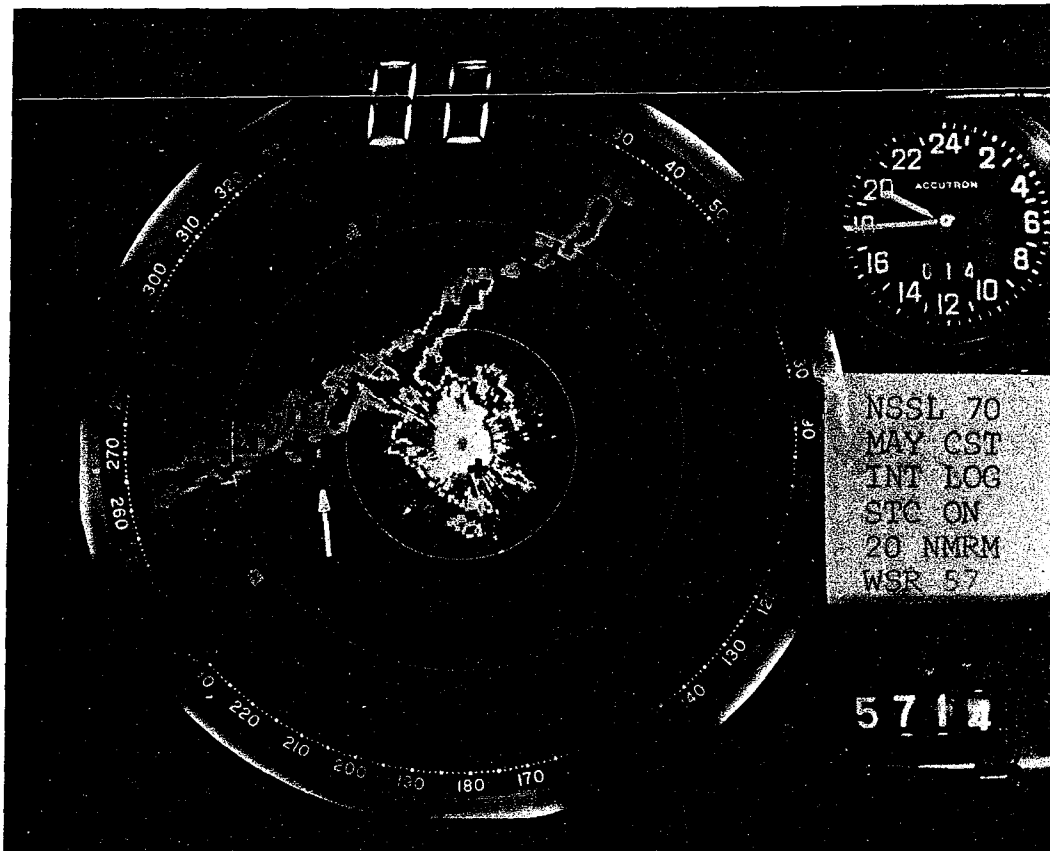
SYNOP - A line of activity developed in the mT air mass ahead of a slow-moving mP front. The mP front moved southeastward across the state during the day and out of the state by midnight. At 500 mb a short wave trough moved across northwestern Oklahoma.

RADAR\* - LN BRKN TRW/NC 46/173 357/50 328/31 250/172 5W 2910 CELLS 2515  
MAX TOP 440 AT 302/40 LN SCTD TRW-/NEW 264/18 244/70 2W MAX TOP 320 AT  
262/20

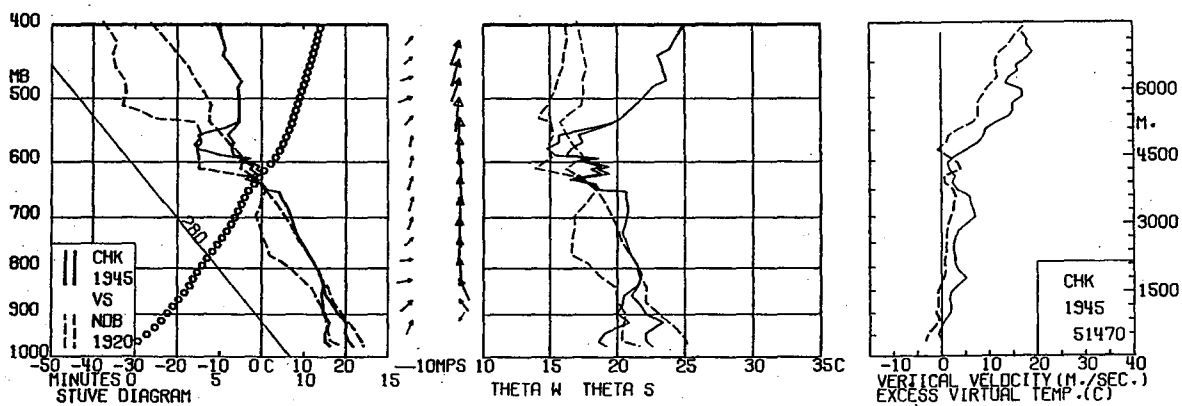
Balloon apparently entered developing radar echo approximately 7 km ahead of squall line.

SFC WX AT RLS TIME - 2/10 CB 4/10 STRATUS - ENVIRONMENT WX - 2/10 CU  
5/10 CI

\*NOTE: Full scope is only 50 n mi.



CASE 24



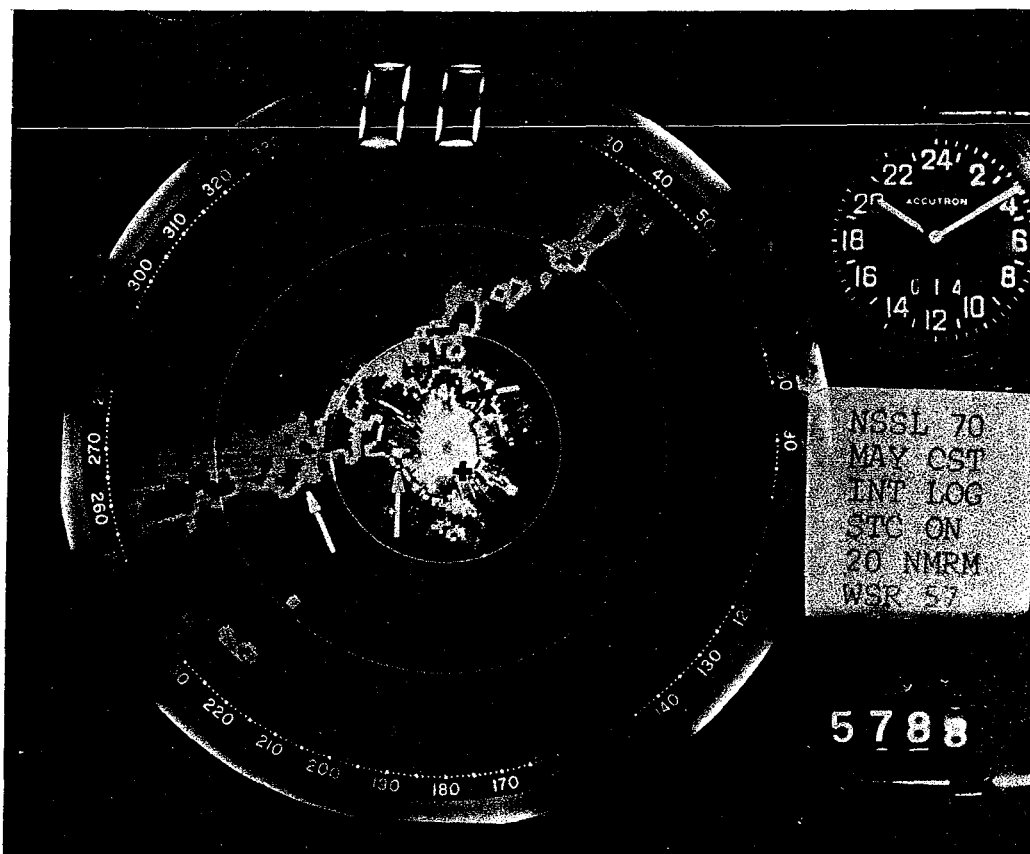
SYNOPSIS - A line of activity developed in the mT air mass ahead of a slow-moving mP front. The mP front moved southeastward across the state during the day and out of the state by midnight. At 500 mb a short wave trough moved across northwestern Oklahoma.

RADAR\* - LN OVC TRW/NC 50/183 11/34 266/55 251/127 245/14 7W 2910 CELLS  
2510 MAX TOP 430 AT 306/27 AREA BRKN TRW/NC 239/79 D20 CELLS 2510 MAX  
TOP 420 AT 243/85 CELL TRWU 216/139 D8

Balloon entered an echo that only appeared on radar at 8 and 10 degree tilts.

SFC WX AT RLS TIME - 3/10 CB 5/10 STRATOCU FQT LTGICCCCG NNW - ENVIRONMENT WX - 3/10 CB 3/10 ALTOCU 2/10 CIRROSTRATUS

\*NOTE: Full scope is only 50 n mi.



CASES 25, 26 & 27

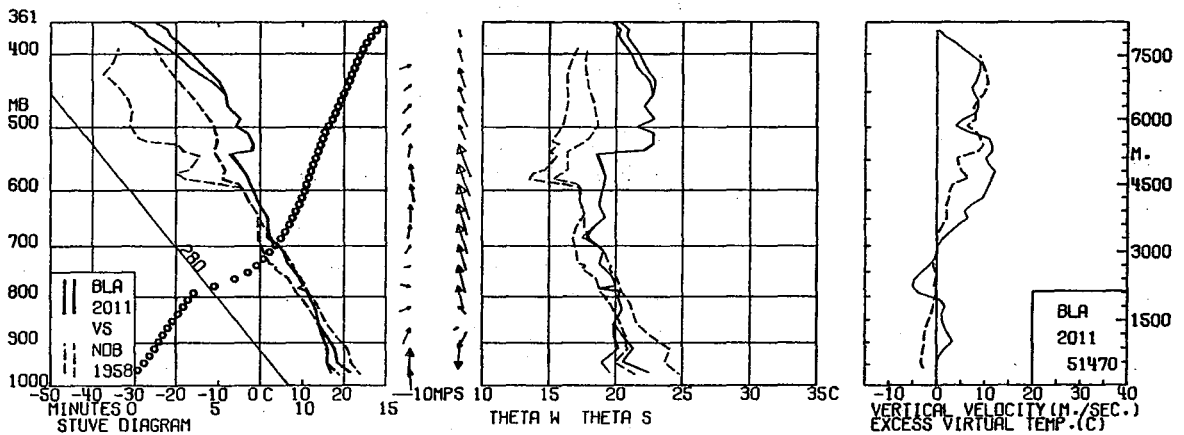
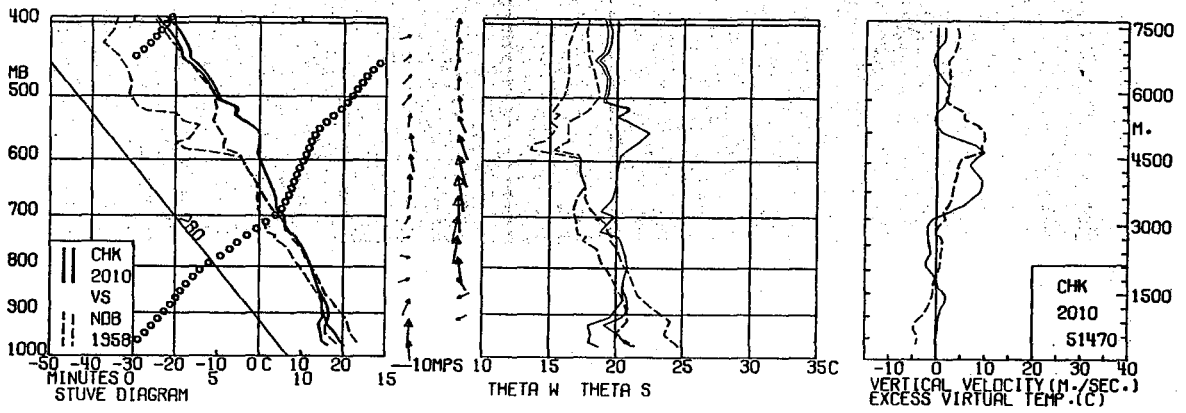
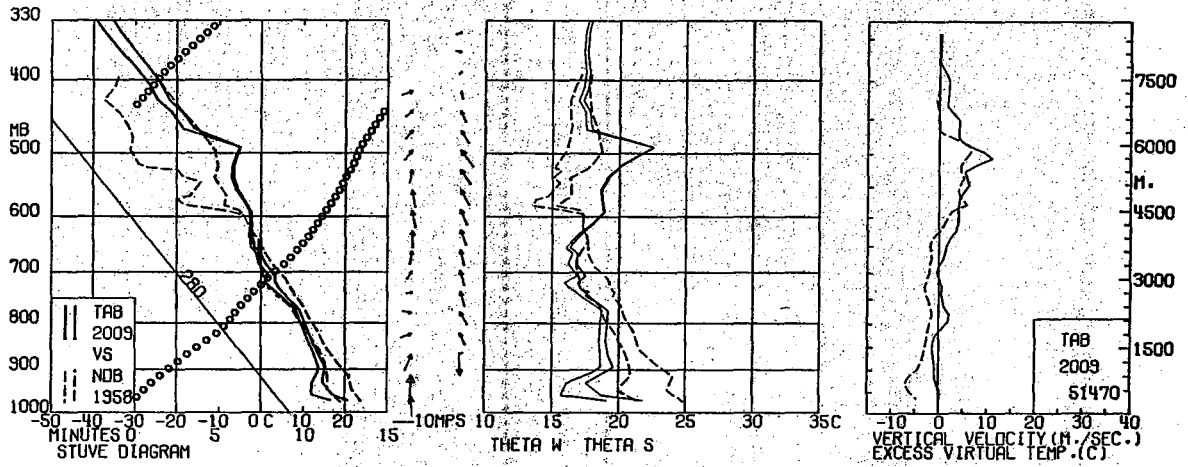
SYNOPSIS - A line of activity developed in the mT air mass ahead of a slow-moving mP front. The mP front moved southeastward across the state during the day and out of the state by midnight. At 500 mb a short wave trough moved across northwestern Oklahoma.

RADAR\* - LN OVC TRW/NC 50/183 11/34 266/55 251/127 245/161 7W 2910 CELLS 2510 MAX TOP 430 AT 306/27 AREA BRKN TRW/NC 239/79 D20 CELLS 2510 MAX TOP 420 AT 243/85 CELL TRWU 216/139 D8

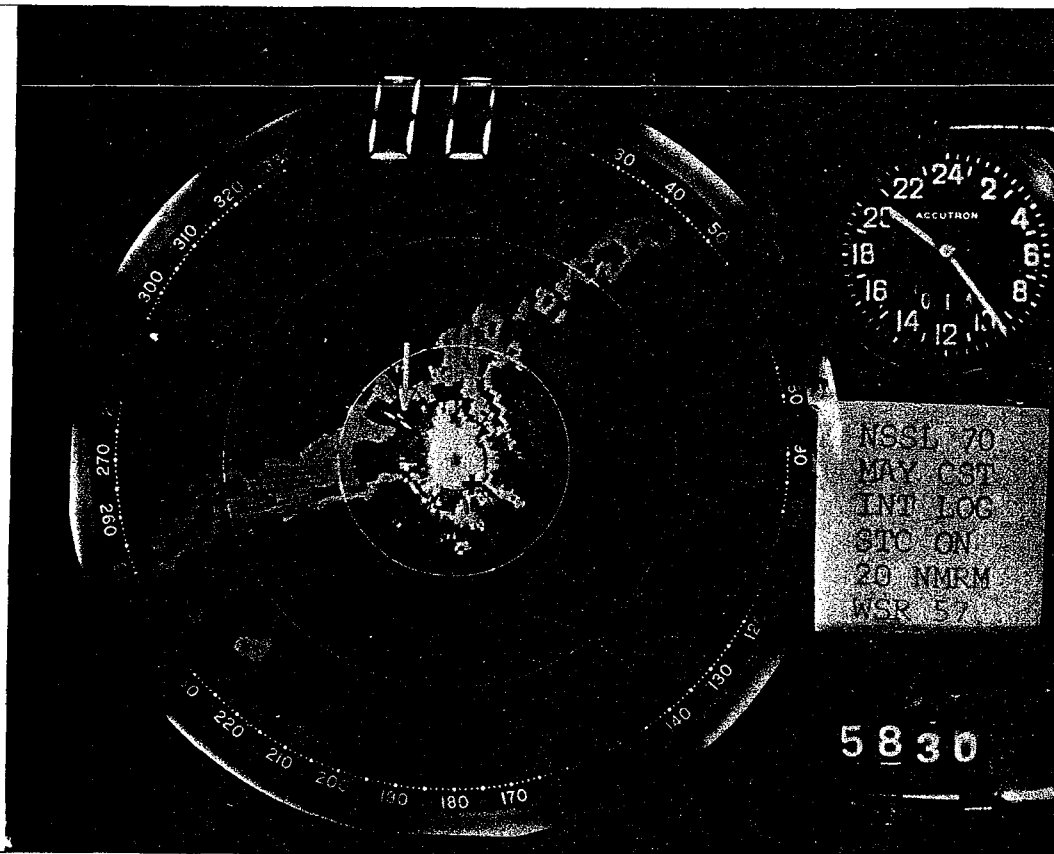
Case 25 - Balloon entered rt. front of radar echo near tight reflectivity gradient. Case 26 - Balloon entered rt. front of radar echo with tight reflectivity gradient near indentation. Case 27 - Balloon entered rt. front of radar echo with tight reflectivity gradient near indentation.

SFC WX AT RLS TIME - Case 25 - 10/10 CB. Case 26 - 5/10 CB 5/10 STRATOCU HEAVY THUNDER IN PROGRESS, FQT LLGICCCCG W-N-E. Case 27 - 10/10 CB. ENVIRONMENT WX - 3/10 CB 5/10 CU 1/10 CIRROSTRATUS

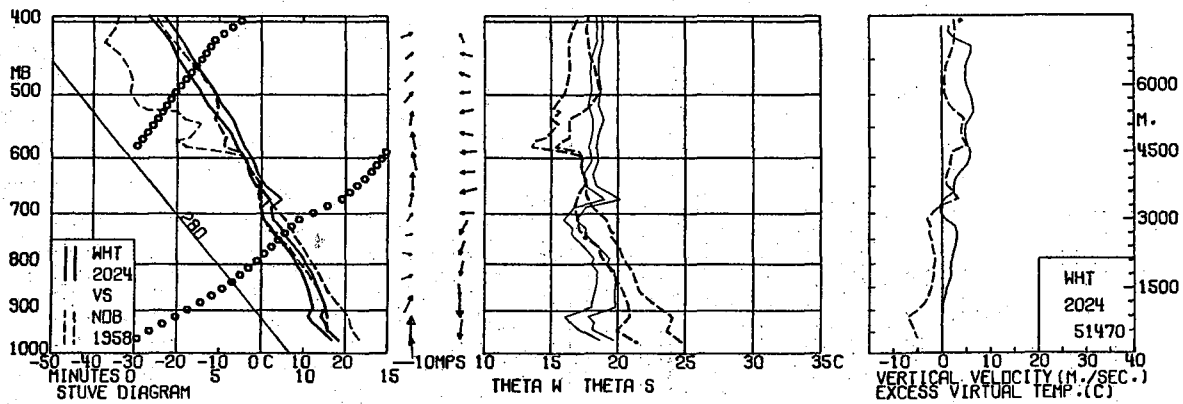
\*NOTE: Full scope is only 50 n mi. Case 25 is northeastern most arrow; Case 26 is southwestern most arrow; Case 27 is middle arrow.



CASES 25 (TOP), 26 (MIDDLE), 27 (BOTTOM)



CASE 28



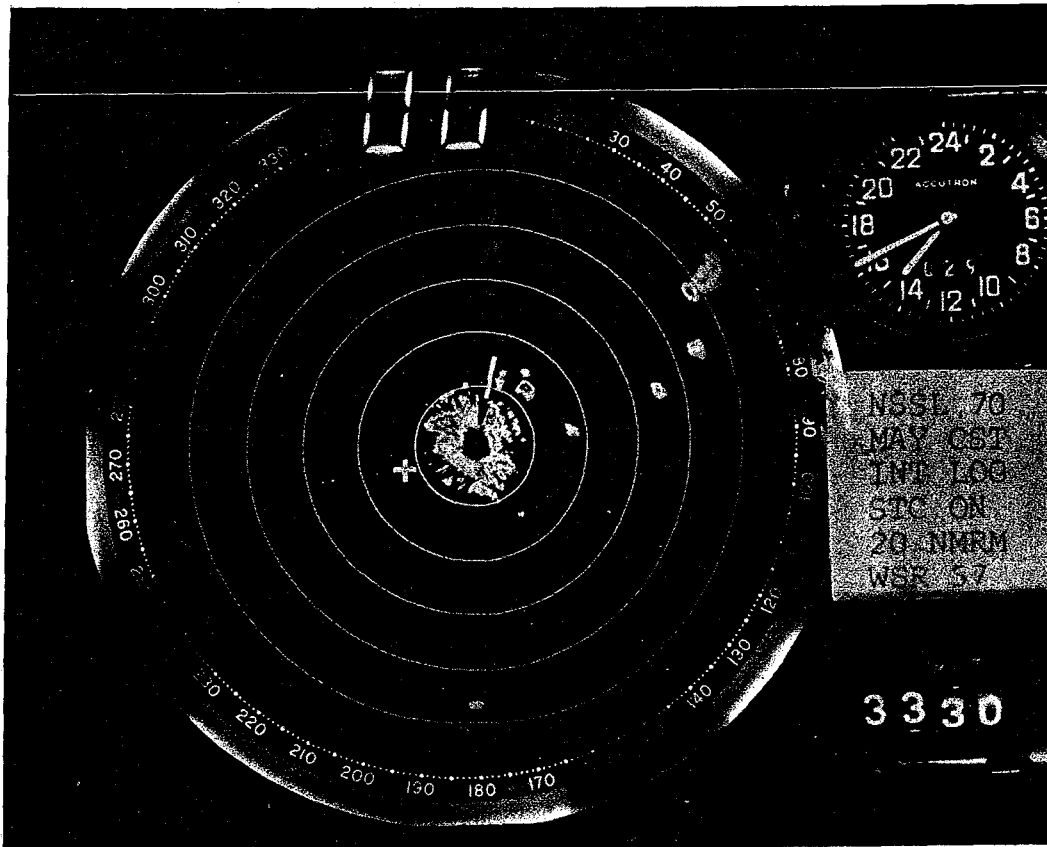
SYNOPSIS - A line of activity developed in the mT air mass ahead of a slow-moving mP front. The mP front moved southeastward across the state during the day and out of the state by midnight. At 500 mb a short wave trough moved across northwestern Oklahoma.

RADAR\* - LN BRKN TRW/NC 48/158 42/53 253/51 243/135 15W 2912 MAX TOP 460  
AT 250/64 CELLS TRW~/NEW 294/93 288/104 D3 TOP 300 AT 294/93

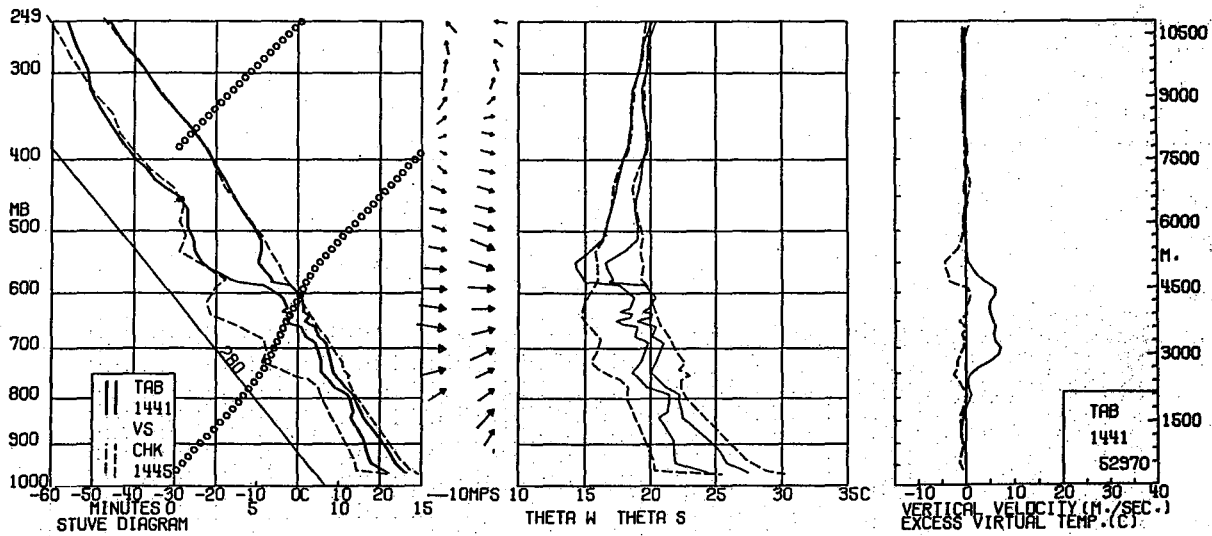
Balloon entered the back side of the slow-moving squall line.

SFC WX AT RLS TIME - 4/10 CB 6/10 STRATUS WITH A HEAVY RAIN SHOWER IN  
PROGRESS - ENVIRONMENT WX - 3/10 CB 5/10 CU 1/10 CIRROSTRATUS

\*Note: Full scope is only 50 n mi.



CASE 29

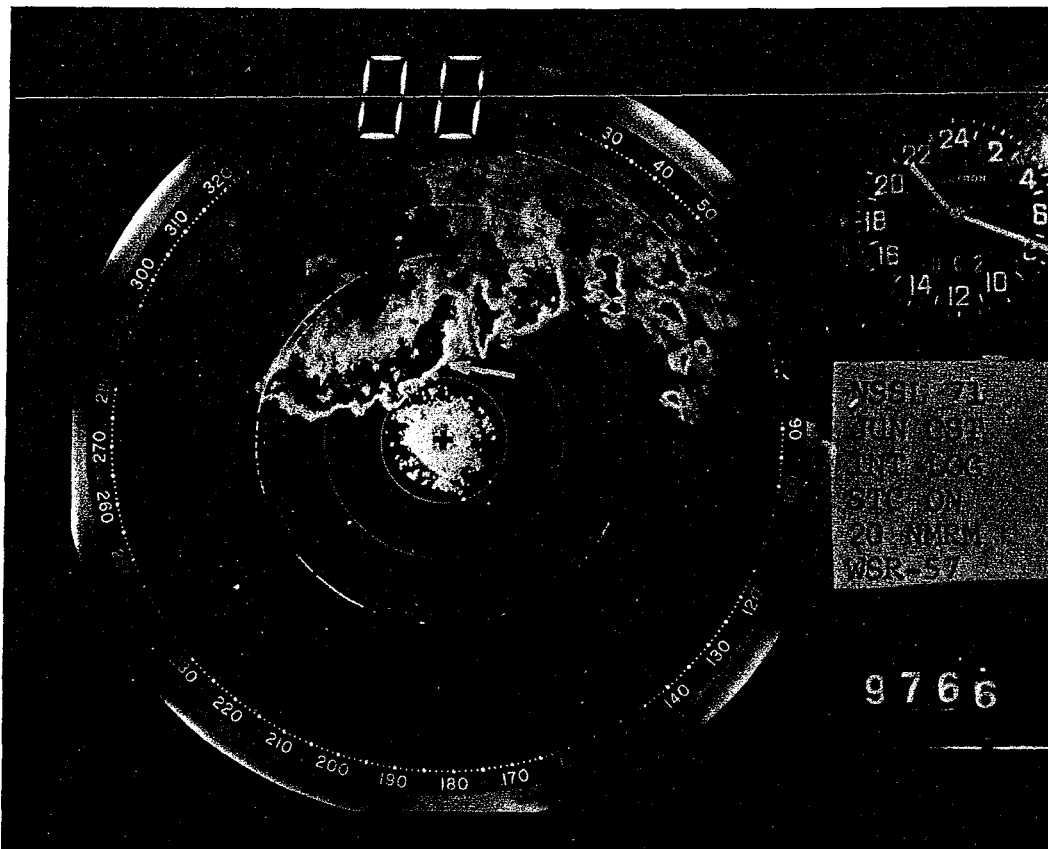


SYNOPSIS - Thunderstorms developed in the mT air south of a quasi-stationary mP front in northwestern Oklahoma. Surface dew points were extremely high as moderate southerly flow continued throughout the day. A 500 mb low moved slowly eastward across the state.

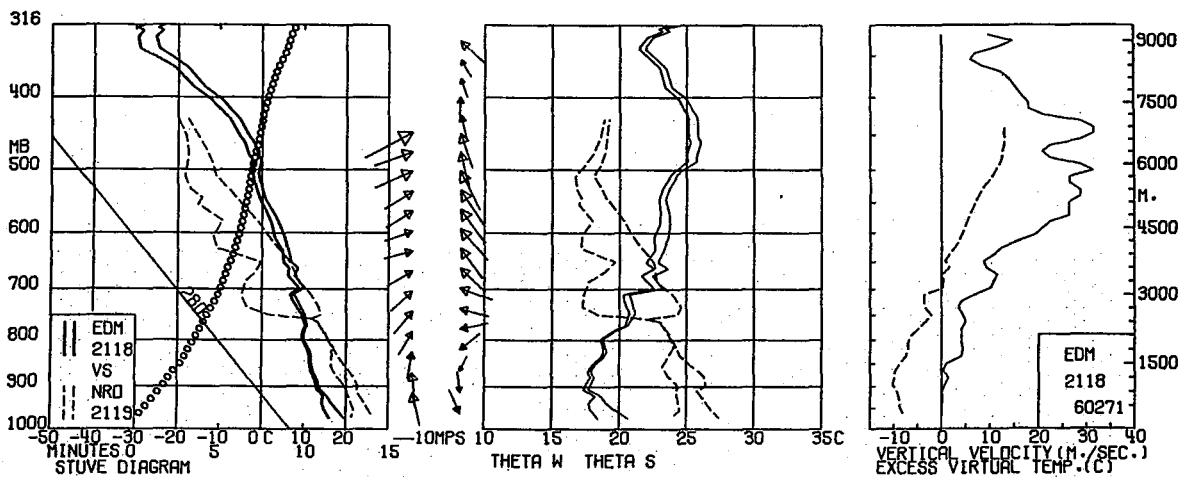
RADAR - LN BRKN TRW/NEW 55/131 62/94 10W MAX TOP 460 AT 60/98 CELLS TRW-/NEW 74/91 78/70 86/32 43/26 D3 MAX TOP 460 AT 43/26

Balloon entrained into echo inside radar ground clutter pattern.

SFC WX AT RLS TIME - CU SKY AMOUNT MISSING - ENVIRONMENT WX - 6/10 CU



CASE 30

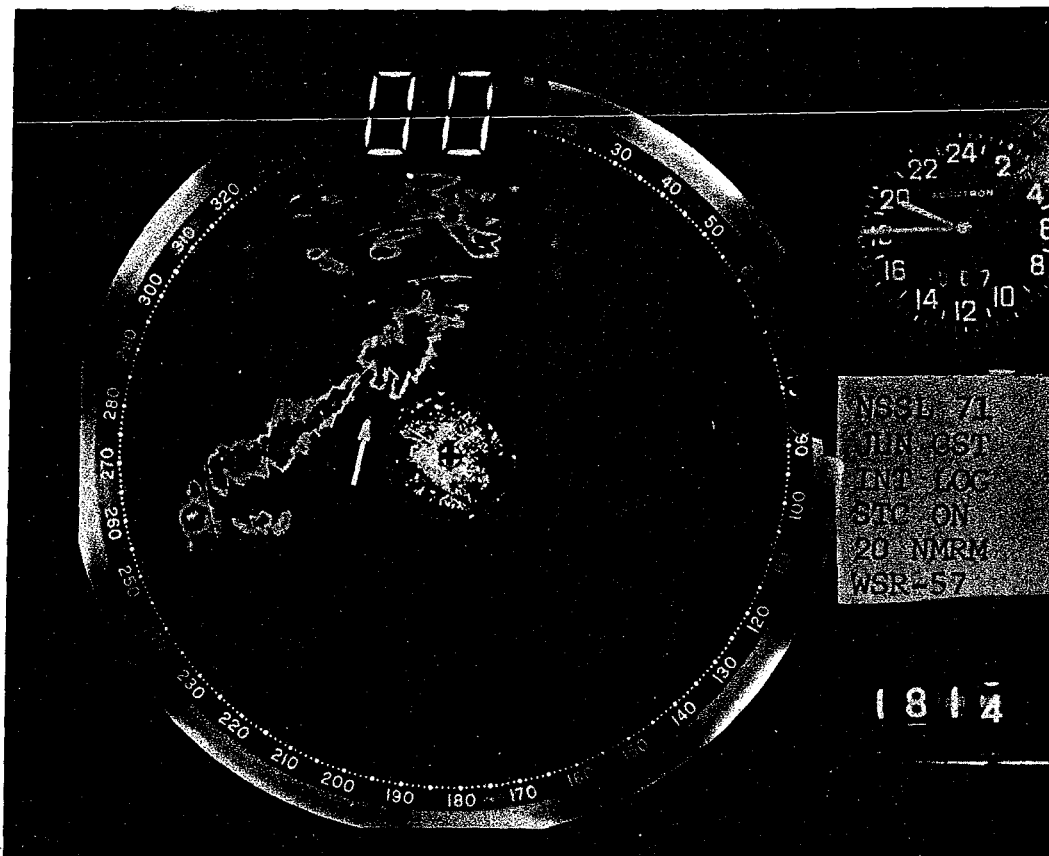


SYNOP - Thunderstorms developed in a very humid mT air mass south of a slow-moving cP front. At 500 mb a vigorous short wave with associated cold air advection moved across the state. Severe weather occurred near time of release - gusts 70 mph, 3/4 inch hail.

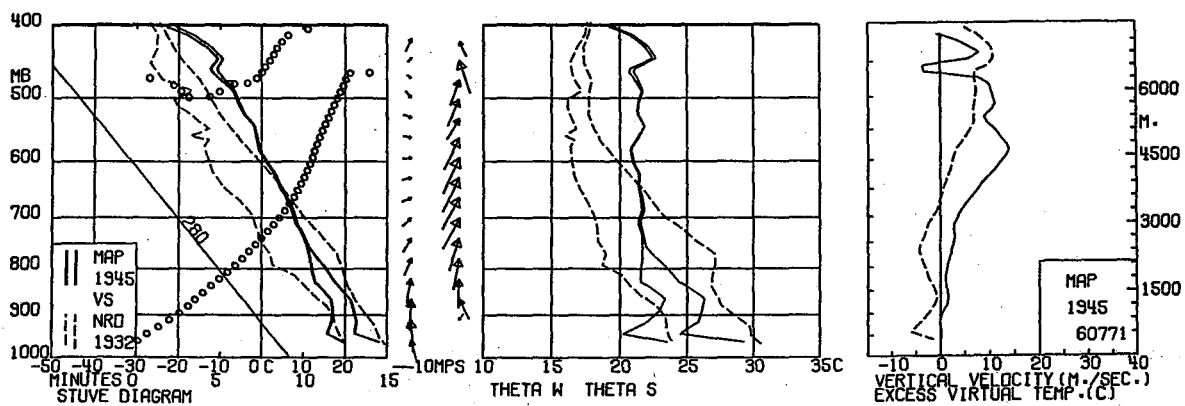
RADAR - AREA BRKN - TRW+/NC 360/152 51/142 77/96 285/88 312/113 3420 MAX TOPS 560 AT 21/58 AND 339/42 AND 331/44

Balloon entered left front of echo. Radar analysis of this feature indicates it was a new updraft in squall line.

SFC WX AT RLS TIME - 10/10 CB WITH TRW- IN PROGRESS - ENVIRONMENT WX - 1/10 CB 9/10 CIRROSTRATUS WITH LTGICCG N



CASE 31

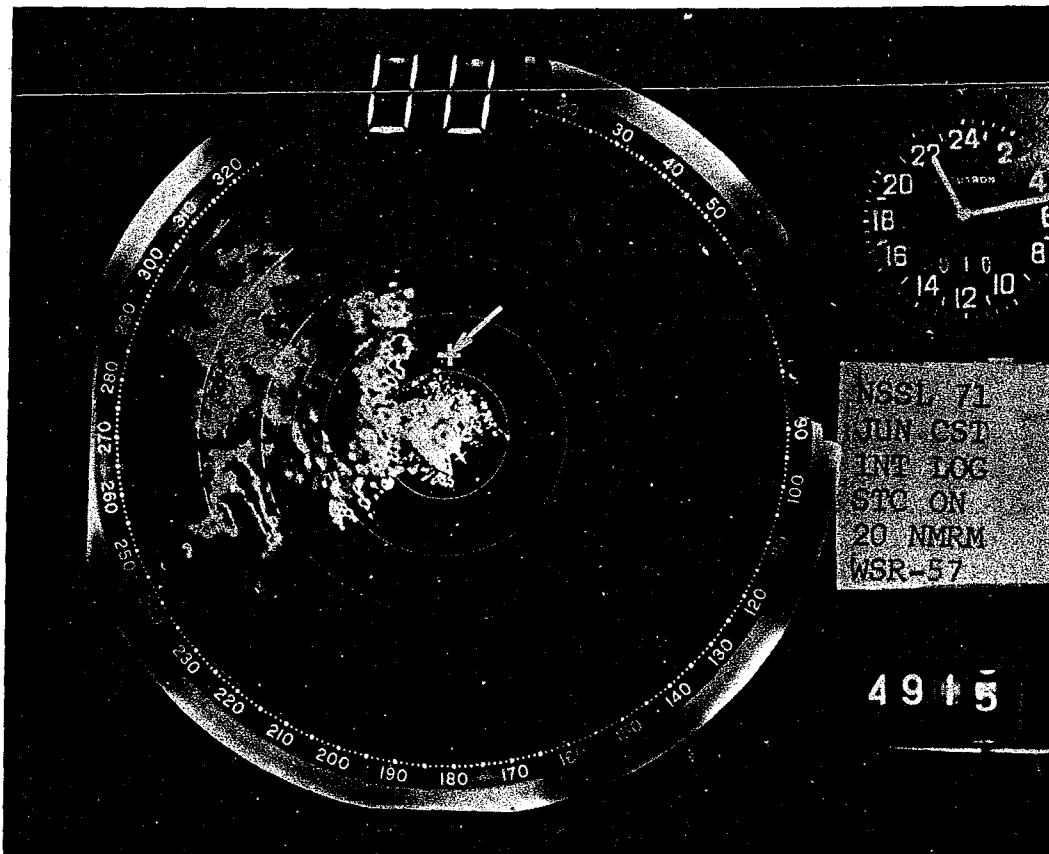


SYNOP - Thunderstorms developed in mT air mass east of a quasi-stationary mP front. Activity seems to have been initiated by 500 mb short wave and associated cold air advection.

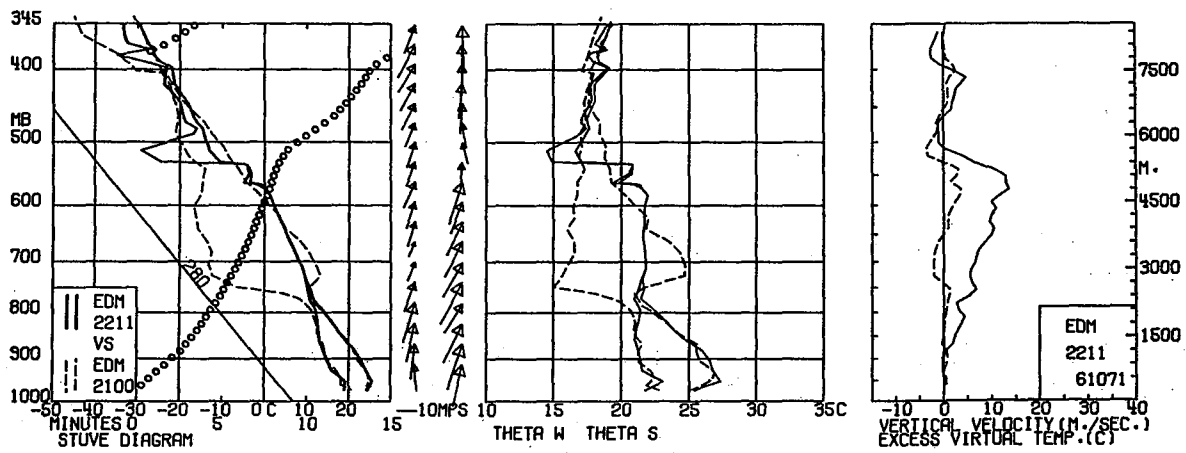
RADAR - AREA BRKN TRW+/NC 331/139 25/123 237/149 225/131 CELLS 2212 MAX  
TOP 580 AT 343/120

Balloon entered apparent convection ahead and to the right of the pre-existing squall line.

SFC WX AT RLS TIME - 10/10 CB - ENVIRONMENT WX - 2/10 CB 2/10 CUMAM 4/10  
CIRROSTRATUS



CASE 32

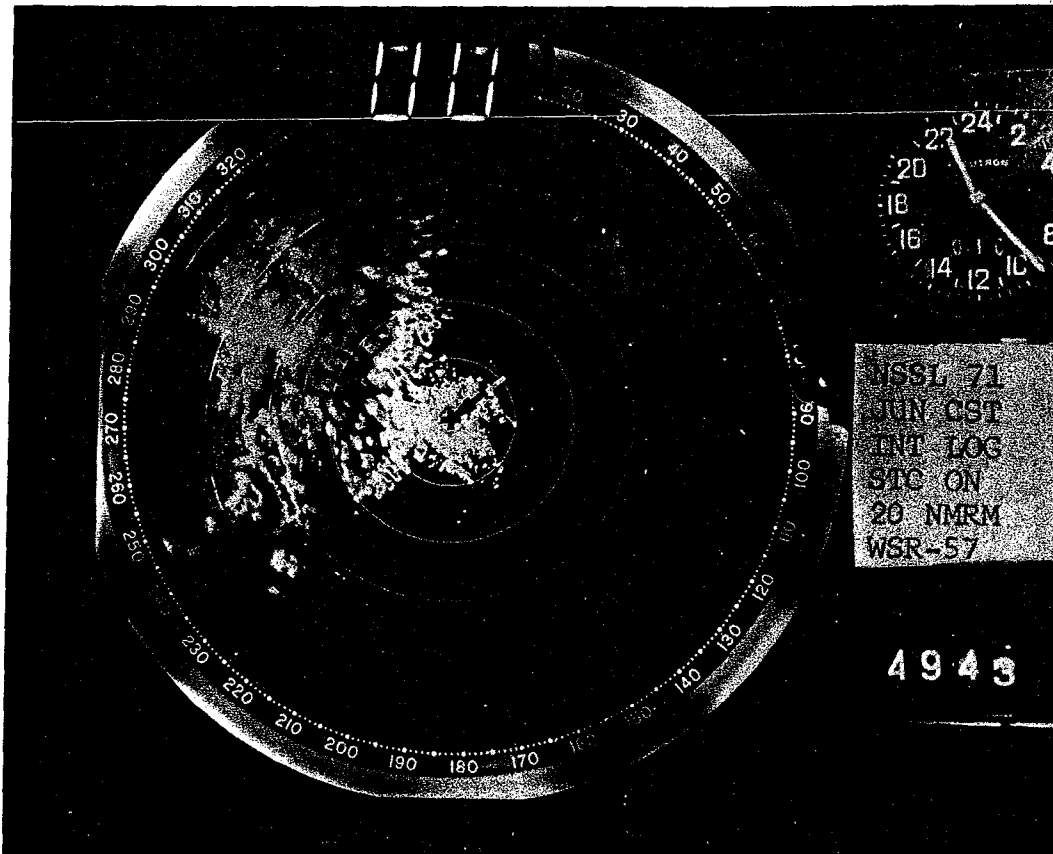


SYNOPSIS - Thunderstorms developed in the mT air mass. There was no salient feature at the surface.

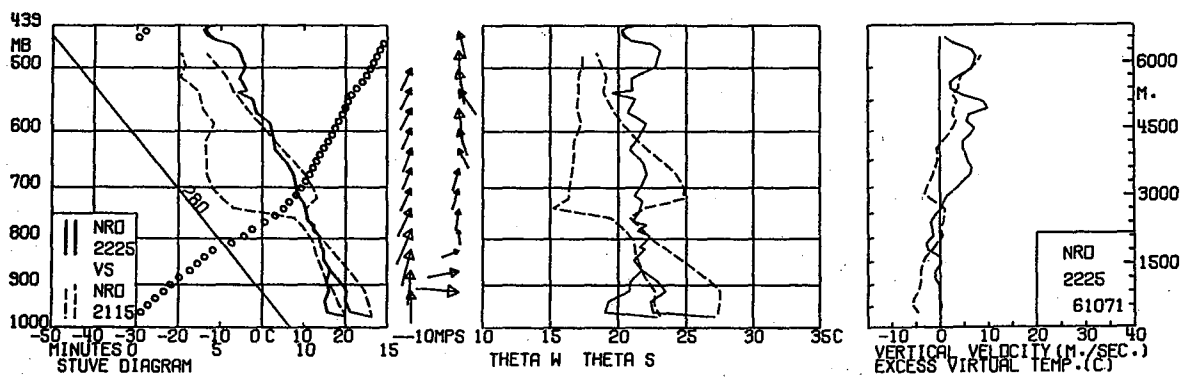
RADAR - AREA BRKN TRW+/NC 342/139 291/34 234/73 241/125 294/111 CELLS  
2430 MAX TOP 470 AT 250/99 CELLS TRWU 355/168 13/160 D5 2425

Balloon apparently was entrained into a new updraft. No radar echo was visible.

SFC WX AT RLS TIME - 10/10 CB WITH TRW-- IN PROGRESS - ENVIRONMENT WX -  
6/10 CB



CASE 33

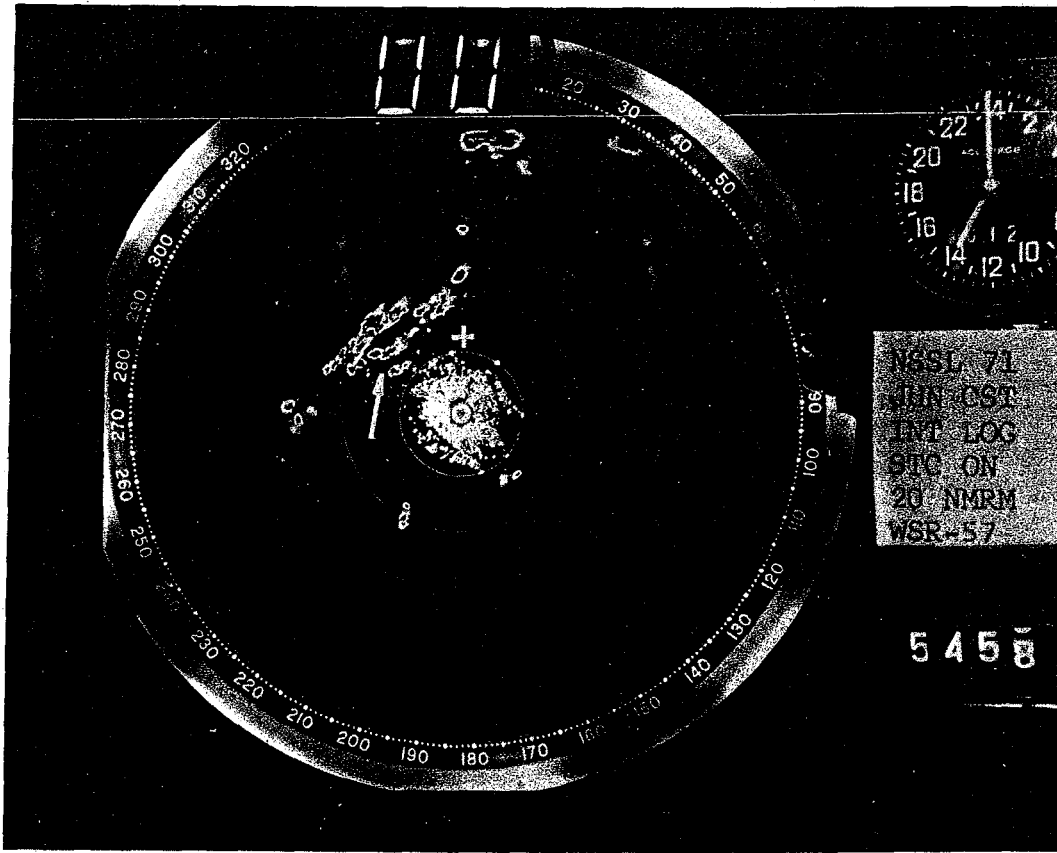


SYNOP - Thunderstorms developed in the mT air mass. There was no salient feature at the surface.

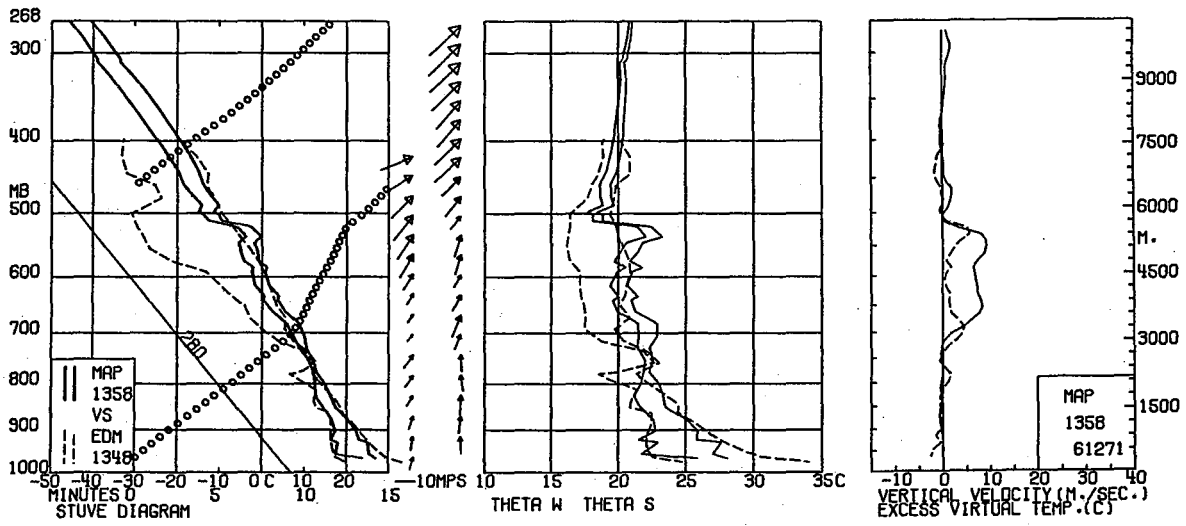
RADAR - AREA BRKN TRW+/NC 342/139 291/34 235/73 241/125 294/111 CELLS  
2430 MAX TOP 470 AT 250/99 CELLS TRWU 355/168 13/160 D5 2425

Balloon was entrained into echo 1 km north of radar site.

SFC WX AT RLS TIME - 5/10 CB 5/10 CIRROSTRATUS - ENVIRONMENT WX - 1/10 CB  
1/10 STRATOCU 8/10 CIRROSTRATUS WITH LTGIC N



CASE 34



SYNOP - Thunderstorms developed along weak instability line in western Oklahoma in mT air mass. Weak cold air advection was present at 500 mb.

RADAR - AREA SCTD TRW/NC 50/197 2/113 50W 2715 MAX TOP 400 AT 6/91 CELLS  
TRW/NEW 305/42 D10 TOP 320 267/58 D9 TOP 300 151/27 D5 TOP 260 CELLS 2125  
CELLS TRWU 297/147 D15 2125

Balloon entered right rear of radar echo with tight reflectivity gradient.

SFC WX AT RLS TIME - 4/10 CB 4/10 CU 2/10 CIRROSTRATUS - ENVIRONMENT WX -  
6/10 TCU

## APPENDIX B

### THERMODYNAMIC ENERGY EQUATION

The thermodynamic energy equation used in the model is

$$\begin{aligned}
 & \left[ 1 + \frac{c_w}{c_p} (q_s + Q) + \frac{\epsilon L^2 q_s (1 + q_s/\epsilon)}{c_p R T^2} + \frac{q_s}{c_p} \frac{dL}{dT} \right] \frac{\partial T}{\partial z} \\
 & = \frac{-g T_v}{c_p T_{v_e}} (1 + q_s) \left[ 1 + \frac{L q_s}{R T} \right] - \frac{\rho_e}{\rho} \frac{2\alpha}{b} \left[ (T - T_e) + \frac{L}{c_p} (q - q_e) \right]
 \end{aligned}$$

where  $z$  is height,  $T$  temperature,  $T_v$  virtual temperature,  $q$  mixing ratio,  $q_s$  saturation mixing ratio,  $Q$  liquid water mixing ratio,  $\rho$  density,  $b$  updraft radius,  $g$  acceleration due to gravity,  $c_p$  specific heat of air at constant pressure,  $c_w$  specific heat of water,  $R$  gas constant for dry air,  $\epsilon = 0.622$ ,  $L$  latent heat of condensation,  $\alpha$  entrainment coefficient, and subscript  $e$  refers to the environment.

In the limit of no entrainment ( $\alpha = 0$ ),  $Q = 0$  (pseudo-adiabatic rather than moist adiabatic ascent) and  $T_v/T_{v_e} = 1$ , this equation yields the expression given in the Smithsonian Tables (1958, p. 323) for the pseudo-adiabatic lapse rate (after use of the Clausius-Clapeyron equation).

## NATIONAL SEVERE STORMS LABORATORY

The NSSL Technical Memoranda, beginning with No. 28, continue the sequence established by the U. S. Weather Bureau National Severe Storms Project, Kansas City, Missouri. Numbers 1-22 were designated NSSL Reports. Numbers 23-27 were NSSL Reports, and 24-27 appeared as subseries of Weather Bureau Technical Notes. These reports are available from the National Technical Information Service, Operations Division, Springfield, Virginia 22151, for \$3.00, and a microfiche version for \$0.95. NTIS numbers are given below in parentheses.

- No. 1 National Severe Storms Project Objectives and Basic Design. Staff, NSSL. March 1961. (PB-168207)
- No. 2 The Development of Aircraft Investigations of Squall Lines from 1956-1960. B. B. Goddard. (PB-168208)
- No. 3 Instability Lines and Their Environments as Shown by Aircraft Soundings and Quasi-Horizontal Traverses. D. T. Williams. February 1962. (PB-168209)
- No. 4 On the Mechanics of the Tornado. J. R. Fulks. February 1962. (PB-168210)
- No. 5 A Summary of Field Operations and Data Collection by the National Severe Storms Project in Spring 1961. J. T. Lee. March 1962. (PB-165095)
- No. 6 Index to the NSSL Surface Network. T. Fujita. April 1962. (PB-168212)
- No. 7 The Vertical Structure of Three Dry Lines as Revealed by Aircraft Traverses. E. L. McGuire. April 1962. (PB-168213)
- No. 8 Radar Observations of a Tornado Thunderstorm in Vertical Section. Ralph J. Donaldson, Jr. April 1962. (PB-174859)
- No. 9 Dynamics of Severe Convective Storms. Chester W. Newton. July 1962. (PB-163319)
- No. 10 Some Measured Characteristics of Severe Storms Turbulence. Roy Steiner and Richard H. Rhyne. July 1962. (N62-16401)
- No. 11 A Study of the Kinematic Properties of Certain Small-Scale Systems. D. T. Williams. October 1962. (PB-168216)
- No. 12 Analysis of the Severe Weather Factor in Automatic Control of Air Route Traffic. W. Boynton Beckwith. December 1962. (PB-168217)
- No. 13 500-Kc./Sec. Sferics Studies in Severe Storms. Douglas A. Kohl and John E. Miller. April 1963. (PB-168218)
- No. 14 Field Operations of the National Severe Storms Project in Spring 1962. L. D. Sanders. May 1963. (PB-168219)
- No. 15 Penetrations of Thunderstorms by an Aircraft Flying at Supersonic Speeds. G. P. Roys. Radar Photographs and Gust Loads in Three Storms of 1961 Rough Rider. Paul W. J. Schumacher. May 1963. (PB-168220)
- No. 16 Analysis of Selected Aircraft Data from NSSL Operations, 1962. T. Fujita. May 1963. (PB-168221)
- No. 17 Analysis of Methods for Small-Scale Surface Network Data. D. T. Williams. August 1963. (PB-168222)
- No. 18 The Thunderstorm Wake of May 4, 1961. D. T. Williams. August 1963. (PB-168223)
- No. 19 Measurements by Aircraft of Condensed Water in Great Plains Thunderstorms. George P. Roys and Edwin Kessler. July 1966. (PB-173048)
- No. 20 Field Operations of the National Severe Storms Project in Spring 1963. J. T. Lee, L. D. Sanders and D. T. Williams. January 1964. (PB-168224)
- No. 21 On the Motion and Predictability of Convective Systems as Related to the Upper Winds in a Case of Small Turning of Wind with Height. James C. Fankhauser. January 1964. (PB-168225)
- No. 22 Movement and Development Patterns of Convective Storms and Forecasting the Probability of Storm Passage at a Given Location. Chester W. Newton and James C. Fankhauser. January 1964. (PB-168226)
- No. 23 Purposes and Programs of the National Severe Storms Laboratory, Norman, Oklahoma. Edwin Kessler. December 1964. (PB-166675)
- No. 24 Papers on Weather Radar, Atmospheric Turbulence, Sferics, and Data Processing. August 1965. (AD-621586)
- No. 25 A Comparison of Kinematically Computed Precipitation with Observed Convective Rainfall. James C. Fankhauser. September 1965. (PB-168445).

- No. 26 Probing Air Motion by Doppler Analysis of Radar Clear Air Returns. Roger M. Lhermitte. May 1966. (PB-170636)
- No. 27 Statistical Properties of Radar Echo Patterns and the Radar Echo Process. Larry Armijo. May 1966. The Role of the Kutta-Joukowski Force in Cloud Systems with Circulation. J. L. Goldman. May 1966. (PB-170756)
- No. 28 Movement and Predictability of Radar Echoes. James Warren Wilson. November 1966. (PB-173972)
- No. 29 Notes on Thunderstorm Motions, Heights, and Circulations. T. W. Harold, W. T. Roach, and Kenneth E. Wilk. November 1966. (AD-644899)
- No. 30 Turbulence in Clear Air Near Thunderstorms. Anne Burns, Terence W. Harold, Jack Burnham, and Clifford S. Spavins. December 1966. (PB-173992)
- No. 31 Study of a Left-Moving Thunderstorm of 23 April 1964. George R. Hammond. April 1967. (PB-174681)
- No. 32 Thunderstorm Circulations and Turbulence from Aircraft and Radar Data. James C. Fankhauser and J. T. Lee. April 1967. (PB-174860)
- No. 33 On the Continuity of Water Substance. Edwin Kessler. April 1967. (PB-175840)
- No. 34 Note on the Probing Balloon Motion by Doppler Radar. Roger M. Lhermitte. July 1967. (PB-175930)
- No. 35 A Theory for the Determination of Wind and Precipitation Velocities with Doppler Radars. Larry Armijo. August 1967. (PB-176376)
- No. 36 A Preliminary Evaluation of the F-100 Rough Rider Turbulence Measurement System. U. O. Lappe. October 1967. (PB-177037)
- No. 37 Preliminary Quantitative Analysis of Airborne Weather Radar. Lester P. Merritt. December 1967. (PB-177188)
- No. 38 On the Source of Thunderstorm Rotation. Stanley L. Barnes. March 1968. (PB-178990)
- No. 39 Thunderstorm - Environment Interactions Revealed by Chaff Trajectories in the Mid-Troposphere. James C. Fankhauser. June 1968. (PB-179659)
- No. 40 Objective Detection and Correction of Errors in Radiosonde Data. Rex L. Inman. June 1968. (PB-180284)
- No. 41 Structure and Movement of the Severe Thunderstorms of 3 April 1964 as Revealed from Radar and Surface Mesonet Data Analysis. Jess Charba and Yoshikazu Sasaki. October 1968. (PB-183310)
- No. 42 A Rainfall Rate Sensor. Brian E. Morgan. November 1968. (PB-183979)
- No. 43 Detection and Presentation of Severe Thunderstorms by Airborne and Ground-Based Radars: A Comparative Study. Kenneth E. Wilk, John K. Carter, and J. T. Dooley. February 1969. (PB-183572)
- No. 44 A Study of a Severe Local Storm of 16 April 1967. George Thomas Haglund. May 1969. (PB-184-970)
- No. 45 On the Relationship Between Horizontal Moisture Convergence and Convective Cloud Formation. Horace R. Hudson. March 1970. (PB-191720)
- No. 46 Severe Thunderstorm Radar Echo Motion and Related Weather Events Hazardous to Aviation Operations. Peter A. Barclay and Kenneth E. Wilk. June 1970. (PB-192498)
- No. 47 Evaluation of Roughness Lengths at the NSSL-WKY Meteorological Tower. Leslie D. Sanders and Allen H. Weber. August 1970. (PB-194587)
- No. 48 Behavior of Winds in the Lowest 1500 ft in Central Oklahoma: June 1966 - May 1967. Kenneth C. Crawford and Horace R. Hudson. August 1970.
- No. 49 Tornado Incidence Maps. Arnold Court. August 1970. (COM-71-00019)
- No. 50 The Meteorologically Instrumented WKY-TV Tower Facility. John K. Carter. September 1970. (COM-71-00108)
- No. 51 Papers on Operational Objective Analysis Schemes at the National Severe Storms Forecast Center. Rex L. Inman. November 1970. (COM-71-00136)
- No. 52 The Exploration of Certain Features of Tornado Dynamics Using a Laboratory Model. Neil B. Ward. November 1970. (COM-71-00139)
- No. 53 Rawinsonde Observation and Processing Techniques at the National Severe Storms Laboratory. Stanley L. Barnes, James H. Henderson and Robert J. Ketchum. April 1971. (COM-71-00707)

- No. 54 Model of Precipitation and Vertical Air Currents. Edwin Kessler and William C. Bumgarner. June 1971. (COM-71-00911)
- No. 55 The NSSL Surface Network and Observations of Hazardous Wind Gusts. Operations Staff. June 1971. (COM-71-00910)
- No. 56 Pilot Chaff Project at the National Severe Storms Laboratory. Edward A. Jessup. November 1971. (COM-72-10106)
- No. 57 Numerical Simulation of Convective Vortices. Robert P. Davies-Jones and Glenn T. Vickers. November 1971. (COM-72-10269)
- No. 58 The Thermal Structure of the Lowest Half Kilometer in Central Oklahoma: December 9, 1966 - May 31, 1967. R. Craig Goff and Horace R. Hudson. July 1972. (COM-72-11281)
- No. 59 Cloud-to-Ground Lightning Versus Radar Reflectivity in Oklahoma Thunderstorms. Gilbert D. Kinzer. September 1972. (COM-73-10050)
- No. 60 Simulated Real Time Displays of Velocity Fields by Doppler Radar. L. D. Hennington and G. B. Walker. November 1972. (COM-73-10515)
- No. 61 Gravity Current Model Applied to Analysis of Squall-Line Gust Front. Jess Charba. November 1972. (COM-73-10410)
- No. 62 Mesoscale Objective Map Analysis Using Weighted Time-Series Observations. Stanley L. Barnes. March 1973. (COM-73-10781)
- No. 63 Observations of Severe Storms on 26 and 28 April 1971. Charles L. Vicek. April 1973. (COM-73-11200)
- No. 64 Meteorological Radar Signal Intensity Estimation. Dale Simans and R. J. Doviak. September 1973. (COM-73-11923/2AS)
- No. 65 Radiosonde Altitude Measurement Using Double Radiotheodolite Techniques. Stephan P. Nelson. September 1973. (COM-73-11934/9AS)
- No. 66 The Motion and Morphology of the Dryline. Joseph T. Schaefer. September 1973. (COM-74-10043)
- No. 67 Radar Rainfall Pattern Optimizing Technique. Edward A. Brandes. March 1974.
- No. 68 The NSSL/WKY-TV Tower Data Collection Program: April - July 1972. R. Craig Goff and W. David Zittel. May 1974.
- No. 69 Papers on Oklahoma Thunderstorms, April 29-30, 1970. Stanley L. Barnes, et al. May 1974.
- No. 70 Life Cycle of Florida Key's Waterspouts. Joseph H. Golden. June 1974.
- No. 71 Interaction of Two Convective Scales Within a Severe Thunderstorm: A Case Study and Thunderstorm Wake Vortex Structure and Thunderstorm Wake Vortex Structure and Aerodynamic Origin. Leslie R. Lemon. June 1974.